BAJECE

e-mail: editor@bajece.com

Balkan Journal of Electrical & Computer Engineering

An International Peer Reviewed, Referred, Indexed and Open Access Journal

www.bajece.com

Vol : 2
No : 3
Year : 2014
ISSN : 2147-284X

Sponsored by the

- Kirklareli University,
- Klaipeda University
- Inonu University
- Istanbul Technical University
- Sriwijaya University

This journal is accredited by the Kirklareli University subsidy purposes. It is abstracted and indexed in Copernicus, Index Google Scholarship, the PSCR, DOAJ, Research Bible, Indian Open Access Journals (OAJ), Institutional Repositories (IR), Journal TOCs, J-Gate (Informatics India), Ulrich's, ResearchGate, International Society of Universal Research in Sciences, DRJI, EyeSource.

General Publication Director & Editor-in-Chief
Ş.Serhat Seker

Vice Editor
Eleonora Guseinovienė, Klaipeda University, Lithuania
Amir Tokić, University of Tuzla, Bosnia and Herzegovina

Editorial board
Deris Stiawan, Sriwijaya University, Indonesia
Hafiz Alisoy, Namik Kemal University, Turkey
Tahir Cetin Akinci, Kirklareli University, Turkey

Scientific Committee
YangQuan Chen (USA)
Gunay Karlı (Bosnia and Herzegovina)
Arif M. Hasimov (Azerbaijan)
Aleksandar Georgiev (Bulgaria)
Ahmet Hamdi Kayran (Turkey)
Murari Mohan Saha (Sweden)
Ferhat Sahin (USA)
Vladimir Berzan (Moldova)
Sabih Atadan (Turkey)
Daniela Dzhonova-Atanasova (Bulgaria)
Vitalijus Volkovas (Lithuania)
Tuiebakhova Zoya Kaimovna (Kazakhstan)
Tahir M. Lazimov (Azerbaijan)
Okyay Kaynak (Turkey)
Jan Izykowski (Poland)
Javier Bilbao Landatxe (Spain)
H. Selcuk Nogay (Turkey)
Yevgeni Dimitriyev (Russia)
Arunas Lipnickas (Lithuania)
Kunihiko Nabeshima (Japan)
Ozgur E. Mustecaplioglu (Turkey)
Belle R. Upadhyaya (USA)
Mourad Houabes (Algerie)
Mehmet Korurek (Turkey)
Onur Toker (Turkey)
Sead Berberovic (Croatia)
Muhammad Hadi (Australia)
Milena Lazarova (Bulgaria)
Hakan Temeltaş (Turkey)
Tulay Adali (USA)
Ibrahim Akduman (Turkey)
Marija Eidukeviciute (Lithuania)
Seta Bogosyan (USA)
Gursel Alici (Australia)
Ali Karci (Turkey)
Brijender Kahanwal (India)
Audrius Senulis (Lithuania)
Rumen Popov (Bulgaria)
Marcel Istrate (Romania)
Veselina Nedeva (Bulgaria)
Lambros Ekonomou (Greece)

Aim & Scope

The journal publishes original papers in the extensive field of Electrical-Electronics and Computer engineering. It accepts contributions which are fundamental for the development of electrical engineering, computer engineering and its applications, including overlaps to physics. Manuscripts on both theoretical and experimental work are welcome. Review articles and letters to the editors are also included.

Application areas include (but are not limited to): Electrical & Electronics Engineering, Computer Engineering, Software Engineering, Biomedical Engineering, Electrical Power Engineering, Control Engineering, Signal and Image Processing, Communications & Networking, Sensors, Actuators, Remote Sensing, Consumer Electronics, Fiber-Optics, Radar and Sonar Systems, Artificial Intelligence and its applications, Expert Systems, Medical Imaging, Biomedical Analysis and its applications, Computer Vision, Pattern Recognition, Robotics, Industrial Automation.

BAJECE

Balkan Journal of Electrical & Computer Engineering

An International Peer Reviewed Refereed indexed and Open Access Journal

© BAJECE

ISSN: 2147- 284X
Vol: 2
No : 3
Year: September 2014

CONTENTS

BALKAN JOURNAL OF ELECTRICAL & COMPUTER ENGINEERING
(An International Peer Reviewed, Refereed, indexed and Open Access Journal**)**

Contact
https://www.bajece.com **e-mail:** editor@bajece.com

The Microwave Energy Harvesting by Absorbent Structures Based on Composite Materials

J. Dikun, V. Jankunas, E. Guseinoviene, A. Senulis, T.C. Akinci

***Abstract*— This study presents two types of Salesbary Screen models which can be used for the microwave EMR harvesting in the occupational areas for the prevention case of the EMF impact for human health. The proposal structures operate on the 6-18GHz frequency electromagnetic radiation and allow collecting heating energy of the defined range. There are two types of fillers of 3% MWCNTs and 3% CNFs where considered in meaning of well electromagnetic radiation absorbency properties. The special attention had been paid for the outer, spacer and back layers thickness evaluation. The specific power as well as the total power in the proposal structures were calculated.**

Index Terms— **Radar absorbent materials; Electromagnetic radiation; Energy harvesting.**

I. INTRODUCTION

ELECTROMAGNETIC fields (EMF) are presented everywhere in our environment but they are invisible and insensitive to the human. Electromagnetic radiation (EMR) depending on wave's length or frequency is divided by several ranges [1]. Nowadays the exposure of EMR for the human health is well studied [2], [3]. The EMR effect level for human body and tissues strongly depends on electromagnetic waves (EMW) frequency or, in other words, on the wave length as well as on the time duration in the EMF. However, the most harmful effects are applied by the high frequency electromagnetic waves (HFEMW). HFEMW are radiated by various kinds of higher frequency radio waves using to transmit the information weather via TV antennas, radio stations or mobile phone base stations can dramatically affect for the human health [3], [4], [5] and [6]. The time limitation under HFEMW is defined by World Health Organization and it must not exceed 6 min [7]. People can be radiated for short time by HFEMW in open or general areas..

J. DIKUN, is with Department of Electrical Engineering University of Klaipeda, Klaipėda, Lithuania, (e-mail: jeldik@bk.ru).

V. JANKUNAS, is with Department of Electrical Engineering University of Klaipeda, Klaipėda, Lithuania, (e-mail: valdas.jankunas@hotmail.com).

E. GUSEINOVIENE, is with Department of Electrical Engineering University of Klaipeda, Klaipėda, Lithuania, (e-mail: eleonora.guseinoviene@ku.lt).

A. SENULIS, is with Department of Electrical Engineering University of Klaipeda, Klaipėda, Lithuania, (e-mail: audrius.senulis@ku.lt).

T.C. AKINCI is with Department of Electrical & Electronics Engineering, Kirklareli University, Kirklareli, Turkey, (e-mail: cetinakinci@hotmail.com).

This exposure can be neglected if the sources of HFEMW are sufficiently far from the defined areas Nevertheless; there are a lot of occupational areas where the workers, operators and technical staff are under direct contact with the broadcasting and communications fields in the form of cellular telephones and towers. This contact is possible in the health care industry for medical treatment, in the food industry for the processing and cooking of food, in the wood, textile, and glass fiber industries for drying materials as well as in the automotive, electrical, rubber, and plastic products industries for fusing and sealing operations. The scientific researches indicate a relationship between exposure to microwave radiation and birth defects, such as mongolism (Down's syndrome) and central nervous system damage. The HFEMW may also cause damage to the male testis genital organs [3], [5], [6]. For the prevention of damage to human health the radar absorbing material and structures should be used. This study presents the radar absorbing structure based on the Salesbary Screen (SS) for the EMR heat energy harvesting. The proposal model of SS (Fig.1) consists of a simple structure of thin resistive graphite film, a dielectric spacer layer, and a backside metal reflector. In terms of transmission line theory, the front resistive sheet is placed a quarter wavelengths away from the metallic backside reflector in this structure.

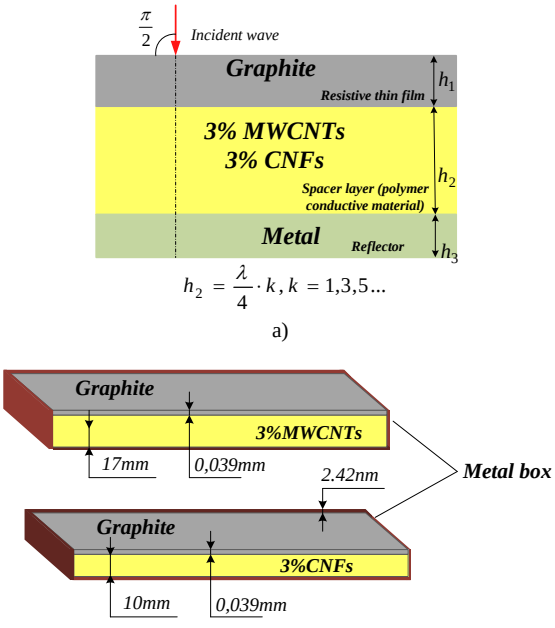

Fig.1. Proposal structure of Salesbary Screen

According to [8] the best reflection is achieved when incident angle of the wave is 900 and the distance between resistive thin film and reflector is smaller. Also the worst reflection occurs with 377 Ohms resistance sheet. Despite the fact that there are a lot of new composite fillers, to assess the absorbent capacity of SS in these study composite fillers, which electrical parameters had been well studied in a certain frequency range, were used [9]. The dielectric permittivity, magnetic permeability, electrical conductivity and optical refractive index of most sample as well as composites fillers are defined as a function of frequency. And, they are complex valued quantities, which can be established only empirically by measurements [10]. For this reason of the proposal absorbing structure, mathematical modelling of the composite materials based on different weight (wt) percentage of carbon nanopowders with respect to the epoxy resin have been analyzed. Particularly, wt of 3% for MWCNTs (Multiwall Carbon Nanotubes) based composite materials and wt of 3% for CNFs (Carbon Nanofibers) based composite materials. For two composite fillers as well as graphite, real and imaginary parts of dielectric permittivity variation on 6-18GHz frequency range are shown in Table 1.

TABLE I
REAL AND IMAGINARY COMPONENT OF PERMITTIVITY OF NANOSTRUCTURED COMPOSITE MATERIALS AND GRAPHITE UNDER THE 6 - 18 GHz FREQUENCY BAND [9],[10]

Type of fillers	Frequency, GHz													
	6		8		10		12		14		16		18	
	ε_r'	ε_r''	ε_r'	ε_r''	ε_r'	ε_r''	ε_r'	ε_r''	ε_r'	ε_r''	ε_r'	ε_r''	ε_r'	ε_r''
3 % MWCNTs	18.1	14.5	17.8	14.1	17.4	13.8	17.2	13.6	17	13.4	16.8	13.3	16.6	13.1
3 % CNFs	14.7	5.2	13.6	5.3	12.9	5.4	12.3	5.5	11.8	5.55	11.4	5.6	11	5.7
graphite	13.5	8.1	12.2	7.8	11.1	7.0	10.7	6.6	10.1	6.4	9.8	6.2	9.5	6.0

II. MATHEMATICAL BACKGROUND

With the reason of collecting the more energy in the proposal structure, the precise calculation of layers heights is necessary. The EMW propagation through the different materials is based on optics laws [14], [15]. The task of the energy harvesting by SS means that the incident EMW has freely propagate through the first and second layers and has not transmitted through the third layer. In this case the reflected wave from the back layer returns to the medium and outer layers and goes out beyond the structure. The resonance should be achieved in the spacer layer for the energy collecting.

2.1 The model layers thickness calculation

In this chapter, the outer, spacer and back layers thicknesses had been obtained.

2.1.1 Resistive sheet thickness

For the wave that freely passed through the graphite layer, it is required that its resistivity would be equal to the air resistivity, namely 377 Ω. Outer layer' impedance can be calculated:

$$\frac{Z_m}{Z_{air}} = \sqrt{\frac{\mu_r^*}{\varepsilon_r^*}} \tag{1}$$

Where: Z_m – is medium impedance, [Ω];
Z_{air} – is the air impedance, [Ω]; $Z_{air} = 377\Omega$;
μ_r^* and ε_r^* – are the complex permeability and permittivity respectively.

Taking in account graphite diamagnetic properties it is assumed that its permeability is equal to 1. Therefore the Eq. (1) can be presented as:

$$Z_m = \frac{377}{\sqrt{\varepsilon_r^*}} \tag{2}$$

The complex permittivity is calculated:

$$\varepsilon_r^* = \frac{\varepsilon' - i \cdot \varepsilon''}{\varepsilon_0} \tag{3}$$

Here: ε_r^* – is the relative permittivity of the medium directly contacted with air;
ε' – is the real part of complex permittivity;
ε'' – is the imaginary part of complex permittivity;
ε_0 – is dielectric constant.

As a graphite layer thickness the depth h_1 should be calculated according to the skin depth for non-metals at high frequencies formula [12]:

$$h_1 = d(f) = \frac{c \cdot \sqrt{\varepsilon_r}}{f \cdot \varepsilon_r''} \tag{4}$$

Where: c – is light speed in vacuum, [m/s];
f – is frequency, [Hz];
$d(f)$ – is skin depth as function of frequency, [m].

2.1.2 Spacer layers thickness

In respect that proposal structure should absorb all 6-18GHz frequencies range EMW, it is needed to evaluate the skin depth for the MWCNTs and CNFs composites under defined frequency range, and as the spacer layer height the maximum penetration depth must be considered as:

$$h_2 = d(f)_{max} \tag{5}$$

The relative permeability of the composites is also equal to 1, therefore, for the spacer layer, thickness evaluation the equation (4) can be used. For the resonance which is the key to successful absorption it is necessary that the number of wave length quarter must be equal to odd number in the spacer layer. The number of wave length quarter is calculated as:

$$\tau = \frac{d(f)_{max}}{\frac{\lambda_i}{4}} \tag{6}$$

Here: τ – is the quarter number of wave length;

i – is the certain frequency wave length index.

Wave length in the composites medium is calculated as:

$$\lambda = \frac{c}{f\sqrt{\varepsilon_r}}. \quad (7)$$

Complex permittivity is calculated by following equation:

$$\varepsilon_r = \sqrt{(\varepsilon_r')^2 + (\varepsilon_r'')^2}. \quad (8)$$

Where: ε_r' and ε_r'' – are the real and imaginary parts of relative permittivity accordingly.

2.1.3 Back layer thickness

EMW cannot penetrate from the metal surface with thickness which is larger than the skin depth. For this reason the thickness of back layer is calculated as:

$$h_3 > d_{Me}(f) = \sqrt{\frac{1}{\pi f \mu \sigma}}, \quad (9)$$

Here: σ – is the electric conductivity, [S/m].

2.2 Absorbance factor calculation

Taking in account that for polymer conductive material, the permeability is equal to 1, the equations of absorbency factors are:

$$\alpha = 1 - \left| \frac{\sqrt{\varepsilon}\cdot\left(1 + j\cdot ctg(k\,h_2)\right) - \frac{1}{\rho_{rs}}}{\sqrt{\varepsilon}\cdot\left(1 - j\cdot ctg(k\,h_2)\right) + \frac{1}{\rho_{rs}}} \right|^2 \quad (10)$$

Where: k – is wave number, [m^{-1}];

h_2 – is the thickness of dielectric layer (polymer conductive material), [m];

ρ_s – is the resistivity of outer layer, [Ωm].

Wave number is calculated as:

$$k = 2\pi f\sqrt{\varepsilon\mu_0\varepsilon_0} = 2.1\cdot 10^{-8} f\sqrt{\varepsilon}. \quad (11)$$

The resistivity of dielectrics namely of outer layer can be represented by conductivity which is the frequency function:

$$\sigma = 2\pi f\,\varepsilon_0\varepsilon_r'' \approx 55{,}63\cdot 10^{-12} f\,\varepsilon_r'' \quad (12)$$

Here: σ – is the electric conductivity [S/m].

Therefore formula (10) can be rewriten as:

$$\alpha = 1 - \left| \frac{\sqrt{\varepsilon}\cdot\left(1 + j\cdot ctg(k\,h_2)\right) - \sigma_{rs}}{\sqrt{\varepsilon}\cdot\left(1 - j\cdot ctg(k\,h_2)\right) + \sigma_{rs}} \right|^2 \quad (13)$$

II.3. Power calculation

This chapter presents the specific power index as well as total power calculation results for the proposal structures.

II.3.1 Specific power factor calculation

Specific power released in the form of heat per unit volume in material is determined by the following relationship:

$$P_S = 5.55\cdot\varepsilon_r\cdot tg\varphi\cdot f\cdot E^2\cdot 10^{-11}, \quad (14)$$

Where: P_S – is specific power, [W/m^3];

E – is electric field strength inside of medium; [V/m],

$tg\varphi$ –is the loss tangent.

Loss tangent is defined as the ratio:

$$tg\varphi = \frac{\varepsilon_r''}{\varepsilon_r'}. \quad (15)$$

Intrinsic electric field in interested layer could be obtained by using the following formula:

$$E = \frac{E_0}{\varepsilon_{r_{gr}}\cdot\varepsilon_{r_{sl}}}, \quad (16)$$

Here: E_0 – is external electrical field strength, [V/m];

$\varepsilon_{r_{gr}}$ – is relative permittivity of graphite;

$\varepsilon_{r_{sl}}$ – is relative permittivity of the spacer layer's material.

2.3.2 The structure total power calculation

Total power can be calculated as:

$$P = P_S\cdot V = P_S\cdot h\cdot l\cdot w, \quad (17)$$

Where: h, l, w - structure's height, length and width respectively, [m].

III. CALCULATIONS RESULTS

Here the layers thicknesses and power calculation results are presented.

III.1 Layers' thicknesses

The layers thicknesses had been given as shown in Table 2. Calculation results are presented in the Tables 2 and 3:

TABLE II
GRAPHITE LAYER PROPERTIES CALCULATION RESULTS

f ,[GHz]	ε_r	$d(f)$,[m]	Z, [Ω]	σ, [S/m]
6	15.66	0.024	286	2.70
8	14.48	0.018	297	3.47
10	13.21	0.016	311	3.89
12	12.57	0.013	319	4.41
14	12.04	0.012	326	4.98
16	11.60	0.010	332	5.52
18	11.32	**0.009**	336	6.01

As it is shown in Table 2, the impedance of 336 Ω under the frequency of 18 GHz is very close to the air impedance. Therefore the outer layer thickness should be defined as equal to 9 mm. However it is necessary to evaluate the absorbency factor for this layer under the applied frequency range of 6-18GHz. Calculation had been done using Equations (9) - (12). These results are presented in the Table 3.

TABLE III
ABSORPTANCE AND TRANSMİTTANCE FACTORS FOR OUTER LAYER

h_1=d(f) ,[m]	f , [GHz]							Average value of absorptance	Average value of transmittance
	6	8	10	12	14	16	18		
0.024	0.54	0.29	0.50	0.52	0.63	0.76	0.82	0.58	0.42
0.018	0.38	0.87	0.92	0.31	0.46	0.97	0.82	0.68	0.32
0.016	0.96	0.73	0.28	0.97	0.60	0.52	0.98	0.72	0.28
0.013	0.10	0.89	0.46	0.84	0.67	0.78	0.78	0.65	0.35
0.012	0.20	0.96	0.18	0.95	0.26	0.93	0.42	**0.56**	**0.44**
0.010	0.93	0.03	0.96	0.46	0.74	0.92	0.07	0.59	0.41
0.009	0.94	0.48	0.55	0.97	0.16	0.81	0.92	0.69	0.31

The results of Table 3 indicate that the most suitable outer layer thickness is 12 mm, because for this chosen value the average absorbency factor under the applied frequency range is the lowest, namely 0.56; and as a result the transmission factor through the graphite layer is highest, namely 0.44. It means that only 44% incident EMW with different length would be penetrating to resistive sheet. For the effectively energy collection by proposal structures it is necessary to evaluate the graphite layer height such that the transmission factor would be approaching to 1. Therefore, Table 4 presents calculations of the most appropriate outer layer height. As it is seen, average value of the highest transmittance occurred if the graphite layer height is equal 0.039mm.

TABLE IV
OUTER LAYER THICKNESS EVAULATION RESULTS

Estimated height h_1, [mm]		5.000	2.500	1.250	0.625	0.313	0.156	0.078	0.039
f ,[GHz]	λ , [mm]	Transmittance factors							
6	12.63	0.3318	0.9654	0.9864	0.7319	0.9198	0.9789	0.9947	0.9987
8	9.85	0.9895	0.9900	0.9778	0.6136	0.8733	0.9657	0.9912	0.9978
10	8.25	0.3081	0.9629	0.9686	0.5149	0.8271	0.9517	0.9875	0.9969
12	7.05	0.0210	0.8503	0.9574	0.4214	0.7750	0.9347	0.9830	0.9957
14	6.18	0.0486	0.6130	0.9451	0.3417	0.7222	0.9163	0.9779	0.9944
16	5.51	0.4182	0.2270	0.9317	0.2745	0.6698	0.8965	0.9724	0.9930
18	4.95	0.9800	0.0051	0.9167	0.2162	0.6165	0.8746	0.9660	0.9913
Average value of transmittance		0.4425	0.6591	0.9548	0.4449	0.7720	0.9312	0.9818	**0.9954**

For the evaluation of absorbency of middle structures layers, the wave lengths and thickness had been calculated. For the properties of composites, calculation results for 3% MWCNTs and 3% CNFs fillers are shown in Tables 5 and 6.

TABLE V
COMPOSITES FILLERS ELECTRICAL PROPERTIES

	3 % MWCNTs				3 % CNFs			
f,[GHz]	ε_r	d(f), [m]	Z, [Ω]	σ , [S/m]	ε_r	d(f), [m]	Z, [Ω]	σ , [S/m]
6	23.19	0.017	78.28	4.84	15.60	0.038	95.45	1.74
8	22.71	0.013	79.11	6.28	14.57	0.027	98.77	2.37
10	22.21	0.010	80.00	7.68	14.00	0.021	100.76	3.03
12	21.93	0.009	80.51	9.08	13.48	0.017	102.68	3.68
14	21.65	0.007	81.03	10.44	13.06	0.014	104.33	4.35
16	21.43	0.007	81.44	11.84	12.70	0.012	105.78	4.98
18	21.15	0.006	81.98	13.12	12.39	0.010	107.11	5.71

TABLE VI
WAVE LENGTH AND SPACER LAYER THICKNESS CALCULATION RESULTS

f,[GHz]	3% MWCNTs				3% CNFs			
	d(f), [cm]	λ, [cm]	λ/4, [cm]	τ	d(f), [cm]	λ, [cm]	λ/4, [cm]	τ
6	**1.700**	1.037	0.26	7	**3.800**	1.266	0.316	12
8	1.300	0.786	0.20	9	2.700	0.982	0.245	16
10	1.000	0.637	0.16	11	2.100	0.802	0.201	**19**
12	0.900	0.534	0.13	13	1.700	0.681	0.170	22
14	0.700	0.461	0.12	15	1.400	0.594	0.148	26
16	0.700	0.405	0.10	17	1.200	0.527	0.132	**29**
18	0.600	0.362	0.09	19	1.000	0.473	0.118	32

Presented results show that odd number of quarte wave length very well matches with the depth that is defined as 1.7cm for the 3% MWCNTs filler. However for the 3% CNFs filler it is not so well. It means that the most possible absorbency factors can be achieved only at frequencies of 8 and 16 GHz. With the reason of optimizing this situation, the absorbency factor was

calculated under the frequency range of 6-18GHz for all possible thicknesses which are represented in Table 6. The calculation results are presented in Table 7.

TABLE VII
ABSORBENCY FACTOR FOR 3% CNFs FILLER LAYER

h_2=d(f), [m]	f,[GHz]							Avrg
	6	8	10	12	14	16	18	
0.038	0.01	0.76	0.97	0.61	0.46	0.98	0.24	0.58
0.027	0.99	0.24	0.03	0.39	0.54	0.02	0.76	0.42
0.021	0.01	0.76	0.97	0.61	0.46	0.98	0.24	0.57
0.017	0.88	0.97	0.77	0.00	0.78	0.96	0.64	0.71
0.014	0.7	0.45	0.97	0.36	0.80	0.9	0.15	0.62
0.012	0.27	0.98	0	0.99	0.10	0.97	0.2	0.50
0.001	0.5	0.66	0.77	0.85	0.91	0.95	0.97	**0.80**

Finally, the thicknesses of 1.7cm and 1.0 cm were chosen for 3% MWCNTs and 3% CNFs fillers of spacer layer. The absorbency factor for them is shown in Fig.1.

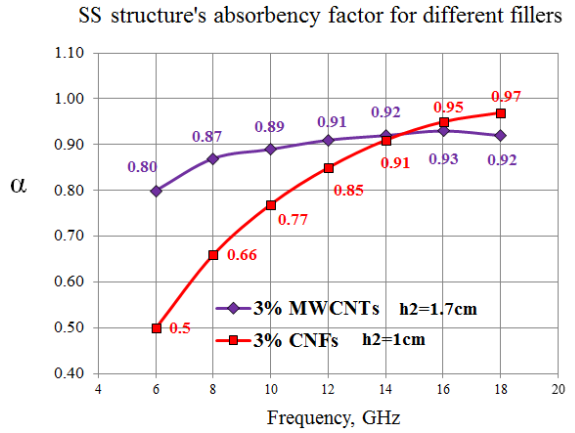

Fig.1.Spacer layers absorbency factor evaluation under 6-18GHz frequency range

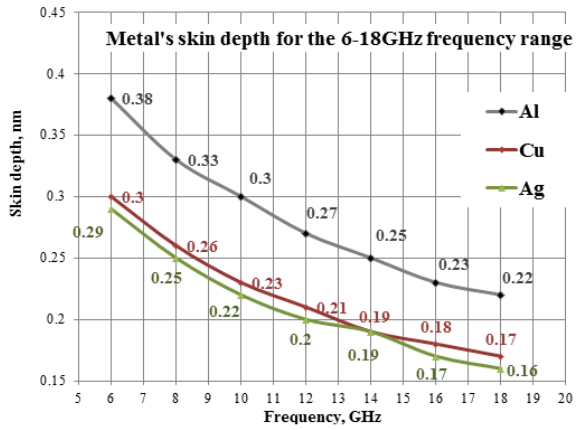

Fig.2. Back layer skin depth evaluation under 6-18GHz frequency range

In order to evaluate the thickness of back layer there are used three metals namely aliuminium, cooper and silver. For the best shelding ability it is recommended to use of 3d(f), 5d(f) and 11d(f) for the minimum, medium and exelent shielding respectively [11]. For these three metals the depth skin were calculated under the frequency range of 6-18GHz assuming the magnetic permeabilities which have the values of $\mu_r = 1$ [11]. Calculation results are shown in Fig. 2. Most lower skin depth is appeared for the cooper. The average value of cooper skin depth under applied frequency range is 0.22nm. Therefore, as it was discussed above, finally the back layer material is choosen cooper and the thikness equal to 2.42 nm.

III.2. Power evaluation

The specific power factor was calculated using Equations 14-16. The external electric field strength with extremely high frequency must not exceed the value of 5V/m in Lithuania [12]. Therefore, for the calculation of specific power factor the outside electric field value of 5V/m was considered. Graphical representation of power factors is shown in Fig. 3.

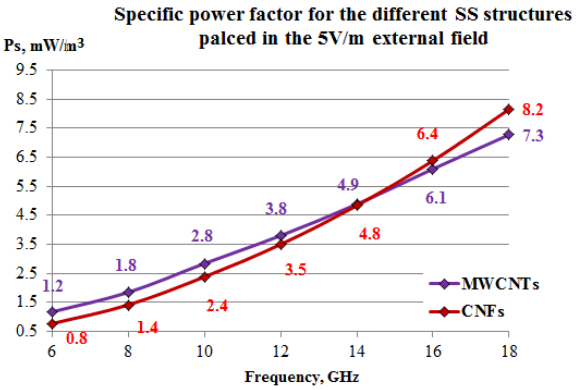

Fig.3. Specific power calculation results

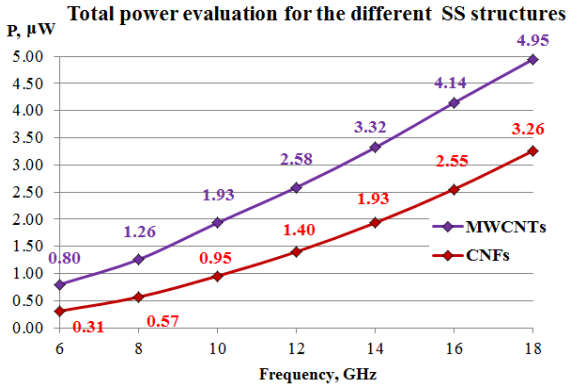

Fig.4. Total power calculation results for the SS structures: $w = l = 0{,}2m$

Equation (17) defines the total power dependency on the geometrical parameters of spacer layer. It is clear that increasing the structures width and length the total collected power increases. Nevertheless, the precise calculations were done assuming the equality of the length and width. The total collected power in certain volume of the composite material is presented by Fig. 4.

IV. DISCUSSIONS

The layers of proposal structures were used because of the data [9,10]. Also the graphite as outer layer has very good ability to collect the heating because of its high thermal coefficient that is very relevant in term of further study on the energy converter by these structures. The layers thicknesses

were obtained to achieve the resonance in the spacer layers which directly influences to the heating properties of composites. Therefore the thicknesses of the proposal structures as well as the spacer layers thicknesses are calculated so that they can operate with all frequencies within the microwave frequency range of 6-18GHz. Average absorbency factor for the 3% MWCNTs with optimal thickness 1.7cm is 0.89. For the SS with 3% CNFs and thickness size of 1cm the average absorbency factor is equal to 0.8.The total calculated harvesting power values are very small, average total power for SS with 3% MWCNTs and with 3% CNFs not exceeds the value of 2.71μW and 1.57μ W respectively. The main reason is the low value of electric field applied for the calculation. Although the legislation limits of the high frequency electromagnetic field up to 5V/m, there are a lot of investigations which find out much more electric field strength values then 5V/m. As an example, police's radar system used in speed tacking can radiate from 17V/m to 142V/m for high frequency electromagnetic waves [13]. Therefore, the electric field value of 5V/m could not be assumed as a constant or limit value.

V. CONCLUDING REMARKS

In this study, two proposal models with microwave absorbing composites as a spacer layer, graphite resistive sheet and cooper back layer of Salesbary Screen are presented. SS structures provide the best operation which will be possible for only incident electromagnetic waves. The mathematical calculation shows that it is possible to collect electromagnetic microwaves energy. As a further study these types of devices should be constructed and tested in real electromagnetic radiation condition. Also it is needed to evaluate the temperature conditions inside the structure using the thermodynamical physics and obtain the heat exchange processes on the graphite-composite, composite-cooper boundaries. Then it is possible to consider the applying of the Peltier elements for the convert the heating energy to electrical energy by proposal structures. Moreover, the use of such structures is relevant for electromagnetic (EM) protection from natural phenomena (lightning), in nuclear physics for shielding and protection from the nuclear EM pulses; in electromagnetic compatibility (EMC) for equipment-level shielding, for protection from the high-intensity radiated fields (HIRF), and for mitigation of exposure to be considered in human health.

ACKNOWLEDGMENT

The authors thank Project "Lithuanian Maritime Sector's Technologies and Environment Research Development", Subsidy contract No: VP1-3.1-ŠMM-08-K-01-019, 2012-2015 for the possibility to complete a scientific research.

REFERENCES

[1] J.G. Van Bladel, *Electromagnetic Fields*, John Wiley & Sons, 2007, p.1176.

[2] L. Hardell, C. Sage, "Biological effects from electromagnetic field exposure and public exposure standards", Biomedicine & pharmacotherapy, Vol.62, No.2, 2008, pp.104-109.

[3] P. Jacob, D. Stram, "Late health effects of radiation exposure: New statistical, epidemiological, and biological approaches", International journal of radiation biology, January 2013, pp.1-11.

[4] I. Calvente, M.F. Fernandez, J. Villalba, N. Olea, M.I. Nunez, "Exposure to electromagnetic fields (non-ionizing radiation) and its relationship with childhood leukemia: A systematic review", Science of the Total Environment; Vol.408, No.16, 2010, pp.3062-3069.

[5] W. Joseph, P. Frei, M. Roosli, G. Thuroczy, P. Gajsek, T. Trcek, J. Bolte, G. Vermeeren, E. Mohler, P. Juhasz, V. Finta, L. Martens, "Comparison of personal radio frequency electromagnetic field exposure in different urban areas across Europe", Environmental Research; Vol.110, No.7, 2010, pp.658-663.

[6] S. Heinrich, S. Thomas, C. Heumann, R. Kries, K. Radon, "The impact of exposure to radio frequency electromagnetic fields on chronic well-being in young people--a cross-sectional study based on personal dosimeter", Environment international, Vol.37, No.1, 2011, pp.26-30.

[7] Electromagnetic Fields (300 Hz to 300 GHz), Environmental Health Criteria 137, World Health Organization, Geneva, Switzerland, 1993.

[8] A.A. Hebeish, M.A. Elgamel, R.A. Abdelhady, A.A. Abdelaziz, "Factors affecting the performance of the radar absorbent textile materials of different types and structures", Progress In Electromagnetics Research B, Vol.3, pp.219-226, 2008.

[9] D. Micheli, C. Apollo, R. Pastore, R.B. Morles, G. Gradoni, M. Marchetti, Chapter of Book: Advances in Nanocomposites - Synthesis, Characterization and Industrial Applications, ISBN 978-953-307-165-7, p.966. Title of chapter: Electromagnetic characterization of Composite Materials and Microwave Absorbing Modeling; INTECH Open Access Publisher, 2011.

[10] M. Hotta, M. Hayashi, M.T. Lanagan, D.K. Agrawal, K. Nagata, Complex Permittivity of Graphite, Carbon Black and Coal Powders in the Ranges of X-band Frequencies (8.2 to 12.4 GHz) and between 1 and 10 GHz; ISIJ International, Vol.51, No.11, 2011, pp. 1766–1772.

[11] R.B. Tabrizi, "Electircal and Magnetic Properties of Metals", ASM International, 2011, p.270.

[12] Electromagnetic fields in the occupational and general environment, (2011); The 10 kHz - 300 GHz frequency bands normalized parametersvalues and measurement requirements, HN 80, No.V-199, 2011.

[13] E.D. Mantiply, R.P. Kenneth, S.W. Poppell, J.A. Murphy, "Summary of Measured Radiofrequency Electric and Magnetic Fields (10 kHz to 30 GHz) in the General and Work Environment", Bio electromagnetics 18, 2007, pp.563–577.

[14] J.A. Stratton, *Electromagnetic Theory*. *Hoboken*, NJ: Wiley-IEEE Press, 2007.

[15] P. Saville, *Review of Radar Absorbing Materials*, Defence R&D Canada – Atlantic, 2005.

BIOGRAPHIES

JELENA DIKUN was born in Klaipeda, Lithuania. She received the B.Sc., and M.Sc., degrees from Klaipeda University, in Electrical Engineering Department, in 2011 and 2013 respectively. Currently, she is a Ph.D. student at Prof. K. Barsausko Ultrasound Research Institute of Kaunas Technology University. Her research interests are in Electromagnetic Wave Theory, Energy Harvesting, Signal Processing Technique, and Ultrasound Non-Distractive Testing.

VALDAS JANKUNAS was born Lithuania, Klaipėda city, in 1976. In 2000-2003, he studied at Klaipėda University and completed the Vehicles bachelor's degree in engineering. In 2003-2005, he studied at Klaipėda University and acquired the electrical engineering master's degree. He received Ph.D. degree in Electrical and Electronics Engineering from Kaunas Technology University, in 2013. His current research interests include Energy Harvesting and Power Electronics.

ELEONORA GUSEINOVIENE was born in Russia, has studied at Kaunas Polytechnic Institute and received qualification of electrical engineer, specialization "Electrical Drives and Automatics of Industrial Equipment" (cum laude). The PhD degree in Electrical and Electronics engineering she received in Kaunas Technology University in 2002. Currently, she is Professor, Head of Electrical Engineering Department and Senior Researcher at Klaipeda University. Research area: Special Electrical Machines, Electromagnetic Wave Theory, and Renewable Energy.

AUDRIUS SENULIS was born in Klaipeda, Lithuania, in 1979. He received the B.Sc. and M.Sc. degrees in Electrical engineering in Electrical Engineering Department of Klaipeda University in 2002 and 2004 respectively. The PhD degree he received in Electrical and Electronics engineering in Kaunas Technology University in 2013. Currently, he is a Assoc. Prof. in Electrical Engineering Department and Researcher at Klaipeda University. Also the engineer-constructor at JSC "Vejo projektai" in Lithuania. His research interests are: Special Oscillating Electrical Drives and Machines, Electromagnetic Wave Theory, Electrical Vehicles.

TAHIR CETIN AKINCI was born in Pınarbası, Turkey. He graduated from Electrical Engineering department at Klaipeda University. He received M.Sc. and Ph.D. degrees from Marmara University of Istanbul, Turkey, in 2002 and 2009 respectively. He received Assoc. Prof. degree in Electrical and Electronics Engineering from High Education Council of Turkey in 2014. His research interests are signal processing, electrical power systems, non-linear dynamical systems, soft computing and condition monitoring techniques.

Smart Grid Implementation in Electricity Distribution of Elektroprivreda B&H – Dequirements and Objectives

E. Bećirović, M. Musić, N. Hasanspahić, S. Avdaković

***Abstract*—In terms of power sector restructuring and electricity market opening there have been significant changes in the functioning of activities at the level of Public Enterprise Elektroprivreda BiH d.d - Sarajevo (EPBiH). Distribution activity in an open electricity market is not a market activity, but the regulated activity, and although does not participate directly in the electricity market, its action must allow unhindered development and functioning of the market in which suppliers competes. The introduction of the smart grid concept in electricity distribution activity is a particularly challenging area of research due to the actuality and importance. The paper presents the elements of the business framework of EPBiH in terms of application of modern technologies in the area of smart grid and the changes that inevitably occur during transition process of energy sector in general.**

Index Terms— **smart grid, regulatory framework, electricity market, distribution activity**

I. INTRODUCTION

IN terms of restructuring the power sector, in general, there is no unique model for the transition from vertical integrated company that performs all activities (generation, transmission, distribution and supply) to separate business activities and open market. In early 90-ies of the last century, countries in transition started with the implementation of comprehensive economic, institutional and political reform, and energy reform are only part of much broader structural adjustment transition countries standards of market economies. The dynamics of power sector restructuring in the SEE countries is significantly affected by the socio-economic circumstances: the transition from the socialist system with a "planned economy" of the democratic system and an economy based on market principles, followed by a lack of domestic and foreign investments entering the country in the region. The main objectives of the restructuring in this area are: improve efficiency (technical and financial) of power system, and reduce the burden of public finance through the elimination of subsidies for the production and transmission of electricity and the privatization of companies in the sector. Along with the requirements for the power sector restructuring, distribution activity needs to meet the requirements and implementation of modern technologies and other technical challenges.

E. Bećirović is with the Department for Development, EPC Elektroprivreda BiH d.d. Sarajevo, 71000 Sarajevo, Bosnia and Herzegovina (e-mail: e.becirovic@elektroprivreda.ba).

M. Musić, is with the Department for Development, EPC Elektroprivreda BiH d.d. Sarajevo, 71000 Sarajevo, Bosnia and Herzegovina (e-mail: m.music@elektroprivreda.ba).

N. Hasanspahić is with the Department for Development, EPC Elektroprivreda BiH d.d. Sarajevo, 71000 Sarajevo, Bosnia and Herzegovina (e-mail: n.hasanspahic@elektroprivreda.ba).

S. Avdaković is with the Department for Development, EPC Elektroprivreda BiH d.d. Sarajevo, 71000 Sarajevo, Bosnia and Herzegovina (e-mail: s.avdakovic@elektroprivreda.ba).

II. ELECTRICITY DISTRIBUTION ACTIVITY IN MARKET ENVIRONMENT

A. Unbundling of electricity business activities

Unbundling of system activities (transmission and distribution) and market activities (generation and supply) is essential for the transparency business of electric power companies according to the EU Directives governing the internal electricity markets [1]. Unbundling implies financial, legal and functional unbundling of traditional vertically organized companies and creation of different stakeholders in electricity markets [2]. After the financial and functional unbundling, the ultimate objective is the legal unbundling of activities within the utilities. Within distribution activity, as it is observed from the current position, the objectives of liberalization are the fact that the supply activity is set aside as a separate market activity, and that the distribution system operator obtains the status of the regulated entity. Overview of interactions among electricity market stakeholders are given on Figure 1.

B. Unbundling of electricity business activities

Having signed the Electricity Policy Statement in 2000, having adopted the entity Laws on electricity, Law on transmission, regulator and system operator of electricity in B&H in 2002, Law on establishment of the company for transmission for electricity in B&H and Law on establishment of Independent System Operator (ISO) for the transmission system of B&H in 2004, the reform of the electric power sector in B&H was initiated. This process has been additionally reinforced by signing of the Treaty on establishment of the Energy Community in the region of the

SEE in 2005. The State Regulatory Commission for electricity (SERC) made Decision on the volume, terms and conditions and timetable of the market opening in B&H (June 2006. and 2009.) based on the Law on transmission, regulator and system operator of electricity in B&H [6].

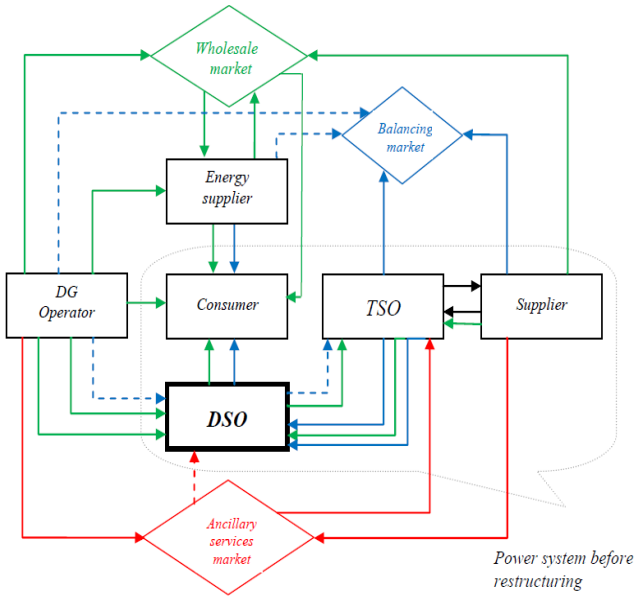

Fig. 1. Interactions among electricity market stakeholder [3], [4], [5]

III. SMART GRID CONCEPT

According to the above noted legislation, today Public Enterprise Elektroprivreda BiH (EPBiH) is conducting licensed activities of generation, production, distribution and supply of electricity, trading, representation and mediation in the domestic electricity market, as well as other activities determined by the applicable documents. Current market activity in B&H is virtually non-existent even the legislation at the level of the power sector is judged as adequate by more competent independent subjects. This refers mainly to the definition of the relationship between distribution and supply activities. In accordance with the practice of some countries, some problems between the distribution system operators and suppliers are expected i.e. the exchange of data, the communications, the vague responsibilities for individual business processes, as well as the appearance of redundant processes. So, well-known processes, reliable IT support and relatively clear responsibility and accountability for their implementation are becoming the new "generator of business risk." The division of responsibilities between business processes and the functional unbundling of activities in accordance with applicable laws and regulations are some of the next targets in EPBiH. By the Law Establishing the Company for the Transmission of Electric Power in B&H (2004.) one joint company for transmission power system (Elektroprijenos/Elektroprenos BiH) is formed officially in 2006. The entity regulatory commissions have made decision on adoption of the Rule book on eligible customer in which the phase dynamics of electricity market opening and eligible customer status are treated [6].

IV. CURRENT STATUS OF IMPLEMENATION OF SMART GRID CONCEPT

A. Advance metering system

One of the business objectives of EPBiH, as determined and defined in appropriate organizational documents, is the implementation of advance metering system as an essential prerequisite for the continued implementation of the smart grid concept. Active engagement in the development of infrastructure for advance metering system (AMR/AMM system) began in late 2009 in EPBiH. The previous implementation of AMR/AMM system implied a multi-phase process, in accordance with business strategy and company organization.

A brief overview of current status of AMR/AMM system implemented in distribution network of EPBiH is given in Table 1.

TABLE I
OVERVIEW OF AMR/AMM SYSTEM IMPLEMENTATION IN DISTRIBUTION NETWORK OF EPBIH

Distribution branch office	Number of installed electronic meters	Number of meters in AMR/AMM system
ED Bihać	5.757	3.427
ED Mostar	3.028	2.281
ED Sarajevo	12.057	7.213
ED Tuzla	9.597	3.099
ED Zenica	12.152	4.217
Total EPBiH	42.591	20.237

Ongoing activity in EPBiH is implementation of Meter Data Management system (MDM) which is a module of total IT system of EPBiH, which will be designed to collect, store, analyze and interpret data from AMR/AMM smart meters independently of type of activity (generation or distribution) [9] .

B. Countermeasures for reduction of losses

Due to the current lack of proper infrastructure of metering in TS 10(20)/0,4 kV, it is not possible to define the adequate allocation of electricity losses on voltage levels. According to available metering data and by using certain approximations and expert experience this allocation is estimated for certain purposes. Also, in accordance with obligations defined in „General Conditions for Electricity Supply“ [10], EPBiH is constantly warning the customers about the need for conduction of reactive power compensation corresponding to average power factor (cos ϕ= 0.95). With adoption of new technical guidelines for substations TS 10(20)/0.4 kV with anticipated installation of reactive power compensation devices, EPBiH started with systematic (planned) reactive power compensation in own electricity distribution network

C. Distributed generation requirements

Total share of distributed generation, mainly small hydro power plants, is continually increasing in distribution network. Since this process takes place in parallel with the process of adjusting the distribution system operator, as well as other participants in the electricity sector to work in a market

environment, it is necessary to take into account the requirements for normal distribution network operation. Distribution system operator analyses the impact of distributed generation to the grid, which can be positive and negative in general. Certain incentives for distributed generation through appropriate legal and regulatory requirements, and the obligation to allow equitable access on distribution network create the business environment in which the distribution activity is faced with the opposite requirements when the results of performed energy analysis show a negative impact of DG on distribution network operation. An example of such situation is the case with an increased level of losses in distribution networks with connected distributed generators (the influence of small hydro power plants in Uskoplje and Fojnica electricity distribution network areas), due to dislocation of DG and „centre of consumption“ in distribution network. Also, it is important to emphasize recent significant increase in interest in the construction and connection of photovoltaic power plants [9].

TABLE II
OVERVIEW OF DG STATUS IN EPBIH – NUMBER OF ISSUED OR REQUESTED PERMISSIONS FOR DG CONNECTION (JANUARY 2013.)

Type of DG	Number of connected DGs	Permitted installed power of connected DG [MW]	Number of requests for DG connection (in process)	Planned installed power of DG as requested[MW]
Small hydro power plant	38	42,00	4	4,6
Photovoltaic power plant	2	0,123	34	9,8

D. *Increase of reliability of electricity supply indices*

In accordance to business plans of EPBiH, modern SCADA/DMS control centres are planned to be implemented. With other power utilities EPBiH participated in the creation of feasibility study for the introduction of SCADA/DMS system in power distribution system [11]. But full implementation of SCADA/DMS system has not yet begun in EPBiH, and the level of automation of the distribution network is quite low, but EPBiH is continuing investments in distribution network automation. During some previous investment programs individual projects of distribution network automation were implemented (i.e. installation of remotely operated circuit breakers and disconnectors and fault locators).

Continual monitoring and calculation of reliability of electricity supply indices (SAIFI: The number of supply interruptions per customer and SAIDI: duration of supply interruptions in minutes per customer) is a process that enables the benchmarking and gives a more detailed insight in distribution network performance of EPBiH). In Figure 2, an increasing trend in reliability of electricity supply is visible. Significant differences in the values of the reliability indices can be noticed in ED Sarajevo due to the network structure and current level of distribution network automation.

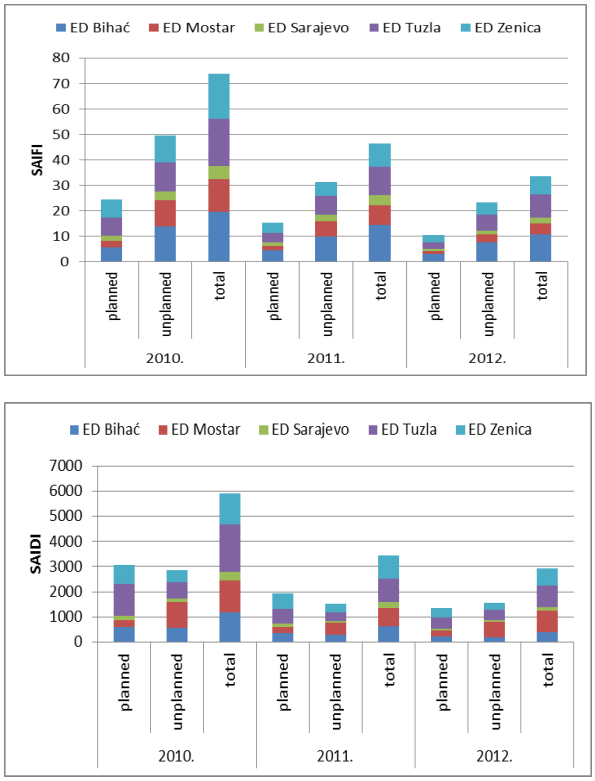

Fig. 2. Reliability of electricity supply indices SAIFI and SAIDI 2010. – 2012.

E. *Electricity demand management and active participation of consumers*

Currently, power utilities in B&H do not have a detailed insight into the structure of electricity consumption, due to the lack of proper infrastructure of metering. The result of this situation is an estimation of load profiles, and also the estimation of total cost of the system during determination process of electricity tariffs accordingly. There is an ongoing project for load profile analysis that is performed in cooperation with the USAID-REAP, regulatory agencies and other power utilities in B&H [9]. According to project documentation, defined goals (direct or indirect) of this project are:

- Determination of adequate consumption groups
- Definition of characteristic consumption profiles for selected categories
- Scheduling of costs in accordance with consumption profiles
- Determination of the maximum consumption and simultaneity
- Effective electricity demand management
- Application to other areas.

F. *Other activities and current business framework requirements*

During the last few years at EPBiH some research were performed with the aim of further education and training of employees with specific requirements for the implementation of smart grid. Some activities were initiated in the selection of pilot projects in order to establish certain functionalities of

smart networks. Among other things, a pilot project for the installation of the first electric vehicle charging station in Bosnia and Herzegovina is started. Also, three pilot projects for testing of equipment and systems for power quality monitoring are realized, in order to prepare for the implementation of this system as a preparation for response to the demands of electricity supply in accordance with EN 50160 from 2015, since this is requested in [10]. Full deployment of smart grid requires full support of legislative and regulatory bodies, as well as the participation of all other electricity sector stakeholders: distribution system operators, regulatory agencies, final customers of electricity, and distributed generation connected to distribution network

V. CONCLUSION

In terms of power sector restructuring, the distribution activity or distribution system operator functionality becomes more complex and demanding. In such new conditions, electricity distribution business must be fully customized to modern statutory provisions and regulations that are subject to frequent changes. Additionally, the distribution activity must respond to the technical challenges associated with the integration of DG and electric vehicles, the establishment of the system for collecting, processing, storing, and sharing information with all participants in the market to allow the normal functioning of electricity markets etc. Smart grid concept is the future challenge that will require further implementation of modern information technology in the area of distribution network operation, and also further linking of IT and business process-level activities.

In accordance with its strategic business orientation, EPBiH will follow the further development trend and apply basic technical elements of the smart grid concept, in order to fully comply with the requirements of modern electricity distribution activity.

VI. ACKNOWLEDGMENT

The study is selected from International Symposium on Sustainable Development, ISSD 2013.

REFERENCES

[1] L. Oksanen L. "Distribution system operator as an enabler of the electricity market - Connecting small-scale production and demand response", MSc thesis, Tampere University of Techonology, Finland, 2011.

[2] M. Vuksanić T. Marijanić "Implementation of smart grids concept in Croatian power distribution system regarding European practice", HRO CIRED, 3.(9.) Session (in Croatian), 2012.

[3] ERGEG, Regulation for Smart Grids, 2011.

[4] M. J. N van Werven., M. J. J. Scheepers "The changing role of distribution system operators in liberalised and decentralising electricity markets, DISPOWER report, ECN-C--05-058., 2011.

[5] M. Bošković, T. Cerovečki, Z. Lipošćak Z. "Adaptation of distribution system operator to operation under open electricity market conditions, HRO CIRED, 2.(8.) Session (in Croatian)", 2010.

[6] Last Accessed on 22.02.2013. About power sector in B&H - www.derk.ba; www.nosbih.ba; www.ferk.ba; www.reers.ba

[7] European Commission, "Communication from the Commission to the European Parliament, the council, the european economic and social committee and the committee of the regions, „Smart Grids: from innovation to deployment, COM 202 final, Brussels, 2011.

[8] T. Jakaša, Dž. Drobić, "Advanced power systems - an overview of European projects", 20. International Symposium EIS 2011, Šibenik, Croatia, 2011.

[9] Internal documentation of Elektroprivreda BiH Sarajevo

[10] FERK, General Conditions for Electricity Supply, 2008.

[11] KfW Study report, "SCADA/DMS and Related Telecommunication Facilities, Distribution Level", 2008.

BIOGRAPHIES

Elvisa Bećirović received B.Eng. and M.Sc. degree in electrical engineering from the Faculty of Electrical Engineering, University of Sarajevo and University of Tuzla, respectively. Currently she is a Ph.D. candidate at the Faculty of Electrical Engineering, University of Zagreb. She works at the Department for Strategic Development in EPC Elektroprivreda B&H.

Mustafa Musić received Ph.D. degree in electrical engineering from the Faculty of Electrical Engineering, University of Sarajevo in 2005. He is a Head of Department for Strategic Development in EPC Elektroprivreda B&H, and also an assistant professor in Faculty of Electrical Engineering, University of Sarajevo.

Nedžad Hasanspahić has B.Sc. degree in electrical engineering from the Faculty of Electrical Engineering, University of Sarajevo. He is a M.Sc. student with work in the field of smart grid implementation in electricity distribution.

Samir Avdaković received Ph.D. degree in electrical engineering from the Faculty of Electrical Engineering, University of Tuzla in 2012. He works at the Department for Strategic Development in EPC Elektroprivreda B&H. His research interests are: power system analysis, power system dynamics and stability, WAMPCS and signal processing.

Six-Phase VSI Control Using 8-Bit MCU

A. Pitrėnas, A. Petrovas

***Abstract*—In this paper a generation of six-phase voltage using six leg synchronous Voltage Source Inverter and a low cost 8-bit Micro-Controlling Unit is investigated. A simple and cost effective Sinusoidal Pulse Width Modulation for controlling six-leg VSI is presented. A simulation on generation of six-phase voltage using SPWM method was investigated. The main advantage of presented SPWM method is the simplicity and low resource requirement for MCU.**

***Index Terms*— Scalar control, Six-phase VSI, SPWM method.**

I. Introduction

THE interest of multi-phase drives has grown over the years. The main reasons for that are their advantages over regular drives. Multi-phase drives have less torque ripple, greater reliability, fault tolerant operation and some other advantages compared with three-phase drives. Multi-phase drives require multi-phase Voltage Source Inverters to form a multi-phase voltage for their supply. Multi-phase drives are widely used in electric cars, ships, locomotives and aircrafts. [1] Multi-phase VSI's have different count of so called legs depending on phase count, thus the control of multi-phase VSI's are different.

There are two main methods of induction motor control. First is so called scalar control (in some literature it's called V/Hz control). When scalar control is used the magnitude and frequency of motor's voltages are controlled. The implementation of this method is simple, but the torque response of this method is poorer compared to other methods.

Other control method is called vector control (or Field Oriental Control). When FOC is used it controls phase of motor's current, its amplitude and frequency. This method provides fast torque response. The Direct Torque Control is derived from FOC method. [2] - [3] Vector control is utilized using Space Vector Pulse Width Modulation technique.

The full SVPWM technique is somewhat more complex compared Sinusoidal PWM used in scalar methods and it requires more than ordinary MCU. Mainly the use of Digital Signal Processors or even Field Programmable Gate Arrays or an Application-Specific Integrated Circuits are required. [4] And this raises the complexity and price of the final project or device.

A. Pitrėnas is with the Department of Automation of Vilnius Gediminas technical university, Vilnius, 03227 Lithuania (e-mail: aurelijus.pitrenas@vgtu.lt).

A. Petrovas is with the Department of Automation of Vilnius Gediminas technical university, Vilnius, 03227 Lithuania (e-mail: andrius.petrovas@vgtu.lt).

A lot of methods regarding simplification of the complex FOC of multi-phase drives can be found. This is mainly done to lower required MCU or DSP resources. Some methods go so far that the needed MCU resources for multi-phase SVPWM control are equal to resources required for three-phase SVPWM. Hoverer the majority of these methods balance between needed resources of MCU and the purity of VSI output voltages. [5] - [6]

Summarizing both control methods have their advantages and disadvantages. FOC method controls motors currents so its operate with fast responses. This method is used when motor runs in transient operation; it's a high-performance control technique. Its disadvantage is high price and complexity of driver circuit.

On the other hand scalar control is cheap and well implementable method. It has some disadvantages when dealing with drives that operate with dynamic behaviour, since it gives low responses to transients. Its performance is low, but the technique itself is very stable. Both techniques are applicable over the nominal speed at the expense of torque. [7] This paper will focus on generation of SPWM signals for six-phase VSI control using a low cost 8-bit MCU. Later developed method could be used to develop a scalar control of six-phase induction motor.

II. Generation Of Six-Phase Voltage

To form a six-phase voltage a six-leg Voltage Source Inverters are used (Fig. 1). One leg of VSI is formed using two solid state switches (most often Insulated Gate Bipolar Transistors). These legs are connected to DC bus. DC bus voltage is supplied from AC line using full bridge rectifiers and decoupling capacitors. Load is connected between legs middle points. When VSI is controlled in synchronous mode, the switches of one VSI leg turns on and off synchronously ex. when S1 is on, S7 is turned off. When every leg of VSI is switched in right order the six-phase voltage is fed to the load.

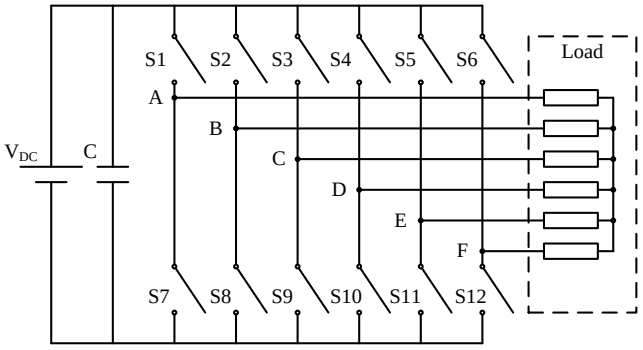

Fig. 1. Two level six-phase VSI

The use of synchronous VSI leads to lower requirements of the MCU and this brings the cost of the system down. For controlling a synchronous six-phase VSI a total of six Pulse Width Modulation outputs of MCU are required. PWM outputs must be formed in the way that they correspond to signal which varies according to sinus function. This method is called Sinusoidal PWM (SPWM) or carrier based PWM. This method is illustrated in Fig. 2.

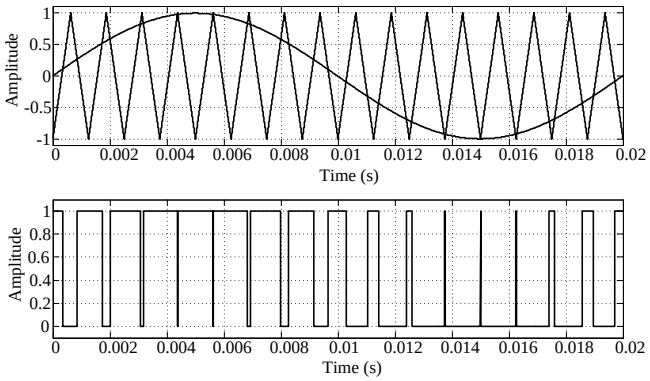

Fig. 2. Generation of carrier based SPWM signal

Carrier based PWM formation works using simple principles: A sinusoidal varied signal is compared to a higher frequency triangle signal, while amplitude of sinusoidal signal is higher than amplitude of triangle signal the output of PWM port is set to HIGH. When amplitude of sinusoidal signal is lower than amplitude of triangle signal, PWM port is set to LOW. The frequency of triangle signal is called carrier frequency. It's should be mentioned that the higher the carrier frequency the less distortions are brought to sinusoidal output. If the amplitude of final VSI output has to be changed then the amplitude of sinusoidal signal is changed while amplitude of triangle signal is kept constant. In the past this type of control algorithm was carried out using analog circuits and in our days this is accomplished using MCU's and DSP's.

III. Six-Phase SPWM Implementation With 8-Bit MCU

A six-phase voltage is shown in Fig 3. To form a six-phase voltage with VSI leads to calculation of six sinus functions by the MCU, but the low cost MCU are incapable of this task, thus the more powerful MCU or DSP should be used, or some simplifications should be carried out.

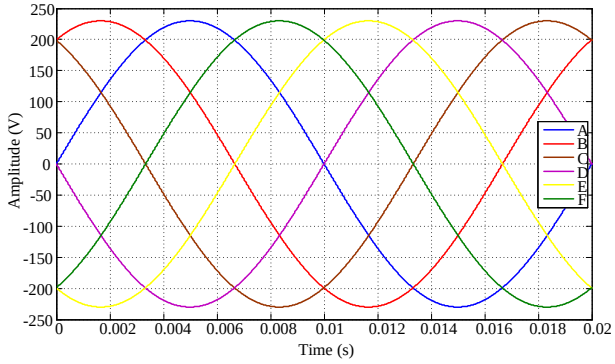

Fig. 3. Six-phase voltage

First simplification comes from that, that all six phases are the same only with 60º degree angle shift between them. This means that MCU has to generate only one SPWM signal and all other can be generated by shifting the first one. Even the low coat modern MCU's have built-in hardware PWM generators which dramatically eases the generation of VSI control signals. Basically the required pulse width of PWM signal is set by writing needed value to according PWM control register.

By using a synchronous VSI control signals of one VSI leg is formed using one PWM channel. The PWM register value has to be changed in every new angle of generating SPWM function. To calculate the needed PWM register value depending on sinus angle following equation is used:

$$R_v = \sin(\alpha) \cdot R_R, \quad (1)$$

where: R_v – register value; α – phase angle in radians; R_R – resolution of register (if register's resolution are 8-bits, then $R_R = 255$).

However the calculated value R_v will be floating number and operations with floating numbers in 8-bit MCU's take longer times and moreover the floating numbers can't be used in 8 bit register. These limitations leads to the need of rounding value R_v, that it could be used as integer type variable. One more thing should be mentioned that when angle of sinus signal goes over 180 º degree, the calculated PWM register's value will be negative and this is not acceptable.

By looking at the one phase sinus signal (Fig. 4) some more simplifications could be done. First of all we notice that sinusoidal signal is symmetrical. This means that we don't need to calculate angles between 180 º and 360 º all we have to do is to invert calculated values for angles from 0 º to 180 º. The simplification of sinus calculation is already a meaningful but this could go a little bit more. In the same manner as before we can see that sinusoidal signal is symmetrical between 0 º to 90 º degrees and 90 º to 180 º degrees. This leads to fact that MCU has to calculate sinus only for angles from 0 º to 90 º and all other needed values could be found by inverting an already calculated ones.

The calculation of all needed PWM registers values of sinus angles could be done in two different approaches. First one is to calculate all 91 values (angle is varied from 0 to 90 including 0) sinus when MCU is turned on, every time, and then store them in Random Access Memory. But this step wastes a big amount of RAM which is critical in low cost MCUs. Second approach is to calculate all needed values in Personal Computer and then store them in MCUs program memory together with the main program. This approach is a lot better because we don't utilize a lot of RAM for variable storage and the MCU don't need to calculate sinus functions at all.

For calculation of all needed values of PWM registers this *Matlab* script could be used:

```
angle_deg = (0:90);
angle_rad = anlge_deg*(pi/180);
```

```
sin_rad = sin(angle_rad);
sin_pwm = sin_rad*255;
spwm = round(sin_pwm);
```

Array *spwm* is then transferred to program memory of MCU together with the main program. The main program of MCU is mainly interrupt based. The values for all six PWM register are transferred using one function. This function is called from timer interrupt routine. Depending on register value of this timer the interrupt is called in different times and this leads to a change of generated six-phase voltage's frequency.

The amplitude is changed by dividing PWM register's value according to the generating frequency of six-phase voltage.

To take this approach one step further one more simplification can be achieved easily, which leads to lowering the needed PWM output of MCU by factor of 2. If we one more time thoroughly look at six- voltage diagram, we can see that some phases are shifted by angle of 180 º degree. This leads to the fact, that three voltages are shifted by angles of 60 º degree and other three is inversion of first ones. This means that MCU could generate only three SPWM signals with phase difference of 60 º degrees, and other phases could be obtained by inverting them. This could be carried out in a hardware level of VSI. For example VSI's first leg's upper switch control signal could be connected to fourths leg's lower switch and first leg's lower switch signal should be connected to fourths leg's upper switch. If we do that for all other legs of VSI, the total required SPWM control signal count drops to 3. This means that six-phase voltage can be generated using the really low end MCU and this is exactly what this paper focuses on. The algorithm of this SPWM generation method is shown in Fig. 4.

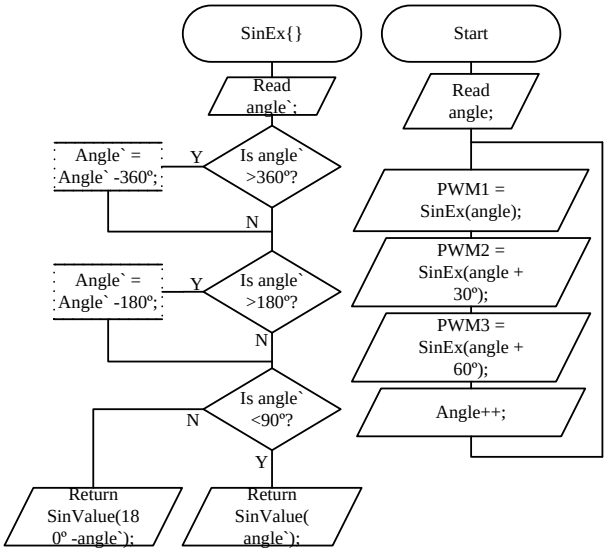

Fig. 4. Algorithm of SPWM signal generation using 3 PWM channels

IV. MODELLING

In this paper modelling of SPWM six-phase voltage formation is carried out using *Matlab Simulink* (Fig. 5). The simulation model consists of three main blocks: generation of SPWM signals, six-phase VSI and 2nd order low pass filter. SPWM signals are generated using carrier base PWM method, because PC have enough resources to calculate sinus functions quick enough and there is no need to simplify the generation of control signals as in case of MCU's. Six-phase VSI is modelled using ideal switches connected to DC bus voltage. 2nd order low pass filter is used to filter the output waveforms of VSI, this block can be found in *SimPowerSystems* toolbox. The filter's cut-off frequency is set to 200 Hz.

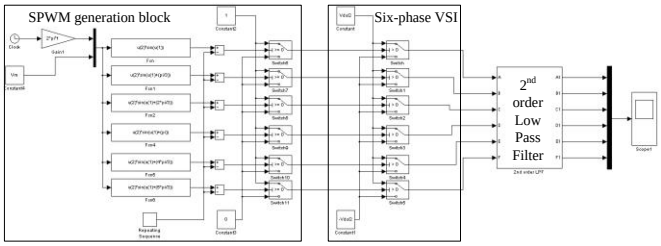

Fig. 5. *Matlab Simulink* model of idealized six-phase VSI with SPWM control

In Fig. 6 a 50 Hz, six phase line to neutral voltage is shown, when voltage of DC bus is set to 200 V and carrier frequency to 2 kHz.

The control SPWM signals for two VSI legs are shown in Fig. 7.

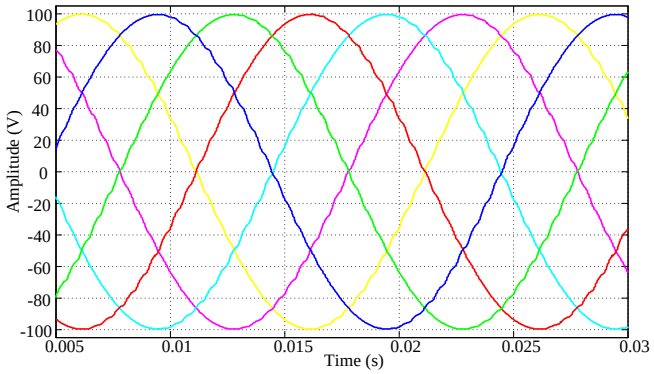

Fig. 6. Modelled six-phase voltage using SPWM method when DC bus voltage is set to 200 V.

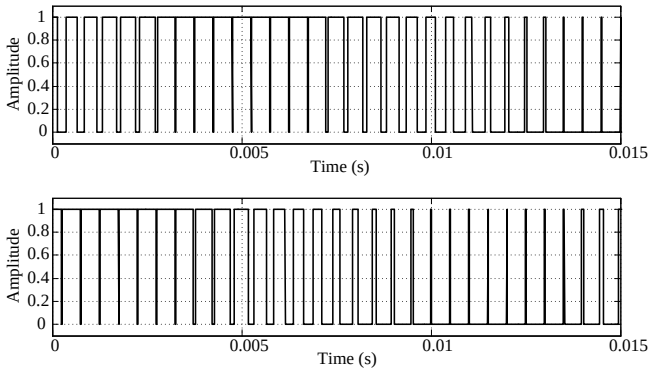

Fig. 7. Modelled SPWM signals for controlling two legs of six-phase VSI

By analysis of modelling results it is clear that simplest SPWM control method of VSI can be used to generate six-phase voltage and moreover the output voltages are almost pure sinusoidal with some switching harmonics which cannot be avoided by any control algorithm which involves any type of switching of VSI legs.

V. Experimental Results

The method of generating SPWM control signals for six-phase VSI described in section III was implemented using Atmel's 8-bit MCU Atmega328. A two SPWM control signals of six-phase VSI is shown in Fig. 8.

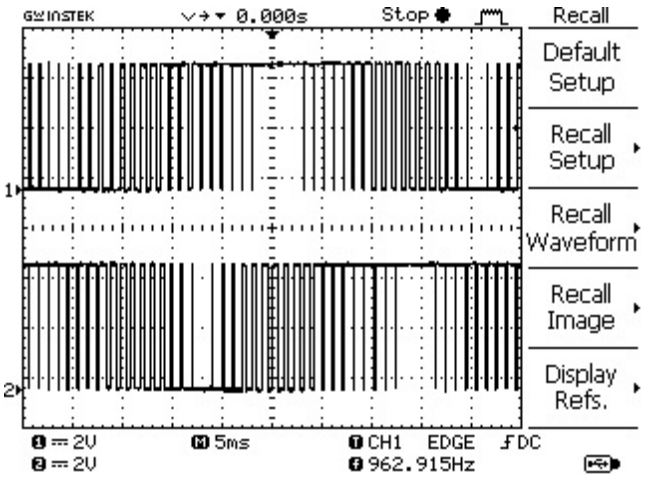

Fig. 8. Two SPWM signals generated with 8-bit MCU shifted by 60 º degrees

These SPWM signals form a near 25 Hz output voltage are different by 60 º degree angle. Using such signals with accordingly connected VSI six-phase voltage can be generated. Two nearest line-to-line voltages would look as shown in Fig. 9.

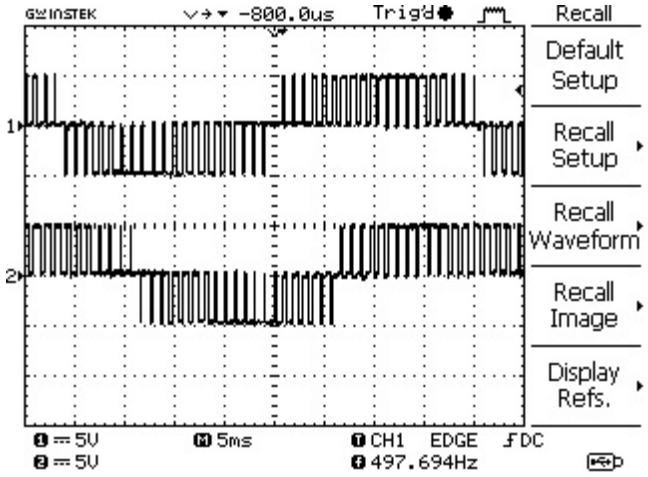

Fig. 9. Line-to-line voltages of VSI

VI. Conclusions

In this paper a simple six-phase voltage generation method using simple and cheap 8-bit MCU are discuses and presented. As observed from modelling results a simple SPWM scheme could be used to form a nearly perfect sinusoidal six-phase voltage. This is important knowing the fact that, when six-phase voltage are generated using more sophisticated methods like SVPWM, the output waveforms may become more disturber when some simplification of method is implemented. It should be noted that these simplifications are needed for lowering the needed computations of MCU. If the simplifications are not used then the output voltage is near sinusoidal, but the complexity of control algorithm rises the need of powerful MCU, DSP or even FPGA and this rises the final cost of a project or a final device it's self.

In conclusion the proposed method will be studied more deeply to investigate the potential of the use of this method for a six-phase induction motor inverter. That type of inverter could be used in areas where torque control is not critical or not necessary at all and the cost of the inverter plays some important role.

References

[1] G. Renukadevi, K. Rajambal. Modeling and Analysis of Multi-Phase Inverter Fed Induction Motor Drive with Different Phase Numbers. Transactions on Systems and Control, vol. 8, pp. 73-80, Jul. 2013.

[2] R. Dharmaprakash, J. Henry. High Performance Control Schemes of Induction Motor – A Review. International Journal of Advanced Research in Electrical, Electronics and Instrumentation Engineering, vol. 2, no. 9, pp. 4336-4347, 2013.

[3] A. Cifci, Y. Uyaroglu, S. Birbas. Direct Field Oriented Controller Applied to Observe Its Advantages over Scalar Control. Electronics and Eelectrical Engineering, vol. 119, no. 3, pp. 15-18, 2012.

[4] G. Renukadevi, K. Rajambal. FPGA Implementation of SVPWM Technique for Seven-Phase VSI. International Journal of Electronics and Electrical Engineering, vol. 1, no. 4, pp. 275-280, Dec. 2013.

[5] E. Levi, R. Bojoi, F. Profumo, H.A. Toliyat, S. Williamson. Multiphase Induction Motor Drives – A Technology Status Review. IET Electr. Power Appl., vol. 4, no. 1, pp. 489 –516, 2007.

[6] T. Lipinskis, A. Baskys, A. Rutkauskas. Six-Phase Voltage Forming Method Using the Largest Magnitude Space Vectors. Elektronika ir Elektrotechnika, vol. 19, no.10, pp. 99-102, 2013.

[7] G. Kohlrusz, D. Fodor. Comparison of Scalar and Vector Control Strategies of Induction Motors. Hungarian Journal of Industrial Chemistry, vol. 39, no. 2, pp. 265-270, 2011.

Aurelijus Pitrėnas is a Ph.D. student at the department of Automation of Vilnius Gediminas Technical University (Lithuania) and works as an assistant in Vilnius Gediminas Technical University. He graduated B.Sc. M.Sc. degrees in electrical engineering, Vilnius Gediminas technical university in 2010 and 2012 respectively. Research interests: automated control systems, embedded systems, power electronics.

Andrius Petrovas recived the B.Sc.,M.Sc and Ph.D. degrees in electrical engineering from the Vilnius Gediminas technical university (Lithuania) in 2001, 2003 and 2007 respectively.
He works as Assoc. Prof. in Automation department of Vilnius Gediminas Technical University, since 2008. The area of scientific interests: automatic control theory, control and modeling of mechatronic systems.

Ecosystem Services for a Sustainable Energy Policy in Bosnia and Herzegovina

L. A. Mesbah

***Abstract* -This paper examines the concept of ecosystem services for a sustainable energy policy, and briefly analyses of current and possible energy sources in Bosnia and Herzegovina (BiH). BiH remains an important cosumer of fossil fuel energies, using both domestic (coal) and imported (petrol and gas) resources. BiH is also using renewable energy sources such as hydropower for electricity production and biomass mainly for heating and has strong potential to further develop other renewable sources of energies. It remains essential but also challenging for the country´s strategy to further develop sustainable energy resources while maintaining functional ecosystems as an important natural capital .**

Keywords-**Ecosystem Services, Sustainable Development, Energy, Renewable Energy, Climate Change, Policy, Bosnia and Herzegovina.**

I. INTRODUCTION

EVERY ecosystem on planet earth fuctions thanks to an input of energy transferred from the sun into the planet earth system that comprises the atmosphere, the hydrosphere and the biosphere. Solar energy, or solar radiations are tranferred to the primary producers (photosynthesis) that provide food (or energy) to the chain of consumers in the ecosystem. This food chain is actually a food web and is a part of the energy transfer where matter is being recycled (the water cycle, carbon, nitrogen, phosphore, sulfur, etc..) and renewed by the decomposers and detritus feeders hailing from the a rich biodiverse ecosystem. What can we learn from ecosystems in terms of energy and its sustainable use ? What kind of resource or services can ecosystems provide us with? What are the oportunities in BIH and the Balkans for a sustainable use of Ecosystem Services ?

L. A. MESBAH is with the American University in Bosnia and Herzegovina, Fra Anđela Zvizdovića 1, 71000 Sarajevo, Bosnia and Herzegovina, (E-mail: lmesbah@aubih.edu.ba)

II. BASIC CONCEPTS

The concept of Ecosystem Services has been defined and outlined at the Millennium Ecosystem Assesment in 2005 (MEA, 2005):

"An ecosystem is a dynamic complex of plant, animal, and microorganism communities and the nonliving environment interacting as a functional unit. Humans are an integral part of ecosystems. Ecosystems vary enormously in size; a temporary pond in a tree hollow and an ocean basin can both be ecosystems. Ecosystem services are the benefits people obtain from ecosystems. These include **provisioning** services such as food and water; **regulating** services such as regulation of floods, drought, land degradation, and disease; supporting services such as soil formation and nutrient cycling; and **cultural** services such as recreational, spiritual, religious and other nonmaterial benefits."

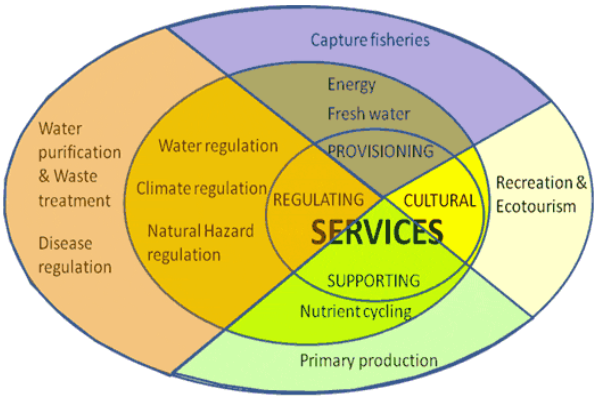

Fig. 1. Schematic description of Ecosystem Services (UNEP and MEA,2005)

Key Definitions as defined by the Ecosystem Millennium Assessment:

Ecosystem. An ecosystem is a dynamic complex of plant, animal, and microorganism communities and the nonliving environment interacting as a functional unit. Humans are an integral part of ecosystems. Ecosystems

vary enormously in size; a temporary pond in a tree hollow and an ocean basin can both be ecosystems.

Ecosystem services. Ecosystem services are the benefits people obtain from ecosystems. These include provisioning services such as food and water; regulating services such as regulation of floods, drought, land degradation, and disease; supporting services such as soil formation and nutrient cycling; and cultural services such as recreational, spiritual, religious and other nonmaterial benefits.

Well-being. Human well-being has multiple constituents, including basic material for a good life, freedom of choice and action, health, good social relations, and security. Well-being is at the opposite end of a continuum from poverty, which has been defined as a ''pronounced deprivation in well-being.'' The constituents of well-being, as experienced and perceived by people, are situation-dependent.

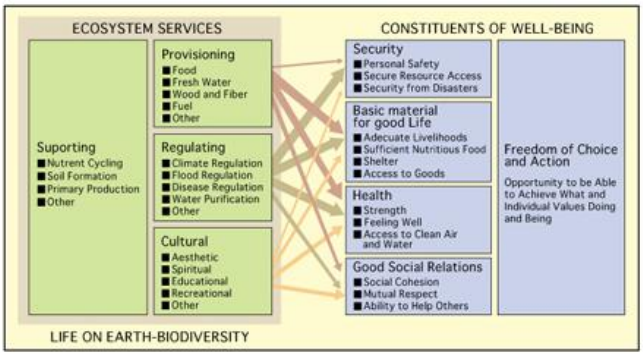

Fig.2. Ecosystem Services providing constituent of human well being (MEA, 2005)

Among supporting services, primary production is essential in making available provisioning services for humanity. The biomass produced becomes then a source of food, wood fiber or fuel. Fossil fuels are also among provisioning services but their life cycle is much longer than food or even wood production. Because of their much longer lifetime at the human time scale, fossil fuels, including petrol, coal and gas, are not considered renewable. Renewable energy sources are increasingly considered important in societies moving towards a post industrial phase. Oil remains the largest source of energy world wide after coal, both fossil fuels, but most experts agree that global peak of oil production have been passed and that it will become increasingly difficult and costly to extract fossil fuels from the underground (Larry Staudt, 2011).

Some of the provisioning services are considered to be a source of energy: Food, fuel and freshwater. With the exception of geothermal, seismic and lunar, energy resources on the planet earth are directly or indirectly solar energy sources. As a result of a constant increase of burning fossil fuel as a source of energy since the industrial revolution, global concentrations of carbon dioxide and their combustion products are steadily increasing.

As clearly outlined and explained in the fourth assessment report of the International Panel on Climate Change (IPCC, 2007), it is the first time in history that human activities have been shown to be responsible for climate change at a global scale. Global warming has consequences in regional climate patterns and distributions, therefore also on human economic, social activities and political decisions. The same report indicated with a high degree of confidence that global warming of atmospheric temperature is due to an increased emission of anthropogenic Green House Gases (GHG) (IPCC, 2007). These gases include mainly carbon dioxide (CO_2) released in the atmosphere after burning fossil fuels but also Methane (CH_4), Nitrate Oxides (NO_X) and other anthropogenic strong GHGs such as PFC and SF_6. The greenhouse effect is storing the heat produced by the sun radiations during the day and keeps the earth's temperature at a level comfortable for life on earth to strive. These greenhouse gases that are released after combustion of fossil fuels as part of the carbon, Nitrogen or water cycle. The speed of accumulation of these gases into the atmosphere is higer that the capacity of the ecosystems to recycle.

A sustainable aproach to meet the needs of an increasing demand for energy, can only be met with a sustainable supply of energy, or renewable sources of energy. Following the post war recovery and reconstruction, and despite a weak industry, BiH has been facing an increasing need for energy.

What are the sources of energy in BiH? Which Ecosystem Services can be a source of renewable source of Energy in BiH? Hydropowers, Biomass, Wind energy, Solar or Geothermal are possibilities. Which one has been developed and which has the most potential for further development? What can be the consequences for the environment and their ecosystems?

III. MATERIALS AND METHODS

This study is a short review. It is therefore the result of desktop research and gathering of information in previous publications and research, and policy documents. The review also reflects a number of discussions and presentations that took place in seminars, and conferences in which the author took part in recent years.

IV. RESULTS AND DISCUSSION

A. Services provided by Ecosystems in BiH.

Ecosystems in BiH are quite diverse due to a large variety of climates and rich topography, from the Mediterranean costal areas, to the semi Mediterranean with mountain influence, the high alpine influence and the continental with the whole range of intermediaries (Mesbah, 2009, 2012). This large variety of climatic conditions

together with a geological diversity creates conditions for a variety of ecosystems which include Mediterranean, deciduous forest, coniferous forests, alpine, even artic at higher elevations. Wetlands can also be found in lowlands, near rivers. These ecosystems provide a large number of services including arable soil for agriculture, wood and non wood products from forests, freshwater, etc… as presented on Fig. 2.

B. Renewable energy in BiH

BiH is dependent on fossil fuels such as petrol and gas imported from outside, but has its own coal reserves (Mesbah, 2009). Electric energy is produced in BiH by hydroelectric power as well as thermoelectric (coal) power plants. In 2008, the total of energy in BiH from renewables was 9.6 % of the total consumption of energy (including tranports), which is low compared to the previous 20 years (UNEP, State of the environment report o be published in 2013). Globally around 13% of the total enegy use come from renewable sources, or 87% come from non renewable sources (International Energy Agency, World Watch Institute).

Among usage of renewable energy, roughly half comes from Biomass (mainly wood) the other half from Hydropower. A very small portion is represented by Goethermal 0.04 % (UNEP, 2013)

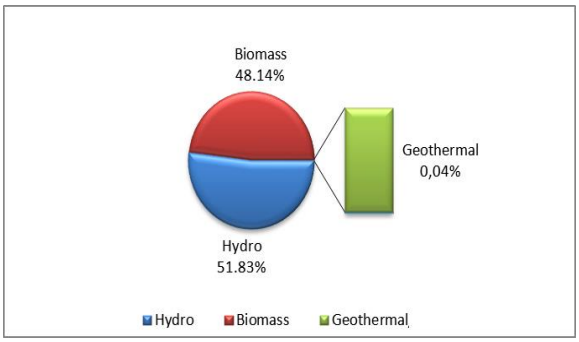

Fig.3. Energy consumption from renewable sources by energy source in Bosnia and Herzegovina, in percentages for 2008 (UNEP, state of the environment report, 2013)

C. Climate Change and Energy

Globale climate change has been shown to be linked with an increasing global emission of green house gaz from anthropogenic burning of fossil fuels. Global climate change is also affecting BiH, with a trend for hotter and dryer summers, milder and shorter winters (Mesbah, to be published in 2013 by UNEP, and Initial National Communication of BiH to the UNFCCC, 2011). In absolute number BiH is not a major emitter of GHG, but it has a relatively high number per capita (UNEP, 2013), and it could be significantly reduced by using more renewable sources of energy and improving energy efficiency.

D. Biomass

Other potentials for renewable energy in BiH include wind energy and non-crop biogas such as wood production in sustainable forestry and agriculture practices. New generation of technologies (ethanol produced from cellulose for example) provide an efficient and economically viable production of bioenergy from biomass obtained from sustainable forestry and meadows management instead of getting biomass from crops which competes with food production over land and water. BiH needs to benefit from these new technologies for bio energy production. Sustainable forestry and agriculture management provides not only significant sources for sustainable energy, it contributes to CO2 sequestration through photosynthesis, but it can also provide habitat and shelter to maintain biodiversity, potential for cultural value and eco-tourism, and a sustainable economy.

Biomass usage includes burning wood but also organic wastes that are part of Municipal Land fills. Sarajevo City Landfill in Smiljevići, Sarajevo Canton has been using its gaz rpoduction due to fermentation of organic wastes since 2001. The output capacity of this plant is 0.35 MW with potential annual production of electrical energy of 0.52 GWh (UNEP and State Ministry of Foregn Tarde of BiH, 2013). Cattle manure can also be used as a biomass. In some countries it is stored for the production of biogas, which can be burned to produce heat and electricity. Grass is an other example of sustianable biomass, produced from perenial plants without much agriculture land management.

E. Hydropower

Hydropower is well developed in BiH with 40% of total electric production in the country but has still strong potential for additional development, as it is one of the less developped Hyrdopower system in the world compared to its potential (aournd 35 % i sactually used (UNEP and State Ministry of Foregn Tarde of BiH, 2013). BiH is mainly mountainous land and supplied with sufficient water flowing through streams and rivers with the current climate. Additional development of power plants is taking place having to take into account environmental as well as social concerns.

F.Wind energy

Bosnia and Herzegovin also has a significant potential for wind energy. Locations with high potential have been indentified and the install capacity being estimated (Ministry of Energy, Mining and Industry of Federation Bosnia and Herzegovina, 2010) UNEP and State Ministry of Foregn Tarde of BiH to be published in 2013).

G. Solar Energy in BiH

Due to its geographic location BiH, compared to other places in Europe, the number of days with sun (especially in Herzegovina) is higer the average in europe. BiH therefore has a has a strong potential for the development of solar energy, but is very little developed. CRP, an NGO from Tuzla indicates that, installing a solar pannel on the roof of a priate house could save the household 50 KM a month for their electricity bill (CRP, 2012). An other project indicates the strong potential in Herzegovina with a project in Grude, Herzegovina.

H. Energy saving

Energy intensity is the amount of energy used compared to the country' s GDP. With a low GDP and a significant amount of energy wasted, BiH has a High Energy Intensity, around 4 times higher than other countries in the western Balkan (EEA, 2010, UNEP, 2013). During the yougoslavia time, BiH already had a much higer energy intensity than other republics of the yougoslavian federation, because of the large number of heavy industries compered to a relatively low population.

BiH still has much progress to make in energy saving measures, including those needed for transport, housing and general efficiency of infrastructure development, maintenance. Many public and private buildings need to be renovated or re-built in order to meet higher standards of energy saving measures. Standardization of more efficient electricity-dependent equipment should be put in place. New policies should aim at moving towards the use of renewable energies in the transport sector which still relies significantly on fossil fuel. BiH is still strongly dependent on imports of fossil fuel such as petrol and gas, but needs to move further towards an increasing use of renewable energy such as bioenergy as well as hydropower, key elements for a sustainable future of the country but also for the preservation of its natural environment.

V. CONCLUSION

Thanks to a rich topography and a combination of continental and Mediterranean climates, BiH offers many services from a rich variety of biodiversity and ecosystems. Among services provided by these ecosystems are renewable forms of energy. Renewable energy represents an important source of energy with additional potential especially in hydropower for electricity. Still in BiH only around 9 % of total energy consumption comes from renewable sources. Biomass and hydropower represent an important potential for further development, but other energy sources have also room development such as Wind energy, Geothermal and Solar Energy.

Recommendations for energy policies have been prepared by the State of the Environment report published in 2013: These recommendations include the adoption of regulations for energy efficiency in buildings, and introduce a system of label or certificates in the energy efficiency of buildings. In additon a system of incentives to increase energy efficiency in households and industry is needed. Replacing imported fossil fuels with energy from domestic renewable sources would contribute to more independency for the country but also to reduce green house gas emissions.

The energy sector in Bosnia and Herzegovina is key for economic development, but needs to grow while maintaining functional ecosystems, in order to maintain the services they provide.

Such a balance between development and sustaning functional ecosystems needs to be taken into account when developping strategies and policies in the energy sector but also in other sectors of the country strategies. Policies aimed at encouraging the use of renewable energy include Clean Development Mechanism (UNFCCC, 2013, National focal point in BiH), an international financial mechanism meant to reduce greenhouse gases from burning of fossil fuels and encourage investments in renewable energies.

ACKNOWLEDGMENT

The study is selected from *International Symposium on Sustainable Development*, ISSD 2013.

REFERENCES

[1] CRP, NGO based in Tuzla, Bosnia and Herzegovina (2012): the Power of solar energy http://zastitaokolisa.crp.org.ba/index.php?option=com_content&view=article&id=185%3Asnaga-sunceve-energije&catid=3%3Aaktuelnosti&Itemid=139&lang=en

[2] Green Rhino Energy (2013) Solar Photovoltaic project in Bosnia and Herzegovina last access in March 2013 http://www.greenrhinoenergy.com/projects/bih/

[3] European Environmnetal Agency (EEA) (2010) Total energy intensity http://www.eea.europa.eu/data-and-maps/indicators/total-energy-intensity-outlook-from-eea

[4] International Energy Agency (2013) http://www.iea.org/

[5] IPCC (2007) Fourth Assesment Report of the The international Panel on Climate Change (IPCC) 4AR http://www.ipcc.ch/publications_and_data/ar4/syr/en/spms1.html

[6] Millennium Assessment Recommendations (MEA) (2005) available at:

[7] http://www.millenniumassessment.*org*/en/Reports.aspx.

[8] Larry Staudt (2011). Recent Nuclear emergencies, whilst aiming for a sustainable energy future. EBBF publication available at: http://ebbf.org/blog/recent-nuclear-emergencies-whilst-aiming-for-a-sustainable-energy-future/

[9] L. A. Mesbah (2013) *The State of the Environment in BiH* UNEP and State Ministry of Foregn Tarde of BiH, 2013 *(* as Co-author) http://www.unep.ba/soer-data-survey.html.

[10] L.A. Mesbah (2012) Presentation of the Situation in Bosnia and Herzegovina at the EC Workshop on April 18-20, 2012 on Ecosystem Services mapping and assessment of EU enlargement and integration countries, at the *Joint Research Center of the European Comission*, Ispra Italy. http://ies.jrc.ec.europa.eu/index.php?page=81

[11] L.A. Mesbah (2009): Ecosystem services for sustainable development in BiH and the Balkans, UNEP/*University of Geneva* available at http://www.unige.ch/formcont/environmentaldiplomacy/TheseMesbahLaurent.

[12] R.Costanza et al (1997) The value of the world's ecosystem services and Natural Capital *Nature* 387, 253 – 260.

[13] http://www.nature.com/nature/journal/v387/n6630/abs/387253a0.html.

[14] Sutward Chapin, Pamela A. Matson, Peter M. Vitousek (2011).The principles of Terestrial Ecosystems, Springer, 529 p.

[15] UNFCCC (2013) Clean development mechanism of the UN Framework Convention on Climate Change http://cdm.unfccc.int/ and http://www.unfccc.ba/en/unfccc/national-communication and http://www.unfccc.ba/ba/posljednje/novosti/21-bih-adopts-the-initial-national-communication-under-the-united-nations-framework-convention-on-climate-change.

BIOGRAPHY

LAURENT AMINE MESBAH was born in France. He received a B.Sc and a M.Sc from the University of Strasbourg in 1991 and 1993 and completed his PhD in Plant Biology in 2000 at the Free University in Amsterdam, the Netherlands. In 2009, he completed a Certificate of Advanced Studies in Environmental Diplomacy at the University of Geneva. Since 2011, L.A. Mesbah is Associate Professor of Environmental Sciences at the American University in BiH and an expert consultant with International Organizations on environmental issues and climate change in the Balkans and other regions of the world.

On the Harmonic Oscillation of High-order Linear Time Invariant Systems

B.B. Alagoz and H.Z. Alisoy

***Abstract*— Linear time invariant (LTI) systems are widely used for modeling of dynamics systems in science and engineering problems. Harmonic oscillation of LTI systems is an outstanding case of LTI system behavior and it is employed for modeling of many periodic physical phenomenon in nature. This study investigates sufficient conditions to obtain harmonic oscillation by using high-order LTI systems. A design procedure for controlling harmonic oscillation of single-input single-output high-order LTI systems is presented. LTI system coefficients are calculated by solving equation sets, which imposes a stable sinusoidal oscillation solution for the characteristic polynomials of LTI systems. Moreover, these analyses are extended to fractional order LTI systems. Simulation examples are demonstrated for high-order LTI systems and the control of harmonic oscillations are discussed by using Hilbert transform and spectrogram of oscillation signals.**

***Index Terms*— Harmonic oscillation, system theory, fractional-order LTI systems, system modeling, root locus analysis.**

I. Introduction

LINEAR Time Invariant (LTI) system modeling methods have been played an important role in development of science and technology for a century. LTI models have found a widespread utilization in theoretical and numerical analyses of linear dynamic systems. Because, behaviors of dynamic systems can be well characterized by LTI system models and consistency of LTI system analyses with real systems has been proven for numerous applied science and engineering problems. It is obvious that analyses on the base of LTI systems still play a central role in system science, today. Deepened investigation on behaviors of LTI systems promises further contributions in term of modeling and comprehension of physical and electrical system behaviors.

LTI systems are expressed in the form of linear time-invariant differential equations. It is convenient to represent LTI differential equations as a set of first-order differential equations to perform state space analyses. Besides, Laplace transform and transfer functions are mainly preferred because of simplification of the system analyses [1-3]. The characteristic polynomial of the LTI systems provides a valuable tool for the analysis of the character of LTI system [4]. Roots of characteristic polynomial are referred to as eigenvalues (or system poles) of systems. Complex conjugate roots ($\lambda_i = \sigma_i \pm j\omega_i$) lead to harmonic terms, e^{jwt}, in the solution of LTI models, and this results in harmonic components at system output [4,5]. The short-term oscillations, originated from the terms of $e^{\sigma_i t \pm jwt}$ for $\sigma_i < 0$, is transient and they tend to asymptotically damp down in time. A continuous oscillating component at LTI system solutions appears when $\sigma_i = 0$ [4,5]. The current study is devoted for the design considerations of high-order LTI harmonic oscillators emerging in the cases of $\sigma_i = 0$ and $j\omega_i \neq 0$.

Previously, stability boundary locus analyses were used for the design of stable control systems [6,7]. It is based on solving characteristic polynomial equation in s domain for $s = j\omega$ to figure out stability regions of controller coefficients. Indeed, stability boundary locus also indicates to the coefficients that results in oscillation of control systems. We consider stability boundary as the oscillation locus and extend our investigation for the harmonic oscillation of LTI systems.

System oscillation is one of the most prominent concerns for dynamic systems. Oscillation behavior is frequently seen in nature, and oscillation of LTI systems was extensively investigated due to potentials of modeling simplification and analysis consistency. Many applied science and engineering fields have been benefited from oscillation models such as in physics [8-12], in control science [13-16], in electrical system [16,17], in biology [19-21]. For instance, prevalence of harmonic oscillators in physics is obvious, such as while describing motions of an object attached to a string and molecules vibrating in crystals [9]. Oscillation conditions were stated for various oscillators [17-19]. However, investigation of parametric conditions to constitute harmonic oscillation (steady sinusoidal oscillations) of high-order LTI models may further extend our comprehension of complex physical systems, which is, today, modeled by simple second-order harmonic oscillation models, particularly in particle physics [9].

This study investigates sufficient conditions to obtain harmonically oscillating high-order LTI system model. Roots of the characteristic polynomials are mapped to amplitude-angle ($M - \theta$) plane by considering roots of characteristic polynomial in the form of $\lambda = Me^{j\theta}$, and coefficients of the LTI system let to a desired harmonic oscillation were found by arbitrary solutions of linear equations. These arbitrary

Baris Baykant Alagoz, was with Inonu University, Department of Electrical-Electronics, Malatya, Turkey (e-mail: baykant.alagoz@inonu.edu.tr).

Hafiz Z. Alisoy, was with Namık Kemal University, Department of Electronics and Telecomunication, Tekirdag, Turkey (e-mail: alismpei@gmail.com).

solutions impose sinusoidal oscillation solutions for characteristic polynomials. These solutions are extended for fractional order LTI systems. Example designs were demonstrated for integer and non-integer order LTI systems, and results were discussed for the control of harmonic oscillations.

II. METHODOLOGY

A. Theoretical Background

Differential equations of LTI control systems with constant coefficients $\alpha_i \in R$ and a derivative order i [1,2,5] are expressed in a general form as follows,

$$\sum_{i=0}^{n} \alpha_i y^{(i)} = u \tag{1}$$

A LTI system is commonly expressed via state space representation [4] as follows

$$x' = Ax + Bu \tag{2}$$

$$y = Cx + Du\ , \tag{3}$$

,where x is $n\times 1$ state variable vector of the system and y is the system output vector. The tem x' denotes the first derivatives of state variable vector. The vector u represents input vector of the system. The matrix A is $n \times n$ size state transition matrix of system. The matrix B, C and D are model parameters of the dynamic system. For single-input single-output systems, Laplace transform transfer function [4,22,23] was expressed in s-domain domain as,

$$T(s) = \frac{Y(s)}{U(s)} = C(sI - A)^{-1}B + D \tag{4}$$

Characteristic polynomial of this system [4] were expressed as follows,

$$\Delta(\lambda) = \det(\lambda I - A) \tag{5}$$

$\lambda_i \in C$, $i = 0,1,2,3,..,n-1$ is complex eigenvalues of dynamic systems. In order to solve λ_i, one expresses characteristic equation in polynomial form as follows,

$$\Delta(\lambda) = \sum_{i=0}^{n} \alpha_i \lambda^i = 0 \tag{6}$$

The roots of characteristic polynomial yield $\lambda_i = \sigma_i \pm j\omega_i$ complex eigenvalues. For a zero input case ($u(t) = 0$), the time domain solution of LTI system contains sum of $e^{\lambda_i t}$ terms, $y(t) = a_0 e^{\lambda_0 t} + a_1 e^{\lambda_1 t} + .. + a_{n-1} e^{\lambda_{n-1} t}$ [4]. Accordingly, the term $e^{\lambda_i t}$ can be factored as two components as $e^{\sigma_i t} e^{j\omega_i t}$. Here, the terms $e^{j\omega_i t}$ generates harmonics at the output because of $e^{\pm j\omega_i t} = \cos(\omega_i t) \pm j\sin(\omega_i t)$ and this results in sinusoidal components at the angular frequency of $\omega_i = 2\pi f_i$. The component $e^{\sigma_i t}$ specifies evolution of amplitude of $e^{j\omega_i t}$ in time. In the case of $\sigma_i < 0$, it is also commonly referred to as attenuation coefficient and correspondingly time constant of asymptotic attenuation was commonly considered as $\tau_i = -1/\sigma_i$ for physical and electrical system models. These systems damp down any excitation in a limited time period. When $\sigma_i > 0$, the term of $e^{\sigma_i t}$ exponentially grows the amplitude of harmonics $e^{j\omega_i t}$ in time and indicates to instability of the system. If $\sigma_i = 0$, it stabilizes amplitude of the harmonics with the frequency of ω_i. It is well known that root locations in complex plane ($\sigma, j\omega$) tells us following remarks for high-order system behaviors [1,4,5],

(i) If all roots accommodates on the left half plane, so $\mathrm{Re}\{\lambda_i\} = \sigma_i < 0$, $i = 0,1,2,3,,n-1$, the system will be asymptotic stability [4]. Because, all $e^{\sigma_i t}$ terms in solution go to zero, as the time goes infinity ($\lim_{t\to\infty} e^{\sigma_i t} \to 0$) [4]. If there is at least a root, of which $\omega_i \neq 0$, it yields a transient oscillation with time constant $\tau = -1/\sigma_i$.

(ii) If there is at least a root accommodating on the right half plane, so $\mathrm{Re}\{\lambda_k\} = \sigma_k > 0$, $k \in [0, n-1]$, the system will be unstable. Because, at least a term $e^{\sigma_k t}$ in solution goes infinitive as time goes infinity. If $\omega_k \neq 0$, it yields a unstable oscillation with a growing amplitude.

(iii) If there are not a complex root at right half plane and at least a complex conjugate root accommodates on complex axis ($j\omega_i$); $\mathrm{Re}\{\lambda_i\} = 0$ and for the rest of roots satisfies $\mathrm{Re}\{\lambda_k\} = \sigma_k < 0$, $k \neq i$ and $k \in [0, n-1]$, this system oscillates. Because, the solution contains at least one harmonic term (e^{jwt}), which leads to sinusoidal oscillations in time domain solutions.

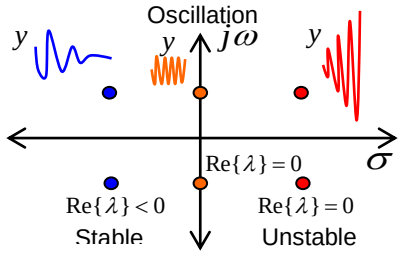

Fig. 1. System responses with respect to root location of characteristic polynomial

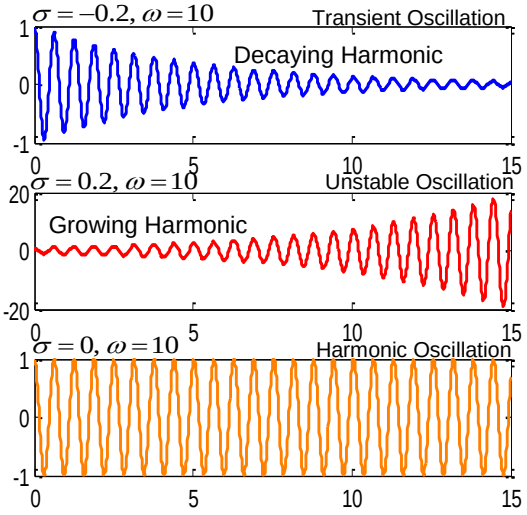

Fig. 2. Oscillation of LTI system for various states of complex roots

($\lambda = \sigma \pm j\omega$)

The system responses are represented with respect to root location of characteristic polynomials in Figure 1. Figure 2 illustrates simulation results obtained for sinusoidal oscillation stereotypes with respect to complex roots.

B. Problem Definition

This study aims to derive fundamental design considerations for harmonic oscillation of high-order LTI systems on the bases of characteristic root placement in complex plane. For this propose, lets express the roots of characteristic polynomial in the form of $\lambda_i = M_i e^{j\theta_i}$ [24, 25]. Here, M_i and θ_i are magnitude and angle of complex roots λ_i, respectively. Transformation from (M, θ) to $(\sigma, j\omega)$ is performed by using,

$$\begin{bmatrix} \sigma \\ \omega \end{bmatrix} = M \begin{bmatrix} \cos\theta \\ \sin\theta \end{bmatrix}. \tag{7}$$

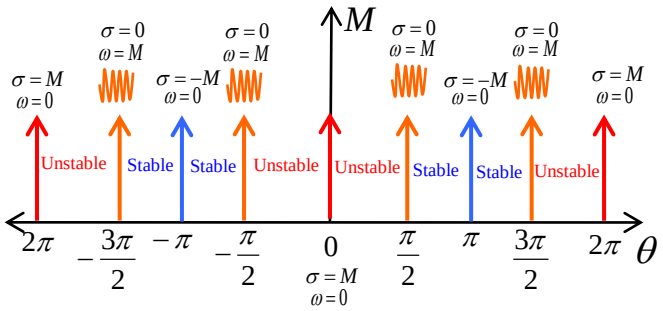

Fig. 3. Root mapping in $M-\theta$ plane and resulting oscillations boundaries

Figure 3 illustrates the character of systems in $M-\theta$ root mapping regions. According to figure, regions of $M > 0$ and $\frac{\pi}{2} + h2\pi < \theta_i < \frac{3\pi}{2} + h2\pi$ for $h \in T$ yields a asymptotically stable LTI systems due to coinciding to left half of complex root plane and regions of $M > 0$ and $-\frac{\pi}{2} + h2\pi < \theta_i < \frac{\pi}{2} + h2\pi$ for $h \in T$ yield unstable LTI systems because of mapping right half of complex root plane. Boundaries between stability and instability mapping regions are referred to harmonic oscillating boundaries due to $\omega_i = M$ and $\sigma_i = 0$. Oscillation-free response of LTI system is possible when all λ_i is mapped over the boundaries of $\theta_i = \pi \pm h2\pi$, $i = 0,1,2,3,,n-1$ due to $\omega_i = 0$ and $\sigma_i = -M$.

Real physical systems in macro scales (mechanical systems) mainly exhibit attenuating harmonic oscillation ($\sigma_i < 0$) for a limited time interval due to friction forces or thermodynamic energy loses. Time constant of this limited time oscillation (transient oscillation) is $\tau = -1/\sigma_i = -1/(M_i \cos(\theta_i))$ and the oscillating frequency is $\omega_i = M_i \sin(\theta_i)$. Steady oscillations can be frequently possible in micro-scale physical systems such as electro-physical and particle systems. However, unstable harmonic oscillation ends with devastation or transformation of the physical systems and this type behaviors can be take place in very short intervals in the nature for instance short-lived particles.

C. Oscillation Locus of LTI systems

Property 1: A LTI system yields steady oscillation if at least one root angle satisfies $\theta_i = \frac{\pi}{2} + h\pi$, $i = 0,1,2,3,,n-1$ and $h \in T$.

Proof: One can write the angle λ_i as $\theta_i = \tan^{-1}(\omega_i / \sigma_i)$ and use it in $\theta_i = \frac{\pi}{2} + h\pi$. In this case, σ_i can be written as,

$$\sigma_i = \omega_i / \tan(\frac{\pi}{2} + h\pi) \tag{8}$$

Since $\tan(\frac{\pi}{2} + h\pi) = \infty$ for $h \in T$, one obtains $\sigma_i = 0$ for $h \in T$. Considering remark (iii), this LTI system oscillates due to $\lambda_i = \pm j\omega$.

Property 2: A n-order LTI system contains harmonic oscillation at the angular frequency ω_k for the first oscillation locus ($h = 0$), when the characteristic polynomial coefficients $\alpha_0, \alpha_1, \alpha_2.., \alpha_n$ satisfy the following conditions,

$$\sum_{i=0}^{n} \alpha_i (\omega_k)^i \cos(\frac{\pi}{2} i) = 0 \text{ and } \sum_{i=0}^{n} \alpha_i (\omega_k)^i \sin(\frac{\pi}{2} i) = 0$$

Proof:
If the characteristic equation of n-order LTI system given by equation (6) is solved for $\lambda_i = M_i e^{j\theta_i}$ mapping, we obtains,

$$\Delta(\lambda) = \sum_{i=0}^{n} \alpha_i (M_i e^{j\theta})^i = 0 \tag{9}$$

Considering Property 1 for the first oscillation locus of system ($h = 0$), one can write the following equation,

$$\sum_{i=0}^{n} \alpha_i (M_i)^i e^{(j\frac{\pi}{2})i} = 0 \tag{10}$$

Since, $e^{j(\frac{\pi}{2})i} = \cos(\frac{\pi}{2} i) + j\sin(\frac{\pi}{2} i)$, equation (10) can be reorganized as follows,

$$\sum_{i=0}^{n} \alpha_i (M_i)^i \cos(\frac{\pi}{2} i) + \sum_{i=0}^{n} \alpha_i (M_i)^i \sin(\frac{\pi}{2} i) = 0 \tag{11}$$

For $\theta_i = \frac{\pi}{2}$, we can write the magnitude as desired oscillation frequency, $M_i = \omega_k$, and rearrange equation (11) as,

$$\sum_{i=0}^{n}\alpha_i(\omega_k)^i\cos(\frac{\pi}{2}i)+j\sum_{i=0}^{n}\alpha_i(\omega_k)^i\sin(\frac{\pi}{2}i)=0 \quad (12)$$

A solution of equation (12) yields the sufficient conditions of harmonic oscillation at the angular frequency ω_k as,

$$\sum_{i=0}^{n}\alpha_i(\omega_k)^i\cos(\frac{\pi}{2}i)=0 \text{ and } \sum_{i=0}^{n}\alpha_i(\omega_k)^i\sin(\frac{\pi}{2}i)=0 \quad (13)$$

Property 2 gives the sufficient conditions for determination of characteristic polynomial coefficients in order to make any n-order LTI system contain harmonic oscillation at the angular frequency ω_k.

One can write equation (13) in open form as,
when the order n are even,

$$\begin{aligned}&\alpha_0-\alpha_2(\omega_k)^2+\alpha_4(\omega_k)^4-\alpha_6(\omega_k)^6+... \\ &\pm\alpha_{n-2}(\omega_k)^{n-2}\pm\alpha_n(\omega_k)^n=0\end{aligned} \quad \& \quad \begin{aligned}&\alpha_1-\alpha_3(\omega_k)^3+\alpha_5(\omega_k)^5-\alpha_7(\omega_k)^7+... \\ &\pm\alpha_{n-3}(\omega_k)^{n-3}\pm\alpha_{n-1}(\omega_k)^{n-1}=0\end{aligned} \quad (14)$$

When the order n are odd,

$$\begin{aligned}&\alpha_0-\alpha_2(\omega_k)^2+\alpha_4(\omega_k)^4-\alpha_6(\omega_k)^6+... \\ &\pm\alpha_{n-2}(\omega_k)^{n-2}\pm\alpha_{n-1}(\omega_k)^{n-1}=0\end{aligned} \quad \& \quad \begin{aligned}&\alpha_1-\alpha_3(\omega_k)^3+\alpha_5(\omega_k)^5-\alpha_7(\omega_k)^7+... \\ &\pm\alpha_{n-2}(\omega_k)^{n-2}\pm\alpha_n(\omega_k)^n=0\end{aligned} \quad (15)$$

These equations also tell us the following important remarks for oscillation condition of LTI systems:

(i) According to equation (13), due to arbitrary solutions, it is always possible to find out a characteristic polynomial coefficients set $\alpha_0,\alpha_1,\alpha_2..,\alpha_n$ in order to oscillate any LTI system with $n>1$ at any ω_k. (*Existence of solution*)

(ii) According to equation (13), the characteristic polynomial coefficients $\alpha_0,\alpha_1,\alpha_2..,\alpha_n$, which oscillates any LTI system at any ω_k, is not unique. So, there is a solution family of $\alpha_0,\alpha_1,\alpha_2..,\alpha_n$ satisfying equation (13). (*Abundance of solution*)

(iii) A special case of oscillating coefficients of characteristic polynomial appears when $\omega_k=1$. A solution family can be obtained as $\alpha_0=\alpha_1=\alpha_2=...=\alpha_n$. (*Balanced solution families*) when the order n are even,

$$\begin{aligned}&\alpha_0-\alpha_2+\alpha_4-\alpha_6+...\pm\alpha_{n-2}\pm\alpha_n=0 \quad \& \\ &\alpha_1-\alpha_3+\alpha_5-\alpha_7+...\pm\alpha_{n-3}\pm\alpha_{n-1}=0\end{aligned} \quad (16)$$

when the order n are odd,

$$\begin{aligned}&\alpha_0-\alpha_2+\alpha_4-\alpha_6+...\pm\alpha_{n-3}\pm\alpha_{n-1}=0 \quad \& \\ &\alpha_1-\alpha_3+\alpha_5-\alpha_7+...\pm\alpha_{n-2}\pm\alpha_n=0\end{aligned} \quad (17)$$

(iv) Oscillation condition given by Equation (13) let to arbitrary selection of $n-1$ coefficient and the rest two coefficients are determined by the following equations,

$$\alpha_v=-\sum_{i=0\&i\neq v}^{n}\alpha_i(\omega_k)^i\cos(\frac{\pi}{2}i) \quad \&$$

$$\alpha_g=-\sum_{i=0\&i\neq g}^{n}\alpha_i(\omega_k)^i\sin(\frac{\pi}{2}i) \quad (18)$$

In order to avoid arbitrary locating of $n-2$ roots of characteristic polynomial and negative effects of this root on harmonic oscillation patterns, we prefer to locate them at $\theta_i=\pi$ with magnitudes $M_1>M_2>...>M_{n-2}$, which mean to $\omega=0$ and $\sigma_1<\sigma_2<...<\sigma_{n-2}<0$. Those roots yield transient asymptotic solutions ($e^{\sigma_i t}$) approximating to zero without any oscillation as time goes to infinity. In other words, we obtain n number of linear equations for n roots and choose only α_0 arbitrary. Additional linear equation for each non-oscillating transient roots ($p=1,2..n-2$) can be written as,

$$\sum_{i=0}^{n}\alpha_i(\sigma_p)^i\cos(\pi i)=0 \quad (19)$$

This equation is useful for vibration free system design. When all roots of a system satisfies this condition, the system response cleans from transient damping harmonics and rippling.

D. Extension of Analyses to Fractional Order LTI systems

Fractional-order system modeling attracts interest of researches, recently. Results in previous section can be easily extended for fractional-order LTI system expressed in a general form as follows

$$\sum_{i=0}^{n}\alpha_i y^{(\sigma_i)}=u \quad (20)$$

Characteristic equation of fractional-order LTI system is written in the following general form,

$$\Delta(\lambda)=\sum_{i=0}^{n}\alpha_i\lambda^{\sigma_i}=0 \quad (21)$$

By considering $\lambda_i^{\sigma_i}=M_i^{\sigma_i}e^{j\theta_i\sigma_i}$, where $\sigma_i\in R$ represents fractional orders.

$$\sum_{i=0}^{n}\alpha_i(M_i^{\sigma_i})^i e^{(j\theta_i\sigma_i)}=0 \quad (22)$$

For $\theta_i=\frac{\pi}{2}$, we can write the magnitude as desired oscillation frequency, $M_i=\omega_k$, and obtains the oscillation condition corresponding to equation (13),

$$\sum_{i=0}^{n}\alpha_i(\omega_k)^{\sigma_i}\cos(\frac{\pi}{2}\sigma_i)=0 \text{ and } \sum_{i=0}^{n}\alpha_i(\omega_k)^{\sigma_i}\sin(\frac{\pi}{2}\sigma_i)=0 \quad (23)$$

For $\theta_i = \pi$ and $M_i = \sigma_i$, additional linear equation for each non-oscillating transient roots ($p = 1,2..n-2$) can be written as,

$$\sum_{i=0}^{n} \alpha_i (\sigma_p)^{\sigma_i} \cos(\pi \sigma_i) = 0 \qquad (24)$$

Equations (23) and (24) are reduced to equations (13) and (19) for integer values of derivative order σ_i. The remarks given in previous section are also valid for fractional order system.

Design procedure for oscillating high-order LTI system ($n > 3$) with no transient oscillation can be summarized as follows:

Step 1: Set $\alpha_0 = 1$ or any real number.

Step 2: Write n number of linear equations such that equation (23) is for oscillating roots and equation (24) is for each non-oscillation roots.

Step 3: Solve linear equations to obtain $\alpha_1, \alpha_2 .., \alpha_n$ polynomials coefficients.

III. NUMERICAL EXAMPLE

In this section, we present an example system for fourth-order LTI systems, expressed in the form of,

$$\alpha_4 y^{(4)} + \alpha_3 y^{(3)} + \alpha_2 y^{(2)} + \alpha_1 y' + \alpha_0 y = u \qquad (25)$$

In order to obtain harmonic oscillation at $\omega_k = 2$ radian/sec according to property 2, one writes equation (13) for $n = 4$ and then solves two equations given bellow,

$$\alpha_0 - 4\alpha_2 + 16\alpha_4 = 0 \text{ and } 2\alpha_1 - 8\alpha_3 = 0 \qquad (26)$$

There are 5 design coefficients ($\alpha_0, \alpha_1, \alpha_2, \alpha_3$ and α_4) and two linear equations, so we choose three coefficients arbitrarily as $\alpha_0 = 1, \alpha_1 = 0.5$ and $\alpha_4 = 1$. Then, by solving equation (26), one obtains $\alpha_2 = 4.25$ and $\alpha_3 = 0.125$. Accordingly, the transfer function of oscillator can be obtained as,

$$T(s) = \frac{1}{s^4 + 0.125s^3 + 4.25s^2 + 0.5s + 1} \qquad (27)$$

State space model in controller canonical form can be written as

$$A = \begin{bmatrix} -0.1250 & -4.25 & -0.5 & -1.0 \\ 1.0 & 0 & 0 & 0 \\ 0 & 1.0 & 0 & 0 \\ 0 & 0 & 1.0 & 0 \end{bmatrix}, B = \begin{bmatrix} 1 \\ 0 \\ 0 \\ 0 \end{bmatrix}, C^T = \begin{bmatrix} 0 \\ 0 \\ 0 \\ 1 \end{bmatrix},$$

$$D = 0 \qquad (28)$$

A Dirac function in the form of $u(t) = g\delta(t)$ was used for the input disturbance of the system. This imposes the initial condition of $y(0) = g$ and $y^{(i)}(0) = 0$, $i = 1,2,3..n$. The amplitude of Dirac (g) can be used for adjusting the amplitude of harmonic oscillation.

Figure 4(a) shows roots ($\lambda_i, i = 0,1,2..4$) in complex plane. Complex conjugate roots $\lambda_{1,2} = \pm 2j$ yields harmonic oscillation at $\omega_k = 2$ radian/sec and the roots $\lambda_{3,4} = -0.0625 \pm 0.4961j$ yield a transient decaying oscillation with a time constant $\tau = -1/(-0.0625) = 16$ sec at the angular frequency of 0.4961 radian/sec. The transient oscillation almost attenuated in $5\tau \cong 80$ sec and the harmonic oscillation at $\omega_k = 2$ radian/sec continues with an amplitude of 0.13 for $u(t) = \delta(t)$. In order to increase the amplitude of harmonic oscillation up to the amplitude of 0.65 as in Figure 4(c), $u(t) = 5\delta(t)$ was applied from the input. This figure confirms that harmonic oscillation amplitude for the high-order LTI system can be controlled via the input signal $u(t)$.

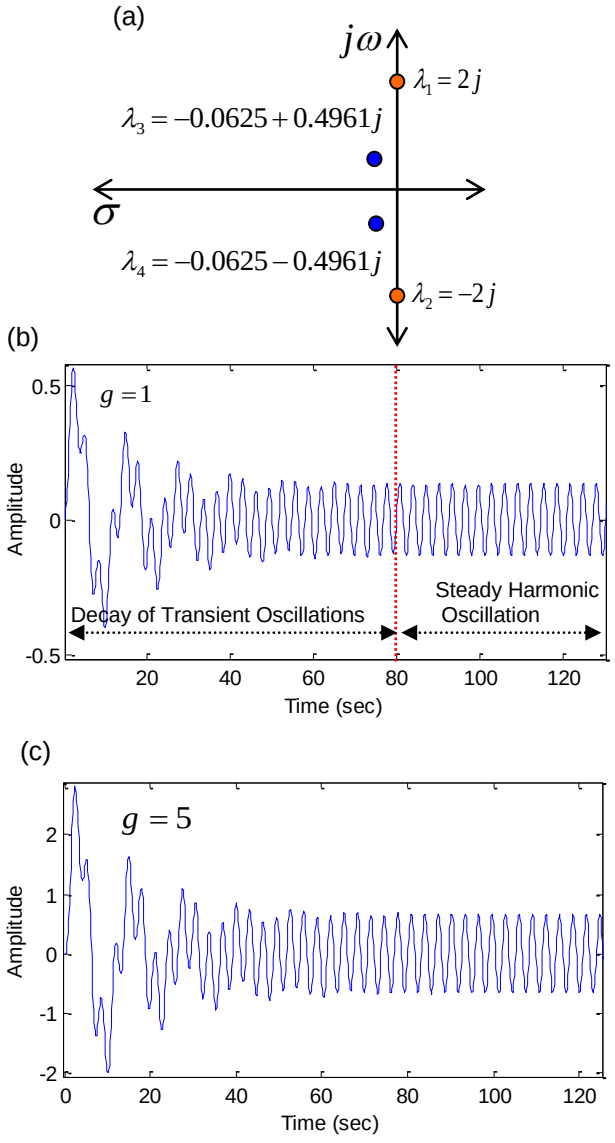

Fig. 4. (a) Root locations in complex plane, (b) LTI system response for $u(t) = \delta(t)$, (c) LTI system response for $u(t) = 5\delta(t)$

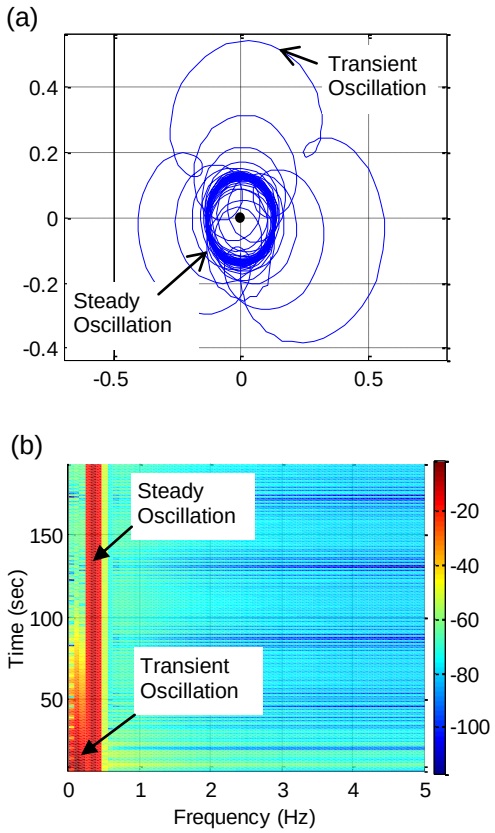

Fig. 5. (a) Discrete-time analytic representation of the output signal. (b) Spectrogram of the output signal

Figure 5(a) shows discrete-time analytic signal of the system output calculated by Hilbert transform. Analytic signal represents signals in a complex plane ($y(t) = |y(t)|e^{j\angle\phi(t)}$), where vertical and horizontal axis are complex part and real part of complex signals. Irregular large circles were formed by transient oscillations in the figure. The circular orbit bands were formed by steady harmonic oscillation obtained at $\omega_k = 2$ radian/sec. This effect can be clearly observed in Figure 5(b) demonstrating spectrogram of the system output. Spectrogram is obtained by moving window short-time Fourier transform of signals. This figure shows damping of transient oscillation at roughly 0.08 Hz (angular frequency of 0.4961 radian/sec) in about 80 sec and a steady harmonic oscillation at 0.31 Hz (angular frequency of 2 radian/sec).

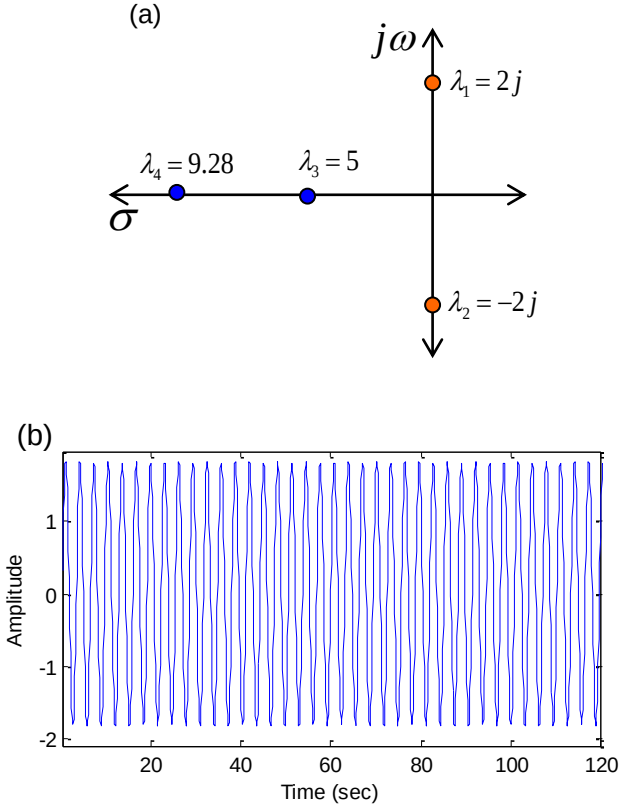

Fig. 6. (a) Root locations in complex plane, (b) LTI system response for $u(t) = \delta(t)$,

In order to remove transient oscillations caused from the complex conjugates roots $\lambda_{3,4} = -0.0625 \pm 0.4961j$, we applied the design procedure for oscillating high-order LTI system with no transient oscillation given in previous section. For this proposes, we preferred decay of non-oscillating two transient components for $\sigma_3 = 5$ and $\sigma_4 = 9.2$ as in illustrated Figure 6(a). Two addition linear equations were written according to equation (19) as,

$$\alpha_0 - 5\alpha_1 + 25\alpha_2 - 125\alpha_3 + 625\alpha_4 = 0 \;\&$$
$$\alpha_0 - 10\alpha_1 + 100\alpha_2 - 1000\alpha_3 + 10000\alpha_4 = 0 \quad (29)$$

For $\alpha_0 = 1$, the solutions of equations (26) and (29) were obtained as $\alpha_1 = 0.3077$, $\alpha_2 = 0.2715$, $\alpha_3 = 0.0769$, $\alpha_4 = 0.0054$ and the differential model of the system can be written as

$$0.0054y^{(4)} + 0.0769y^{(3)} + 0.2715y^{(2)} + 0.3077y' + y = u \quad (30)$$

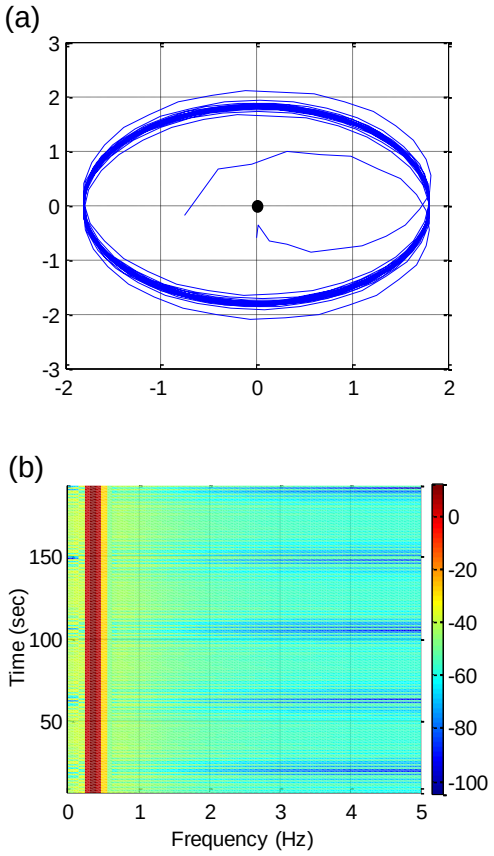

Fig. 7. (a) Discrete-time analytic representation of the output signal. (b) Spectrogram of the output signal

Figure 6(b) shows the system output, where transient oscillations are cleared. To better evaluate harmonic oscillations, Figures 7(a) and 7(b) shows discrete-time analytic signal and spectrogram of the system output. It is evident from figures that transient oscillations were cleared from the system output.

One of the noteworthy property of this oscillator is that one can add a bias level for harmonic oscillation by applying a step function ($u(t)=1, t\geq 0$) to the input. Figure 8(a) and (b) shows step response and discrete-time analytic signal of the system. A bias with a magnitude of one is apparent in these figures. Figure 9 shows results of variable step input applied for a fourth-order LTI system designed for $\omega_k = 1$ radian/sec, $\sigma_3 = 5$ and $\sigma_4 = 9.8$. The differential model of the LTI oscillation control system was obtained as

$$0.0204y^{(4)} + 0.3020y^{(3)} + 1.0204y^{(2)} + 0.3020y' + y = u(t) \quad (31)$$

To better demonstrate amplitude and bias control of oscillations at $\omega_k = 1$ radian/sec via input signal $u(t)$, we applied subsequent delayed Dirac input and a variable step input as control signal. The subsequent delayed Dirac signal was formed as follows,

$$u(t) = 0.5\delta(t) + \delta(t-100) + 1.2\delta(t-150) \quad (32)$$

And, the following variable step input signal was used to disturb the oscillating system.

$$u(t) = \begin{cases} 0.5 & ,t \leq 50 \\ 1 & ,50 < t \leq 100 \\ 2 & ,100 < t \leq 200 \end{cases} \quad (33)$$

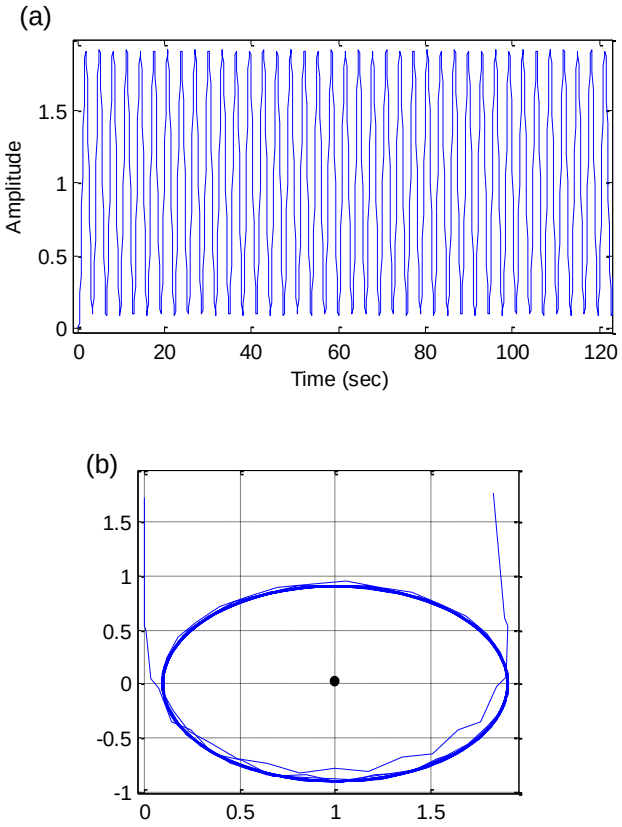

Fig. 8. (a) LTI system response for $u(t) = 1$ exhibiting a bias level of one, (b) Discrete-time analytic representation of the output signal with a bias level of one.

Figure 9(a) and (b) demonstrates control of oscillation amplitude by the subsequent delayed Dirac signal generated by equation (32). Each pulse increases amplitude of harmonic oscillation for a zero bias. Figure 9(c) demonstrates shift of bias of oscillation by altering amplitude of the variable step function according to equation (33). It should be noticed that oscillation control is performed for amplitude by Dirac input and for bias by step input.

Practical harmonic oscillator implementation in circuit design encounters with voltage stability problems and it requires a control circuitry to sustain oscillation voltage stability[26].

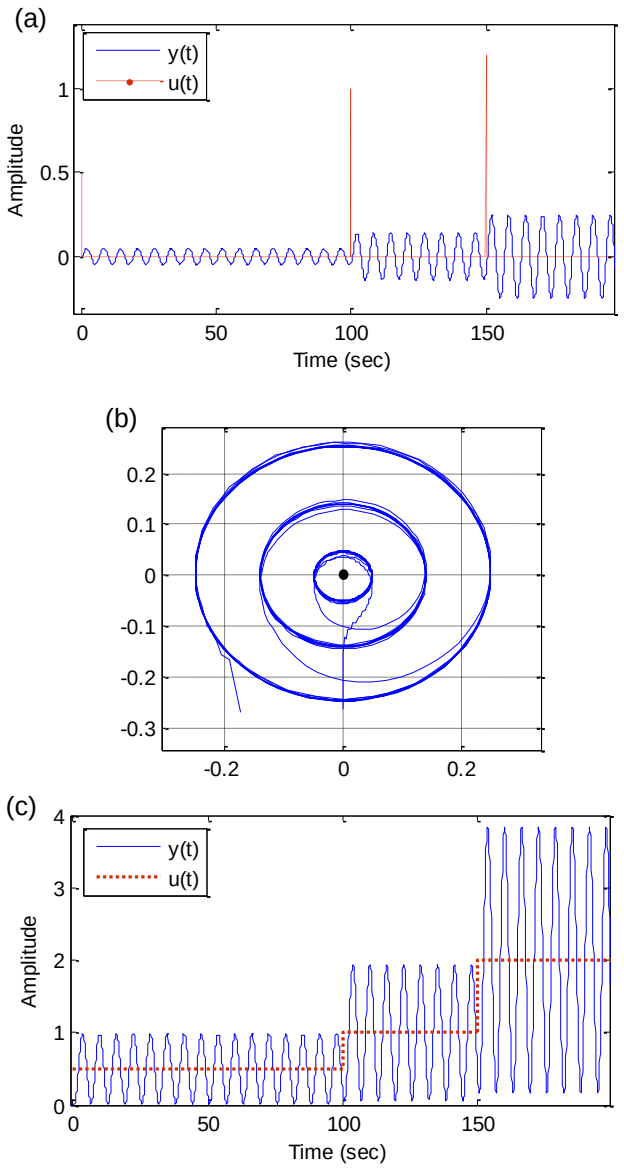

Fig. 9. (a) LTI system response for subsequent delayed dirac input, (b) Discrete-time analytic representation of the output signal for subsequent delayed dirac input, (c) Harmonic oscillation controlled with a variable step input and corresponding bias levels.

We present another example system for fractional-order LTI systems, expressed in the form of,

$$\alpha_3 y^{(3.6)} + \alpha_2 y^{(2.4)} + \alpha_1 y^{(1.2)} + \alpha_0 y = u \qquad (34)$$

In order to obtain harmonic oscillation at $\omega_k = 4$ radian/sec according to property 2, one writes equation (23) for $n = 3$ and then solves two equations given bellow,

$$\alpha_0 + 0.8155\alpha_1 - 1.8195\alpha_2 + 1.6350\alpha_3 = 0 \text{ and}$$
$$2.5099\alpha_1 - 1.3219\alpha_2 - 1.1879\alpha_3 = 0 \qquad (35)$$

There are 4 design coefficients ($\alpha_0, \alpha_1, \alpha_2, \alpha_3$) and two linear equations, $\alpha_0 = 1$ and $\alpha_1 = 0.5$ are chosen arbitrarily. Then, by solving equations (35), one obtains $\alpha_2 = 0.080733$ and $\alpha_3 = 0.013745$. Accordingly, the transfer function of fractional order LTI harmonic oscillator can be obtained as,

$$T(s) = \frac{1}{0.01374s^{3.6} + 0.080733s^{2.4} + 0.5s^{1.2} + 1} \qquad (36)$$

A differential model of fractional order LTI harmonic oscillator was obtained as,

$$0.013745y^{(3.6)} + 0.080733y^{(2.4)} + 0.5y^{(1.2)} + y = u(t) \qquad (37)$$

Fig. 10 shows step response of fractional order LTI system and its discrete-time analytic representation. In order to simulate step response of equation (36), we used Matlab functions presented in [27]. We observed in simulation that amplitude of harmonic oscillation is not steady for a long time as harmonic oscillation of integer order LTI systems. One reason for this amplitude instability can be approximation errors, which are caused from approximate implementation of fractional order terms in numerical simulations.

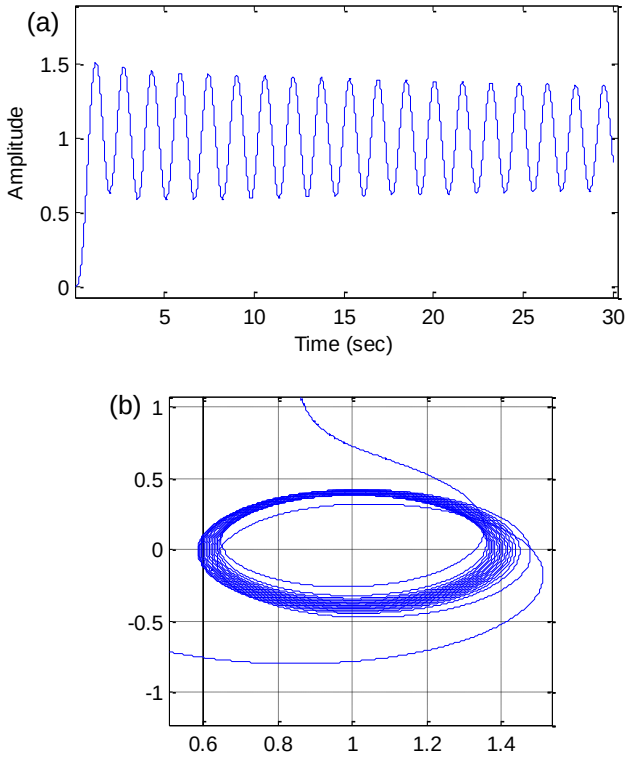

Fig. 10. (a) Step response of fractional order LTI system given by equation (36), (b) Discrete-time analytic representation of the output signal.

IV. CONCLUSIONS

This study presents a harmonic oscillation design and control procedure for high-order LTI systems. The paper discusses sufficient conditions of system coefficients to maintain

harmonic oscillation and to clear transient harmonics from the system output. Moreover, some properties related to oscillating LTI system solutions such as existence of solution, abundance of solutions, balanced solution families are discussed. Equation set for oscillating roots (equation (13)) and non-oscillation roots (equation (19)) placement is derived and a design procedure for oscillating high-order LTI systems with no transient oscillation is presented.

Design and control examples were presented for the fourth-order LTI systems. In these examples, we illustrated removal of undesired transient harmonic oscillation from the system response and controlling the amplitude and bias levels of harmonic oscillations of the systems via input signal.

In physics, harmonic oscillations are widely used to explain mechanisms acting on the periodic events. A notable point should be emphasized that the steady state behavior of a high-order LTI system can mimic a second-order harmonic oscillator, when the complex conjugate roots resulting in transient oscillations moves away the complex axis. This transient components damp down during the transient regime. Steady-state response analysis of physical systems can hide effects of higher-order eigenvalues or roots at the system output. However, the actual orders of harmonically oscillating systems can be estimated by evaluating transient response of systems.

Discussions and examples in the paper can be useful for system engineering and results can contribute to the field of vibration control, electrical systems, modeling and analysis of periodical physical phenomena.

REFERENCES

[1] Blackman P.F., *The pole-zero approach to systems analysis*, Rowse Muir Publications, 1962.

[2] Perkins W.R., Cruz J.B., Engineering of dynamic systems, Wiley, 1969.

[3] Harris C.J., Miles J.E., "Stability of linear systems : some aspects of kinematic similarity", Mathematics in Science and Engineering, Academic Press, 1980.

[4] Gopal M, Modern Control System Theory, New Age International, 1993, pp. 322-324.

[5] Dorf R.C. and Bishop R. H., Modern Control Systems. Addison-Wesley, New York, 1990.

[6] Tan N., "Computation of Stabilizing PI and PID controllers for processes with time delay", ISA Transactions, 44, 2005,pp.213-223.

[7] Moghaddam T.V. and Abbasi Y., "Tuning a Fractional Order PD and PID Controller with Lead Compensator for Integrating Time Delay Systems", Journal of Electrical and Control Engineering 2, 2012, pp.34-41.

[8] Wells J.D., "Effective Theories in Physics", Springer Briefs in Physics, 2012, pp.7-13.

[9] Chiorescu I., Bertet P., Semba1 K., Nakamura Y., Harmans C. J. P. M. and J. E. Mooij, "Coherent dynamics of a flux qubit coupled to a harmonic oscillator", Nature 431, 2004, pp.159-162.

[10] Carloni S.,Troisi A., Dunsby P. K. S., "Some remarks on the dynamical systems approach to fourth order gravity", General Relativity and Gravitation 41, 2009, pp.1757-1776.

[11] Yakovenko S., "Oscillation of Linear Ordinary Differential Equations: On a Theorem of A. Grigoriev", Journal of Dynamical and Control Systems,12, 2006, pp.433-449.

[12] Ibrahim H.H., Tawfik M., "Limit-cycle Oscillations of Functionally Graded Material Plates Subject to Aerodynamic and Thermal Loads", Journal of Vibration and Control 16, 2010, pp.2147-2166.

[13] Kasnakoglu C., "Control of Oscillations in Flow Problems Under Frequency Limitations", Journal of Vibration and Control, 16, 2010, pp.1941-1966.

[14] Saha A., Pandey S.S., Bhattacharya B., Wahi P., "Analysis and control of friction-induced oscillations in a continuous system", Journal of Vibration and Control 18, 2012, pp.467-480.

[15] Chen Y.M., Liu J.K., "Homotopy Analysis Method for Limit Cycle Oscillations of an Airfoil with Cubic Nonlinearities", Journal of Vibration and Control 16, 2009, pp.163-179.

[16] Brigante M and Sumbatyan M.A., "An efficient method in 2D problem on transient oscillations of the elastic half-space interacting with a rigid structure", Journal of Vibration and Control, 2013, doi: 10.1177/1077546313490777.

[17] Radwan A.G., Elwakil A.S., and Soliman A.M., "Fractional-Order Sinusoidal Oscillators: Design Procedure and Practical Examples", IEEE Transaction On Circuits And System 55, 2008, pp.2051-2063.

[18] Atay F.M., "Oscillation Control in Delayed Feedback Systems", Lecture Notes in Control and Information Sciences 273, 2002, pp.103-116.

[19] Wilkins A.K., Tidor B., White J., Barton P.I., "Sensitivity Analysis for Oscillating Dynamic Systems", Siam J. Sci. Comput., 31, 2009, pp.2706-2732.

[20] Jolma I.W., Ni X.Y., Rensing L., Ruoff P., "Harmonic Oscillations in Homeostatic Controllers: Dynamics of the p53 Regulatory System", Biophysical Journal 98, 2010, pp.743–752.

[21] Kaplan, I. Gabay, G. Sarafian, D. Sarafian, "Biological applications of the "Filtered" Van der Pol oscillator", Journal of the Franklin Institute, 345, 2008,226-232.

[22] Abdelaziz T.H.S.,"Robust pole assignment for linear time-invariant systems using state-derivative feedback", Proceedings of the Institution of Mechanical Engineers, Part I: Journal of Systems and Control Engineering, 223, 2009, pp.187-199.

[23] Özgören M.K., "An algebraic method for designing controllers for multi-input multi-output linear systems via s-domain input-output decoupling", Proceedings of the Institution of Mechanical Engineers, Part I: Journal of Systems and Control Engineering, 223, 2009, 263-274.

[24] Gross B. and Braga E.P., Singularities of Linear System Functions, Elsevier Publishing, New York, 1961.

[25] Bayat F.M. and Ghartemani M.K., "On the essential instabilities caused by multi-valued transfer functions", Math. Problems in Engineering Article ID 419046, 2008, 13p.

[26] Kaveh P., Ashrafi A. and Shtessel Y.B., "Robust Sliding Mode Harmonic Oscillator Suitable for Low Frequencies", System Theory, SSST '05 Proceedings of the Thirty-Seventh Southeastern Symposium, 2005, pp.249-252.

[27] Xue D., Chen Y.Q., Atherton D.P., "Linear Feedback Control Analysis and Design with MATLAB", Society for Industrial and Applied Mathematics, Philadelphia, 2007.

BIOGRAPHIES

BARIS BAYKANT ALAGOZ was graduated from University of Istanbul Technical University department of Electronics and Communication Engineering in 1998. He worked for Alcatel Microelectronics and Turkish Telecom for several years. He is following PhD at Inonu University department of Department of Electrical-Electronics Engineering.

HAFIZ Z. ALİSOY was graduated from Moscow Technical University department of Electro-Physics Engineering 1982. He had his PhD degree from USSR Science Academy Physics Institute of P.N. Lebedyev and Doctor of Sciences degree (DSc) from International Ecology-Energy Academy. He became as Full Professor in 1995. He received award of Young Scientist. He works at Namık Kemal University, Department of Electronics and Telecommunication Engineering.

Active Power Filter in a Transformerless Grid Connected Photovoltaic System

B. Boukezata, A.Chaoui, J P. Gaubert, and M. Hachemi

***Abstract*—This paper presents a transformerless grid-connected photovoltaic (PV) with active power filter functions. It compensates for the reactive and injects active power demanded by nonlinear loads simultaneously; the developed PV array model may be directly connected to dc-side of the voltage source inverter with Direct Power Control Algorithm used for grid PV interaction. The system presents increased efficiency when compared to the conventional systems. Simulation results are provided to demonstrate the effectiveness of the proposed system.**

***Index Terms*—Direct Power Control, Active Power Filter, PV, P&O**

I. INTRODUCTION

THE global energy consumption is increasing by leaps and bounds to improve the living standards of mankind's worldwide. However, the conventional fossil fuels which are the primary sources of electric power so far are on the verge of extinction. Also, the extensive use of fossil fuels and nuclear resources causes the serious environment pollution and safety problems. Due to above mentioned facts, world is turning towards environmentally clean and safe renewable energy sources such as PV, wind, fuel cells, etc. [1].

Photovoltaic (PV) energy has great potential to supply energy with minimum impact on the environment, since it is clean and pollution free [2], and it is a suitable choice for a variety of applications mainly due to its capability to be directly converted to electrical energy using solar cells. This useful energy is supplied in the form of DC power from photovoltaic arrays (PV) bathed in sunlight and converted into more convenient AC power through an inverter system [3].

The grid-connected PV system supplies the active power from the PV array to the grid via an inverter. Today, non-linear loads are widely used in residential and office buildings. If the grid-connected PV system is applied to non-linear loads, the power quality is relatively poorer, because of the active power supply by the PV array.

B. BOKEZATA is with the Department of Electrical and Engineering, University of Setif 1, Setif, Algeria (e-mail: bboukezata@yahoo.com)

A.CHAOUI, is with the Department of Electrical and Engineering, University of Setif 1, Setif, Algeria (e-mail: abdelmadjid.Chaoui@ext.univ-poitiers.fr).

J P. GAUBERT, is with the Department of Electrical and Engineering, University of Poitiers, France (e-mail: jean.Paul.Gaubert@univ-poitirs.fr).

M. HACHEMI, is with the Department of Electrical and Engineering, University of Setif 1, Setif, Algeria (e-mail: hacemimabrouk@yahoo.fr)

To solve this problem, the grid-connected PV system should not only supply active power to the system via MPPT, but also improve the power quality (low THD and unity power factor) [4].

In this paper, a transformerless grid-connected photovoltaic (PV) system with a direct power (active and reactive) control algorithm is proposed. This system increases the conversion efficiency (Single stage PV system) and operating as power supply as well as harmonic and reactive power compensator when the sun is available. At low irradiation, the system operates only as harmonic and reactive power compensator (Active Power Filter). The aim is that the system can operate as an inverter of distributed generation or/and as a shunt APF independently or simultaneously .In order to verify the proposed system. The PV system is simulated using Simpower of MATLAB/Simulink.

II. SYSTEM CONFIGURATION

The system that has been simulated consists of a photovoltaic array connected through a DC bus to a three-phase inverter that is connected to a grid through a simple filter and nonlinear load, as shown in Fig. 1.The MPP tracker is integrated in the inverter control (Fig.3), as there is a one stage Grid connected PV system. The inverter is used to transfer the power from PV module, it also assure the compensation of the harmonic currents, reactive power and unbalanced current. The load is represented by three phase of rectifier with R L load.

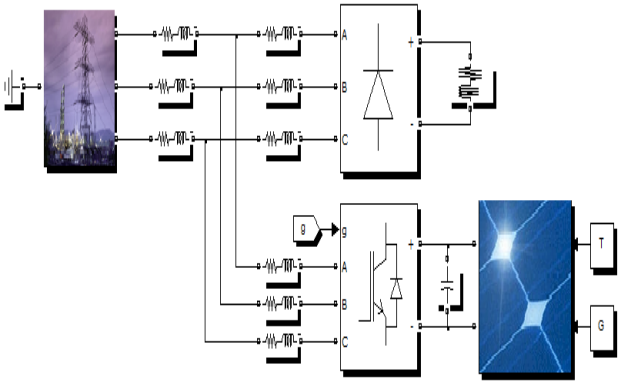

Fig. 1.Three-phase grid connected to the PV module

III. PV ARRAY MODEL

The PV array used in the proposed system is MSX60 and it is simulated using a model based on [5]. In this model, a PV cell is represented by a current source in parallel with a diode and a series resistance as shown in Fig. 2(a). The basic current equation is given in the following equation:

$$I = I_{pv,cell} - I_{o,cell}\left[\exp\left(\frac{qv}{akT}\right)-1\right] \quad (1)$$

where I_(pv,cell) is the current generated by the incident light (directly proportional to sun irradiation), I_(o,cell) the leakage current of the diode, q the electron charge 1.60217646e10_19 C, k the Boltzmann constant, T the temperature of the PN junction, and a is the diode ideality constant. But practically the PV array comprised with many PV cells connected in series and parallel connection. This makes some additional parameters to be added with the basic Eq. (1). The modified equation is shown in the following equations:

$$I = I_{pv} - I_o\left[\exp\left(\frac{V+R_sI}{V_ta}\right)-1\right] - \frac{V+R_sI}{R_p} \quad (2)$$

$$I_{pv} = \left(I_{pv,n} + K_I\Delta_T\right)\frac{G}{G_n} \quad (3)$$

A practical PV array consists of several connected PV modules formed by Ns solar cells connected in series and parallel. Therefore, (1) which presents a single PV cell should be amended into (4) to represent a PV array [6].

$$I = N_{pp}I_{pv} - N_{pp}I_o\left[\exp\left(\frac{V+IR_s\left(N_{ss}/N_{pp}\right)}{V_taN_{ss}}\right)-1\right] - \frac{V+IR_s\left(N_{ss}/N_{pp}\right)}{R_p\left(N_{ss}/N_{pp}\right)} \quad (4)$$

Where:

N_{pp} is the number of PV modules connected in parallel;

N_{ss} is the number of PV modules connected in series.

The PV model is simulated using Solarex MSX60, 60W PV module. The simulated I-V and P-V characteristics of the Solarex PV module at constant temperature and varying insolation are shown in Fig. 2(b) and Fig. 2(c) respectively.

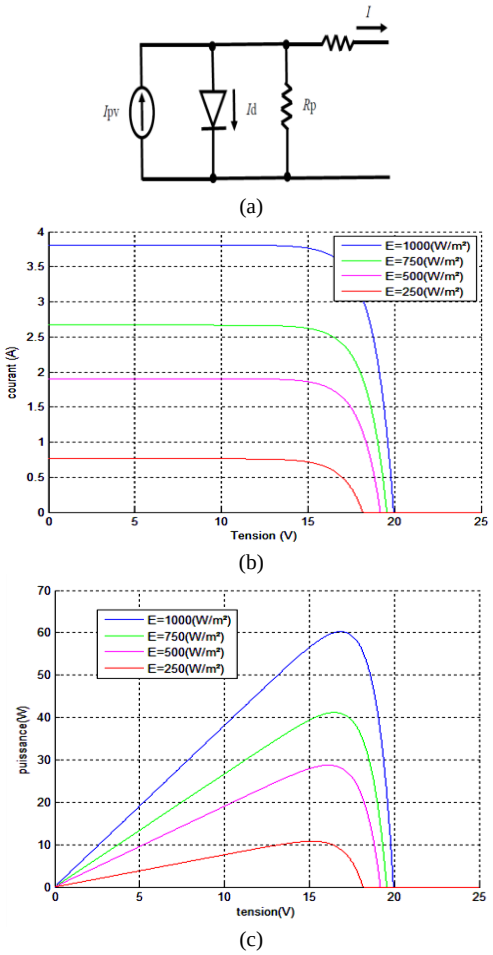

Fig. 2 (a) Equivalent circuit of a PV cell, (b) I-V characteristics, (c) P-V characteristics

IV. MPPT CONTROLLER

Most of the MPPT implementations for photovoltaic inverters output either a dc-link voltage reference to the inverter, or a duty cycle reference to a DC/DC converter depending on the system topology.P&O method is one of the popular methods to track the maximum-power point and probably the most frequently used in practice, mainly due to its easy implementation. [7,8]. The working principle of P&O is depicted by the flow chart in Fig. 3.

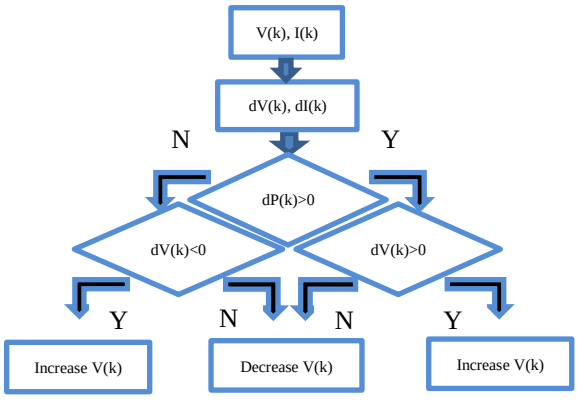

Fig. 3 P&O Flow Chart

V. Active Power Filter

Active power filters (APF) are basically power electronic devices that are used to compensate the current or voltage harmonics and the reactive power flowing in the power grid. The APF may be used as a controlled current source and it has to supply a current wave as close as possible to current reference. [10].

The basic compensation principle of APF is explained in Fig. 4.

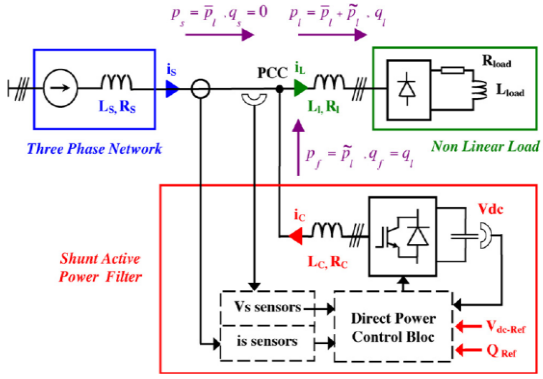

Fig. 4 Shunt active power filter configuration

A. Direct Power Control

The bloc scheme in Fig. 5 gives the configuration of direct power control where the commands of reactive power (set to zero for unity power factor) and active power pref (delivered from the outer integral-proportional (IP) DC voltage controller) are compared with the calculated ps and qs values given by (5), in reactive and active power hysteresis controllers, respectively.

$$s_s = ps + jqs$$

$$ps = vsa \cdot isa + vsb \cdot isb + vsc \cdot isc$$

$$qs = \frac{1}{\sqrt{3}}\left[\left(vsa - vsc\right) isa + \left(vsc - vsa\right) isb + \left(vsa - vsb\right) isc\right] \quad (7)$$

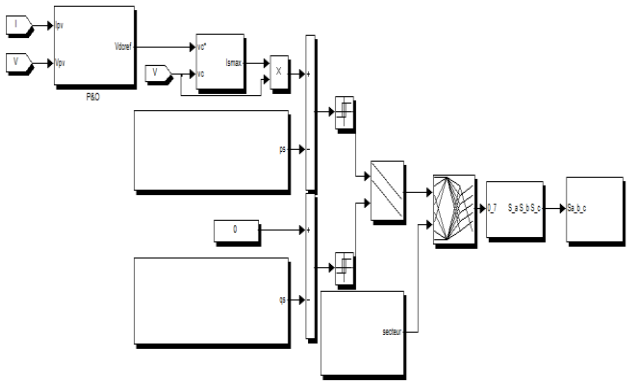

Fig. 5 bloc scheme of DPC with source voltage sensors

The digitized variables d p ,d q and the line voltage vector position θ p = tan-1 (V s β / V s α) form a digital word, which by accessing the address of lookup table selects the appropriate voltage vector according to the switching table. For this purpose, the stationary coordinates are divided into 12 sectors, as shown in Fig. 6, and the sectors can be numerically expressed as:

$$\left(n-2\right)\frac{\pi}{6} \le \theta_n \le \left(n-1\right)\frac{\pi}{6}\, n = 1, 2, ..., 12. \quad (8)$$

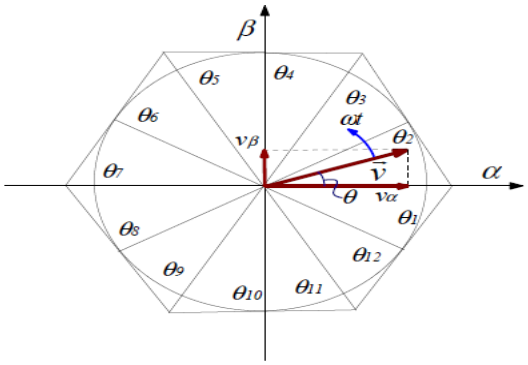

Fig. 6 Sectors on stationary coordinates

The digitized error signals d p, d q and digitized voltage phase θ n are input to the switching table in which every switching state S a ,S b and S c of the converter is stored, as shown in Table 1. By using this switching table, the optimum switching state of the converter can be selected uniquely in every specific moment according to the combination of the digitized input signals. The selection of the optimum switching state is performed so that the power errors can be restricted within the hysteresis bands [9].

TABLE I
SWITCHING TABLE

dp	*dq*	*Θ1 Θ2 Θ3 Θ4Θ5 Θ6 Θ7 Θ8Θ9 Θ10Θ11Θ12*
1	0	101 111 100 000 110 111 010 000 011 111 001 000
1	0	111 000 111 000 111 000 111 000 111 000 111 000
0	0	101 100 100 110 110 010 010 011 011 001 001 101
0	1	100 110 110 010 010 011 011 001 011 101 101 100

VI. Results and Discussion

In Matlab/SIMULINK environment; a SimPower Systems based model has been developed to simulate the behavior of the controlled APF.

Figures 7 a, b, c and d show the dynamic response of the system with the PV system under different variations of the irradiation.

Fig. 8 shows that the dc bus voltage across the grid interfacing inverter is maintained at constant level in order to keep good functionality of the inverter and to facilitate the active power flow.

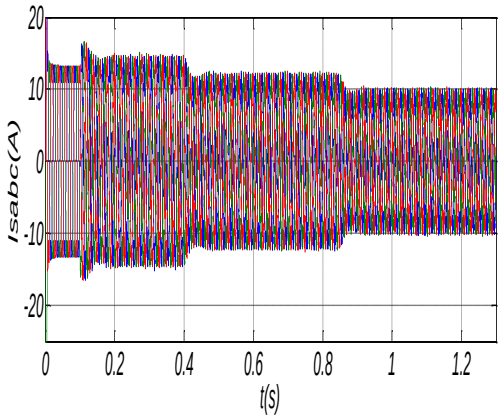

(a) Sources currents.

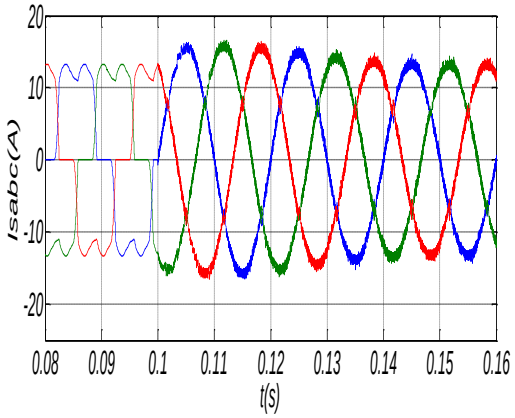

(b) Sources currents, Filter switched on at 0.1s.

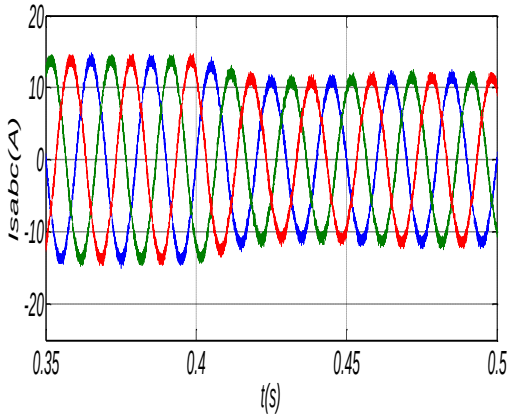

(c) Sources currents, Insolation variation on at 0.4s.

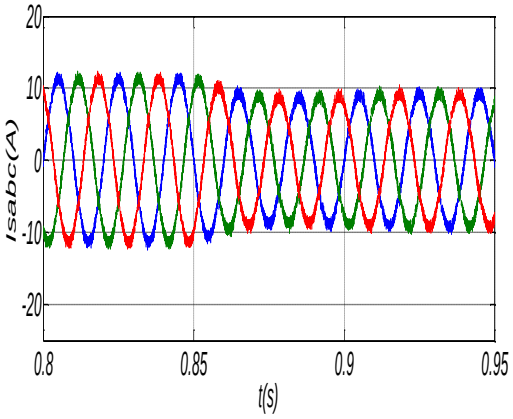

(d) Sources currents, Insolation variation on at 0.85s

Fig. 7 Dynamic response of the system under different variations of the irradiation (a, b, c and d)

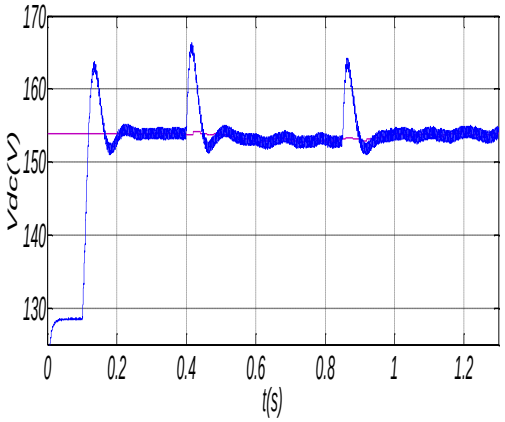

Fig. 8 DC Bus Voltage

In Fig. 9 we can see that the active power followed its nominal value and decreased when the PV system supplies the active power to the load. The reactive power becomes null when the active filter is activated at 0.1s as well as when the insolation is changed (0.4 and 0.85 s).

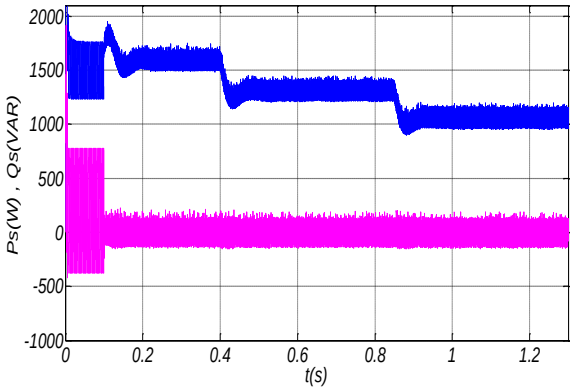

Fig. 9 Active and reactive powers source

Fig. 10 illustrates the FFT result of the grid current after the switch of APF (26.29%).and before (3.24 %), and when the PV supplies the power, the total harmonic distortion (THD) of the grid current is 4.78%.

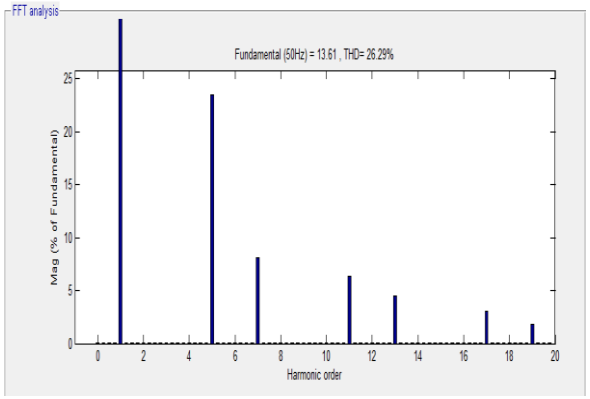

(a)

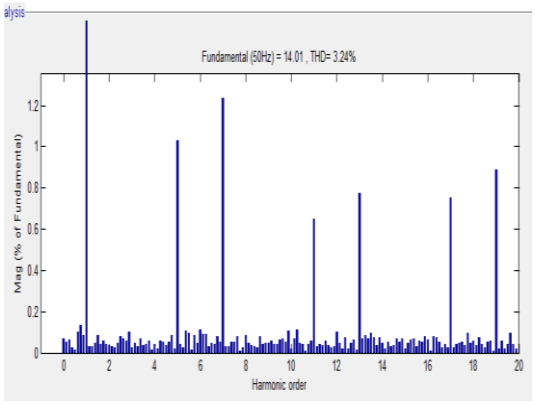

(b)

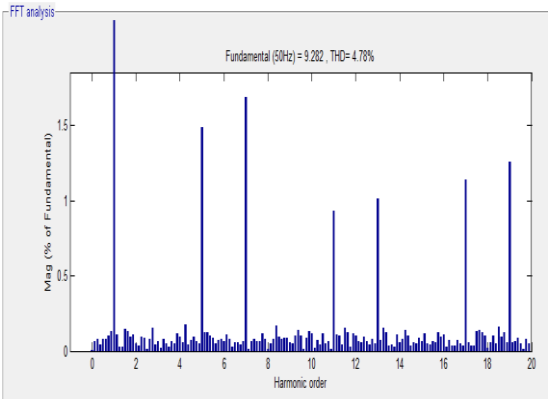

(c)

Fig. 10 a, b, c A grid current THD at steady-state

VII. CONCLUSION

This paper presents a behavioral model and control of a Grid-PV system with active power filter functioning suitable for changing atmospheric conditions. The Solarex MSX60, 60W PV module is used for simulation that has 36 series connected polycrystalline cells. The PV system is developed using one string having 9 series connected PV modules. A DPC for APF has been presented. One can see that the control algorithm is simple, it has a good dynamics, and it offers sinusoidal line currents (low THD). Simulation results verify the performance of the combined PV–APF and the P&O MPPT method.

VIII. ACKNOWLEDGMENT

The study is selected from 1st International Conference on Electrical Energy and Systems October 22-24th

REFERENCES

[1] R. D. Patidar , S. P. Singh and D.K. Khatod , "Single-Phase Single-Stage Grid-Interactive Photovoltaic System with Active Filter Functions", in Power and Energy Society General Meeting IEEE, July 2010, pp.1-7.

[2] M.C. Cavalcanti, G.M.S. Azevedo, B.A. Amaral, and F.A.S. Neves", Unified Power Quality Conditioner in a Grid Connected Photovoltaic System ", Electrical Power Quality and Utilization Journal, Vol.12, No.2, 2006, pp. 59-69.

[3] A.R. Reisi, M.H. Moradi and H. Showkati, "Combined Photovoltaic and Unified Power Quality Controller to Improve Power Quality", Solar Energy, Vol. 88, 2013, pp.154–162.

[4] S.W. Lee, J.H. Kim, S.R. Lee, B.K. Lee, and C.Y. Won", A Tranformerless Grid-Connected Photovoltaic System with Active and Reactive Power Control", In Power Electronics and Motion Control Conference, IPEMC '09, May 2009, pp.2178-2181.

[5] Marcelo GradellaVillalva, Jonas Rafael Gazoli, and Ernesto RuppertFilho, "Comprehensive Approach to Modeling and Simulation of Photovoltaic Arrays", IEEE Transactions on Power Electronics, Vol 24, pp.1198-1208 .

[6] Atiqah Hamizah Mohd Nordin, Ahmad Maliki Omar, "Modeling and Simulation of Photovoltaic (PV) Array and Maximum Power Point Tracker (MPPT) for Grid-Connected PV System", 3rd International Symposium & Exhibition in Sustainable Energy & Environment, 2011, pp.114-119.

[7] J.M. Enrique, J.M. Andu jar, M.A. Bohorquez " A reliable, fast and low cost maximum power point tracker for photovoltaic applications " in Solar Energy 84, 2010, pp.79–89.

[8] E.S. Sreeraj, K. Chatterjee and S. Bandyopadhyay" One-Cycle-Controlled Single-Stage Single-Phase Voltage-Sensorless Grid-Connected PV System, "IEEE Transactions On Industrial Electronics, Vol.60, No.3, 2013, pp.1216-1224.

[9] A. Chaoui, J.P Gaubert, F. Krim, "Power quality improvement using DPC controlled three-phase shunt active filter", in Electric Power Systems Research 80, 2010, pp.657–666.

[10] R. Lohde and F. W. Fuchs, "Improved DPC Method of VSC to Fulfill Low Voltage Ride Through Requirements in Wind Power Applications", 14th International Power Electronics and Motion Control Conference, EPE-PEMC, 2010, pp.T12-35-T12-42.

BIOGRAPHIES

BOUALEM BOUKEZATA was born in Setif, Algeria, on December 23, 1987. He received the License and Master degrees in electrical engineering from the University ofSetif 1, in 2009 and in 2011, respectively.
He is currently working toward the Ph.D. degree in the Department of Electrical and Engineering, University of Setif 1, Setif, Algeria.
His main research interests are analysis, simulation, and design of power converters, circuit and systems for renewable energy sources, and power quality systems (Active Power Filter).

ABDELMADJID CHAOUI was born in Algeria in 1968. He received the Engineering and Master's degrees in electrical engineering from Sétif University, Algeria, in 1990 and 1996 respectively. In 2010, He obtained the PHD degree in Power Electronic and control from Sétif and Poitiers universities', Algeria and France respectively.
He is currently an assistant Member Professor at the Department of Electrical Engineering, University of Setif1, Algeria. Member of Power Electronic and Industrial Control Laboratory, Setif 1 University. His main research interests are Power Electronics control applied to Renewable Energy and Power Quality systems.

JEAN-PAUL GAUBERT, He received the Engineer's degree from the University of Clermont-Ferrand, France, in 1988, the M. Sc. and the Ph.D. degrees from the University of Science and Technology of LILLE, France, in 1990 and 1992, respectively, all in Electrical Engineering. He is actually Professor with the Automatic Control and Industrial Data Processing Laboratory (LAII), Poitiers National School of Engineering (ENSIP), University of Poitiers, France. His current research interests are modeling and advanced control of power converters and power electronics systems and their digital control techniques. The derived topics deal with power quality such as active power filters, PWM rectifiers or renewable energy systems. He is a member of IEEE and EPE association.

HACHEMI MABROUK, was born in Setif (Algeria), on May 08th, 1955. He received his engineering from the University of Oran (Algeria) in 1981 and the magister degrees from the University of Setif (Algeria) in 1992, all in Electrical Engineering. He received his Ph.D. degree from the University of Setif (Algeria) in Electrical Engineering in 2007. He was a professor at the Department of Electrical Engineering University of Setif 1, since 1984. His main research interests are: analysis, simulation and design of electrical machines, energy storage systems and renewable energy.

Dielectric Properties of Triaxial Porcelain Prepared Using Raw Native Materials Without Any Additions

S. Kitouni

Abstract— **in this study, production of porcelain, for the ceramic dielectric applications by using inexpensive natural raw materials or waste materials was undertaken. The principal raw materials of porcelain, such as kaolin, feldspar, and quartz, are relatively inexpensive and readily available. The raw materials used in this study were collected from Algerian source (Kaolin was from Debagh deposit, Quartz from El Oued city and Feldspar from Ain Barbar deposit). The basic electro-porcelain composition was selected consisting of 37% kaolin, 35% potash-feldspar and 28% quartz. The samples synthesized were characterized by X-ray diffraction (XRD) technique.**

The dielectric properties of porcelain bodies prepared without the incorporation of mineralisers or metal oxides, e.g. dielectric constant, dielectric loss tangent (tan δ) and loss factor, were investigated. Dielectric measurements have been carried out at 1 KHz in the temperature range ambient Temperature – 200°C. The dielectric constant ε' and dielectric loss tangent tan δ respectively of porcelain samples sintered at the most proper sintering temperature 1200°C were about 21.22 and 0.006. The value of dielectric constant is higher as compared to conventional porcelain which not exceeds generally 9.

Index Terms— **Dielectric constant, dielectric loss tangent, dielectric loss, feldspar, kaolin, quartz, porcelain,**

I. INTRODUCTION

THE electric power industry tends to develop extra high voltage, large capacity and long distance transmission, the electric porcelain is required. An advantage of electric porcelain over other insulating ceramic materials is the fact that it enables one to make large size high-voltage insulators of a complex configuration. Electro porcelain can be classified as follows based on its purpose and properties: normal high-voltage porcelain used in the production of high-voltage line and apparatus insulators; high-voltage porcelain with an increased quartz content used to make high-voltage apparatus insulators with improved electromechanical properties; high-voltage alumina porcelain for high-voltage apparatus insulators with elevated mechanical strength; low-voltage porcelain used in the production of insulators and insulating parts for plants up to 500 V generating direct and alternating current and weak current plants [1]. It has been estimated that more than 20% of the total outlay for a typical transmission and/or distribution system of electric energy is spent on insulation alone and prominent among them is porcelain [2]. The utilization of ceramic materials as electrical insulators goes back until 1850 when Werner von Siemens introduced in the construction of electrical air lines the use of electrotechnical porcelains. During this long period of time it has been realised that several characteristic properties of porcelain (e.g. mechanical strength, high-power dielectric strength and corrosion resistance) as a ceramic product cannot be obtained in other materials. Today, the growing demand for porcelain in the field of electrical engineering, caused by the importance of electric energy in modern society, motivates many research projects in order to obtain the best properties for the requirements and applications of porcelain insulators [3]. Basically porcelain is an insulator but the rise of temperature as example may damage its insulation property due to decrease in its resistivity and the porcelain body may be employed as conductor [4].

Electrotechnical porcelain is a clever compromise between electrical, thermal and mechanical resistances. Improving performance characteristics of the electrical porcelain involves the updating of its production technology. The characteristics of porcelain insulators depend to a marked degree on the percentage composition of the mixture, sources of the mixture and method of manufacture. The production of electrotechnical porcelain is based predominately on natural raw materials. To this end, kaolin-feldspar-quartz triaxial porcelain was prepared from locally available raw materials and characterized. The characterisation is aimed at comparing the electrical properties of the triaxial porcelain with those of others works and hence explores the possibility of local substitution of the imported variety which is the subject of a future research.

II. EXPERIMENTAL PROCEDURE

A. Raw materials

The raw materials used in the preparation of the triaxial electrical porcelain are kaolin, feldspar, and quartz (in the form of silica sand). The raw minerals used in the present investigation were taken from different deposits in Algeria. The sources of the raw materials and their chemical composition are shown in table 1. This study investigates a

S. KITOUNI, is with the Physics Department, Constantine 1 University, Constantine, 25000, ALGERIE. (e-mail:souad0714@yahoo.fr).

unique porcelain type percentage composition of Kaolin, 37: feldspar, 35: and quartz, 28.

B. Apparatus and Procedure

We attempt to make samples of electro technical porcelain from the local raw materials. The technological process of electro porcelain production consisted of several stages: preparation, combination, and mixing of the initial raw materials in the required proportions; formation of an article with the required shape from powder (mix); heat-treatment (sintering). The samples obtained consisted of 13 mm in diameter cylinders. The samples were prepared by the dry process technique and fired at a temperature of 1200°C with a soaking time of 2 hours for proper sintering. To avoid spurious effects and in order to create a conduction path for electrical measurements on the samples, samples were electroded with silver paste on the top and bottom faces. Electrodes were fired at 300 °C for 20 mn with a heating rate of 5 °C/min. All measurements were undertaken at range temperature 20-190°C on a LCR meter connected to a furnace heating rate of 5 °C/min) as shown in Fig. 1. Effective permittivity was calculated as measured capacitance multiplied by the geometrical factor of a sample. The dielectric constant was determined from the relation where C_0, is the capacitance of a two-electrode system with air as the dielectric, and C is the capacitance with the sample as a dielectric.

$$\varepsilon' = \frac{C}{Co} = \frac{Cl}{\varepsilon oA} \qquad (1)$$

$$\varepsilon'' = \varepsilon' \tan \delta \qquad (2)$$

Where l is the thickness of the sample, A is the effective area between the electrodes and ε_0 is the free space permittivity.
The dielectric loss tangent (tanδ) was measured directly from the instrument.

TABLE I
THE SOURCES AND CHEMICAL COMPOSITION OF THE RAW MATERIALS

Mineralogical Name	chemical composition	Source
Kaolin	$Al_2O_3.2SiO_2.2H_2O$	Debagh deposit
Feldspar	$K_2O.Al_2O_3.6SiO_2$	Ain Barbar deposit
Quartz	SiO_2	El Oued

III. RESULTS

The dielectric constant (ε') of the sintered bodies as a function temperature measured at 1 KHz is shown in Fig. 2. The dielectric constant remains fairly constant in the ambient - ~100 °C, thereafter increases gradually. The dielectric constant is almost constant at low temperatures and the dielectric constant dependence increases with increasing temperature. It is interesting to note that as the temperature increases the dielectric constant increases. The increase in dielectric constant temperature is one of the features of normal dielectrics. The rise in ε' is ascribed to the dc conductivity effect [5]. The electrical properties of the samples were determined beforehand. The room-temperature permittivity at 1 KHz is 21.22. Based on a mixture rule using various theories to predict the dielectric constants of materials, the dielectric constant of the composites was found to be 12~24. Prediction of the dielectric constants is considered on the basis of phases, shape of phases, and porosity [6].

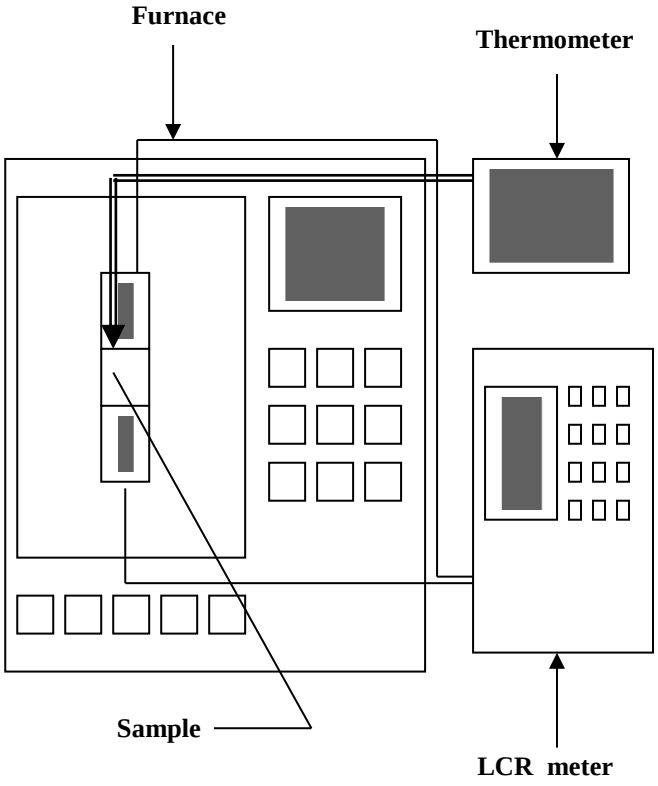

Fig. 1 Test setup for capacitance and dissipation factor

An increase of dielectric constant with increasing temperature results from polarization phenomena at grain boundaries and electrodes [7]. In ceramic materials, ions can be carriers to provide electrical conduction. The degree of conductivity is largely dependent on the energy barrier that must be overcome for the ion to move from one lattice position to the next. At low temperature, conductivity is low. However, if the temperature is high enough to overcome the barrier for lattice diffusion, the conductivity increases.
Other reason which can be given is some form of interactions between the dielectrics and Ag electrodes are responsible for the higher ε'. Moreover, the lattice defects formed could accelerate the mass transport process; the existence of lattice defects such as vacancies and interstitials in the structure aids conduction [5], further promoting grain growth. As is well known, the grain size will influence the dielectric constant [8]. Thus the insulator could be used, as capacitor bushings where low charge storage capacity is very desirable.
Dielectrics with dielectric constant above 12 are generally materials for capacitors and transducers. The ceramic capacitors are one of the most widely used discrete electronic

components that play a very important role in electronic industry. In the recent years, a rapid fast development in the ceramic capacitor technology has been achieved to meet the needs of advancement in microelectronics and communication. It is envisaged that more applications of ceramic capacitors will be found in future [8]. The porcelain sample is suitable for this application in the present form because of the higher dielectric.

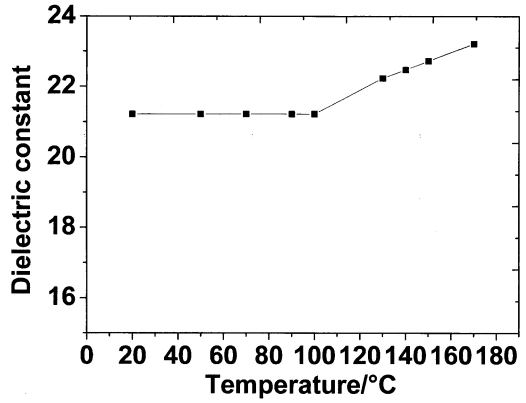

Fig. 2 Temperature versus dielectric constant for samples sintered at 1200 °C for 2 h

The dielectric loss factor (ε") of the sintered bodies as a function temperature measured at 1 KHz is shown in Fig. 3. A similar trend is observed with ε'.

The increase of ε" with temperature can be explained by the relaxation phenomenon which is divided into three parts, conduction losses, dipole losses and vibration losses [9].

At low temperatures conduction losses have minimum value. As the temperature increases ε" conductivity increases and so the conduction losses increase. As a result increase the value of ε" with increasing temperature.

The dielectric loss tangent (tan δ) of the sintered bodies as a function temperature measured at 1 KHz is shown in Fig. 4. Variation of dielectric loss tangent (tan δ) as a function temperature at 1 KHz the samples under study is consistent with the ε' behaviour as shown in Fig. 2 of the corresponding samples.

The room-temperature dielectric loss tangent is 0.006. In the dielectric materials, defects, space charge formation, lattice distortions, etc., in the boundaries could produce absorption current resulting in tan δ [10]. The dielectric loss tangent and dielectric constant of samples increase with increasing temperature. The electron part of polarization in an ionic crystal decreases with increasing temperature due to decreasing density of the material, and the ionic part of polarization is affected by two opposite factors: decreasing density and weakening of elastic bonds, which cause a decrease in the elastic bond coefficient. The dielectric constant of ionic cubic crystals with increasing temperature grows relatively little and is nearly linearly [6].

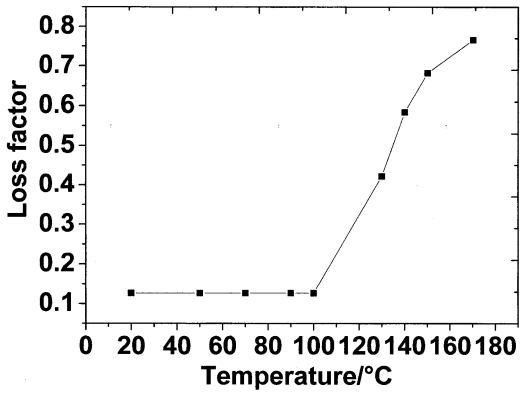

Fig. 3 Temperature versus loss factor for samples sintered at 1200 °C for 2 h

The porcelain body is composed of phases such as mullite, quartz and glass. Its electrical properties are dependent on the properties of each of these phases, both at room and at elevated temperatures. Besides, microstructural characteristics, such as crystal size and size-distribution also contribute to the electrical properties of the body because they influence the passage of current through the body. X-ray structural analysis (DRX) showed the presence of mullite, separated quartz and a glassy phase in the samples. The DRX was elaborated in an earlier paper [11]. In this study, the glassy phase is derived from the potash feldspar and quartz component in the porcelain composition. Glass phase has a dominant influence on electrical and dielectric properties of fired ceramics. These properties are determined by the concentration and mobility of K^+ and /or Na^+ ions in this phase [7]. In the presence of the large amount of glassy phase in the structure [11], the mobile ions such as K^+ finds an easy path to move and hence increases the conductivity [5]. It is known that the dielectric constant of porcelain increases in presence K^+ and Na^+ cations and decreases when they are replaced by Ca^{2+}, Mg^{2+}, and Ba^{2+} cations [12]. On the other hand mullite, which is a crystalline phase, has a vital role on electrical properties. As the matrix of the ceramic sample is clay matrix or the glassy phase, mullite maintain the stress level in a higher order as just in a composite matrix [13].

In addition mullite behaves like semiconductor at high temperature. The band gap energy (E_g) of mullite is 1.43 eV and this value is in the semiconductor interval [12]. Mullite crystal has inherent defect centres as 0^{2-} ion vacancy in its structure and it is a potential ionic conductor.

Substitution of Al^{3+} ion in the (AlO_6) octahedral and (AlO_4) tetrahedral sites of mullite lattice by the transition metal ions, Mn^+ can make it n- type (if n > 3) and p-type (if n < 3) electronic conductor.

Apart from this, substitution of Al^{3+} ion by M^{n+} ion (if n=3) in the octahedral or tetrahedral position and only incorporation of M^{n+} ion in the interstitials or structural channels of mullite lattice can impart electrical conductivity in mullite [4]. In this study, the dielectric constant obtained in the present study is higher than the value for pure mullite (6.9) [14].

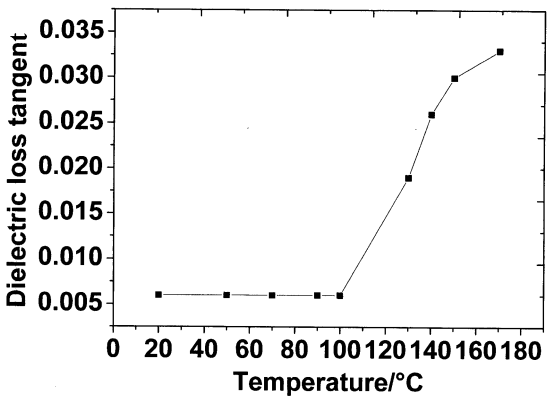

Fig. 4 Temperature versus dielectric loss tangent for samples sintered at 1200 °C for 2 h

IV. CONCLUSION

The present work is an attempt for the elaboration of alumino-silicate porcelain samples with simple techniques. The data obtained show that Local raw materials are quite suitable for fabricating electro technical porcelain. Based on the experimental results obtained in this study, using the locally available raw materials, electrical porcelain with good dielectric properties can be produced. This material can be used for dielectrics in commercial capacitor applications. Thus the insulator could be used, as capacitor bushings where low charge storage capacity is very desirable. The porcelain sample is suitable for this application in the present form because of the higher dielectric.

ACKNOWLEDGMENT

This study was conducted in the ceramics laboratory of physics department (Constantine 1 University, Constantine, Algeria).

REFERENCES

[1] Z. V. Kolpashchikova, E. V. Shcherbakova, N. S. Kostyukov, "Polarization processes in electrotechnical porcelain within a wide frequency range", Glass and Ceram., vol. 60, no.11-12, pp.370-373, 2003.

[2] L.U ANIH, "Characterization of Locally Sourced Kaolin-Feldspar-Quartz Triaxial Porcelain for Insulation Applications", Electric Power Engineering Conference (EPEC), June 2005.

[3] J.M.Amigo, J.V. Clause, E. Vicente, J. M. Delgado, M. M. Revento, L. E. Ochando, T. Debaerdemaeker, F. Martı, "X-ray powder diffraction phase analysis and thermomechanical properties of silica and alumina porcelains", J. of the Eur. Ceram. Soc., vol. 24, no.1, pp.75-81, 2004.

[4] S.P. Chaudhuri, P. Sarkar, A.K. Chakraborty, "Electrical resistivity of porcelain in relation to constitution", Ceram. Inte. vol. 25, no.1 pp.91-99, 1999.

[5] A. S. Demirkiran, R. Artir, E. Avci, "Electrical resistivity of porcelain bodies with natural zeolite addition", Ceram. Inter. vol. 36, no.3, pp.917-921, 2010.

[6] S.J. Hwang, Y.J. Kim, H.S. Kim, "La_2O_3–B_2O_3–TiO_2 Glass/BaO–Nd_2O_3–TiO_2 ceramic for high quality factor low temperature co-fired ceramic dielectric", J Electro. Ceram., vol. 18, no.1-2, pp.121-128, 2007.

[7] V. Tmovcova, I. Fura, F. Hanic," Influence of technological texture on electrical properties of industrial ceramics", J. of Phys. and Chem. of Sol. vol.68, no.5-6, pp.1135-1139, 2007.

[8] Ying-Chieh Lee, "Dielectric Properties and Reliability of $Zn_{0.95}Mg_{0.05}TiO_3$+0.25TiO_2 MLCCs with Different Pd/Ag Ratios of Electrodes", Int. J. Appl. Ceram. Technol.,vol. 7, no.1, pp.71-80, 2010.

[9] H. M. El-Malah, N. A. Hegab, Studies on a.c. properties of Ca1–xSrxTiO3 perovskites, J. Mater. Sci. vol.42, no.1, pp.332-336, 2007.

[10] G.B. Kumar, K. Sivaiah, S. Buddhudu, "Synthesis and characterization of ZnWO4 ceramic powder", Ceram. Inter. vol.36, no.1, pp.199-202, 2010.

[11] S.Kitouni, A. Harabi," Sintering and mechanical properties of porcelains prepared from Algerian raw materials", Cerâmica, vol.57, no.344, pp.453-460, 2011.

[12] V.P. Il'ina, "Feldspar material from Karela for electrical engeneering", Glass and Ceram., vol.61, no.5-6, pp.195-197, 2004

[13] R.A. Islam, Y.C. Chana, M. F. Islam, "Structure–property relationship in high-tension ceramic insulator fired at high temperature", Mat. Sci. and Eng. vol.B106, no.2, pp.132-140, 2004.

[14] V. Viswabaskaran, F.D. Gnanam, M. Balasubramanian, "Mullite from clay–reactive alumina for insulating substrate application", Applied Clay Sci. vol.25, no.1-2, pp.29-35, 2004.

BIOGRAPHIES

S. KITOUNI received Ph.D. degree in physics from the University of Constantine, Algeria in 2013. Her current research interests are dielectrics. Participate in some international conferences in Algeria.

A New PID Tuning Method Based on Transient Response Control

S. E. Hamamci

***Abstract*—In this paper, an efficient PID tuning method for stable, unstable and integrating systems with time delay is introduced. The presented method is based on shaping the transient response of the two-degrees of freedom closed-loop system according to the performance specifications determined before the design. This method gives explicit tuning formulae in terms of plant model parameters and two design parameters which are used to shape the transient response. A graphical optimization technique for tuning of the PID parameters is also introduced. Illustrative examples are given to demonstrate the performance of the method. Significant improvement is provided in comparison with some previous methods.**

***Index Terms*— Time Delay, PID Control, Transient Response Control, Settling Time, Overshoot.**

I. INTRODUCTION

SYSTEMS with energy storage cannot respond instantaneously and exhibit transient responses in the time domain whenever they are subjected to inputs or disturbances. In many practical cases, the performance characteristics of the control systems are described in terms of transient response specifications. The most significant specifications are settling time (t_s) and maximum overshoot (M_p) [1, 2].

It is a very important specialty for a control method to design the control system providing the target performance specifications. The design of controller which results only the desired transient response is called as transient response control. Although good transient response is one of the most significant requirements for the control system design, there are very few results dealing with the transient response control in the literature [3]. Hauksdóttir [4] pointed out that the analytical expressions of transient responses can be obtained if the poles of the transfer function are all real, negative, and distinct. It was also shown that these formulae in closed form can be used to determine the zeros that result in minimum transient time. Jung *et al* [5] and Goodwin *et al* [6] found some limitations on transient response in terms of poles and zeros of the system. An interesting result was also reported by Leon de la Barra [7] who has shown that there are some relations between the nonminimum phase zeros and the case of undershooting [3]. The transient response control studies considered in these methods entirely deal with the relation between the transient response specifications and the poles/zeros of the characteristic polynomial. However, there is a different approach on this topic based on certain relationships between transient response specifications and coefficients of the characteristic polynomial. At first, these relations were introduced by Graham and Lathrop [8] in 1953. They proposed ITAE (Integral Time Absolute Error) standard form method which gives the different forms for each order of characteristic polynomial. This is very inconvenient when the order varies in the course of design [9]. To improve the control system response, a standard form with less oscillation and overshoot was given by Kessler [10]. The control system designed by "Kessler canonical form" is more stable than the ITAE form and has the overshoot of 8% in the unit step response. In addition to these previous forms, various standard forms such as ITSE (Integral Time Squared Error) form [11] and ISTE (Integral Squared Time Error) form [12] which give more successful time domain responses have been proposed recently. However, it is not possible to design the closed loop systems by these methods according to the transient response specifications which are specified prior to the design. In 1969, Naslin [13] observed empirically that the step response of all-pole systems of various orders remains essentially unchanged provided that the coefficients of the characteristic polynomial satisfy certain relationships. Thus, Naslin obtained the explicit formulae between the performance specifications and the coefficients of characteristic polynomial [3, 14]. Using the Naslin's relations, an important contribution in this regard was presented by Manabe [15] who proposed a new control technique, namely Coefficient Diagram Method (CDM), for the linear time-invariant control systems. The most important properties of this method are adaptation of the polynomial representation in the design methodology, use of the two-degrees of freedom (2DOF) control system structure and utilization of Standard Manabe form for obtaining of a unit-step response without overshoot. Furthermore, determination of the desired settling time at the start is another significant feature of the CDM. This is a major advantage which guides to the designer in his design [15, 16]. For the time delay systems, however, Manabe's method is ineffective to obtain the desired transient response. The obtained transient response does not meet the specified settling time value and non-overshooting property because of the time delay element [16]. As a result of this problem, a modification on the CDM technique is needed.

S. E. HAMAMCI is with the Department of Electrical-Electronics Engineering Department, Inonu University, Malatya, Turkey (e-mail: serdar.hamamci@inonu.edu.tr).

In this study, the results of the CDM which has been successfully applied to the linear time-invariant systems are generalized to the case of time delay systems. Since the CDM gives the higher order polynomial controllers whose degrees depend on the degree of the system, a methodology to design the fixed and lowest order controllers as possible such as PID controllers for time delay systems is considered. A new PID tuning method is proposed to achieve the desired settling time and maximum overshoot values which are determined in advance of the design. To achieve this, the first-order plus time delay (FOPTD) model of the stable, integrating or unstable plant is used. Using the 2DOF control system structure, an extra feedforward controller is designed to provide the better closed loop performance focusing on both tracking the desired reference signal and disturbance rejection. This extra controller is tuned in terms of the PID controller. This is an important advantage of the proposed method because the main controller and the extra feedforward controller in other methods are tuned separately [17, 18]. Furthermore, a graphical optimization step is included for modifying the standard Manabe form values to obtain the closed loop response which meets the transient response specifications determined before the design.

II. PID CONTROLLER DESIGN

A. 2DOF PID Control System Structure

A general form of the 2DOF control system is shown in Fig. 1 where $G(s)$ is the plant to be controlled, $C_f(s)$ is the feedforward controller and $C(s)$ is the main controller [20]. Successful reference input tracking and the disturbance rejection are provided if

$$C(0) = \infty, \quad C_f(0)/C(0) = 0 \tag{1}$$

imposes conditions on the controller. The most important result satisfying (1) are that $C(s)$ must contain an integrator and $C_f(s)$ must not. Thus, $C(s)$ can be chosen as

$$C(s) = K_p\left(1 + \frac{1}{T_i s} + T_d s\right) \tag{2}$$

in the form of classical PID controller and $C_f(s)$ is a controller satisfying (1).

The polynomial based CDM block diagram [15] is shown in Fig 2. In this figure, $N(s)$ is the numerator and $D(s)$ is the denominator polynomials of the plant transfer function. $B(s)$ and $F(s)$ are the feedback and reference numerator polynomials while $A(s)$ is the forward denominator polynomial

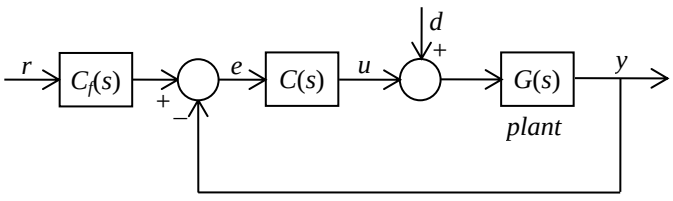

Fig. 1. Two-degrees of freedom control system structure (r: reference input signal, y: output signal, u: control signal, d: external disturbance signal).

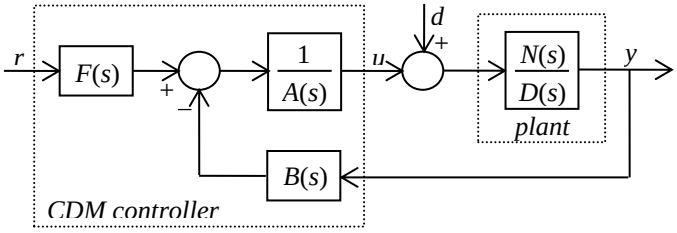

Fig. 2. The block diagram of the CDM control system.

of the controller transfer function. This controller transfer function with two numerators points to a 2DOF system structure. $A(s)$ and $B(s)$ are represented in the polynomial form

$$A(s) = \sum_{i=0}^{p} l_i s^i \quad \text{and} \quad B(s) = \sum_{i=0}^{q} k_i s^i \tag{3}$$

where p and q are the orders of the polynomials. The polynomial $F(s)$ is in fact a proportional controller and used to eliminate the steady-state error. The output equation of the control system in Fig. 2 is

$$y = \frac{N(s)F(s)}{P(s)} r + \frac{A(s)N(s)}{P(s)} d\,. \tag{4}$$

The characteristic polynomial, $P(s)$ is described by

$$P(s) = A(s)D(s) + N(s)B(s) = \sum_{i=0}^{n} a_i s^i\,, \qquad a_i > 0\,. \tag{5}$$

where n is the order of $P(s)$.

If the 2DOF control system structure in Fig. 1 is compared with the CDM control system in Fig. 2, it is clearly seen that $N(s)$ and $D(s)$ in Fig. 2 are the polynomials of $G(s)$ in Fig. 1. Similarly, $A(s)$, $B(s)$ and $F(s)$ in the CDM control system structure shown in Fig. 2 are the polynomials of $C_f(s)$ and $C(s)$ in Fig. 1. Therefore, $C(s)$ is expressed by $B(s)/A(s)$ and $C_f(s)$ have the form of $F(s)/B(s)$. From (1), $B(s)/A(s)$ can be chosen as the PID controller. The controller polynomials then must be chosen as

$$A(s) = l_1 s, \tag{6a}$$
$$B(s) = k_2 s^2 + k_1 s + k_0\,. \tag{6b}$$

Comparing (2) with (6a) and (6b), the parameters of the PID controller are simply obtained as

$$K_p = k_1/l_1, \quad T_i = k_1/k_0 \quad \text{and} \quad T_d = k_2/k_1. \tag{7}$$

B. Modeling

The most encountered model for the time delay systems is the FOPTD model whose transfer function is given by

$$G_m(s) = \frac{K}{T_1 s + T_0} e^{-\theta s} \tag{8}$$

where K is the gain, θ is the time delay and T_1 is the time constant. The value of T_0 in the model is equal to 1 for the stable processes, 0 for the integrating processes, and -1 for the

unstable processes. Many experimental identification techniques for the stable, unstable and integrating FOPTD models has been reported in the literature [21-23].

Since the CDM technique considers the transfer function of the plant as the ratio of two independent polynomials, the LTI dynamical model of the plant over a desired operating range should be chosen. Therefore, first order Pade approximation of the term $e^{-\theta s}$

$$e^{-\theta s} = (1 - 0.5\theta s)/(1 + 0.5\theta s). \quad (9)$$

is used. The first order approximation is compulsory to obtain PID controller because their higher number results more complex controllers. The simulation results show that the first order approximation for the time delay gives good results. Substituting (9) into (8), the equivalent LTI model is obtained as

$$G_m(s) = (-0.5K\theta s + K)/(0.5T_1\theta s^2 + (T_1 + 0.5T_0\theta)s + T_0) \quad (10)$$

Remark 2.1: For unstable time delay systems, the condition of $T_1 \neq 0.5\theta$ must be fulfilled to not occur pole-zero cancellations in the equivalent LTI model in (10).

C. Tuning the PID Controller

From (10), the polynomials of the equivalent LTI model are obtained as

$$N(s) = -0.5K\theta s + K \quad (11a)$$
$$D(s) = 0.5T_1\theta s^2 + (T_1 + 0.5T_0\theta)s + T_0 \quad (11b)$$

Replacing these polynomials and the controller polynomials in (6a-b) into (5), the characteristic polynomial depending on unknown controller parameters (k_i and l_i) is obtained. Then, selecting the CDM design parameters a target characteristic polynomial $P_{target}(s)$ is obtained. According to Manabe [15], the CDM design parameters are stability indices (γ_i) and equivalent time constant (τ) which are specified prior to the design [16].

The *equivalent time constant* which is defined as a measure of time response speed of the control system in the CDM is given as

$$\tau = a_1/a_0, \quad (12)$$

The equivalent time constant is related by the settling time. If τ is increased, t_s is also increased.

The *Stability indices* indicating the relative stability measure of the control system is described by

$$\gamma_i = \frac{a_i^2}{a_{i+1}a_{i-1}}, \quad i = 1\sim(n-1), \quad \gamma_0 = \gamma_\infty = \infty\,, \quad (13)$$

The stability index γ_1 in all indices is much effective on the overshoot. Bigger γ_1 results more relative stability and less overshoot.

For the stability indices, we make use of standard Manabe values in the CDM design. *Standard Manabe form* [15] is the closed-loop performance measure that gives a unit step response without overshoot and with desired settling time. To achieve this, Manabe proposes the values of the stability indices as follows

$$\gamma_i = \{2.5, 2, 2, \ldots\ldots, 2\} \quad i = 1\sim(n-1) \quad (14)$$

The choosing of these values gives the unit-step response without overshoot. When the Manabe's standard values are used, the relation between t_s and τ is obtained as

$$t_s \cong 2.5\tau \quad (15)$$

From (12) and (13), the coefficients a_i of $P(s)$ in (5) can be written as

$$a_i = \tau^i a_0 / \prod_{j=1}^{i-1} \gamma_{i-j}^j = Z_i a_0. \quad (16)$$

Thus, the coefficients of the $P(s)$ in (5) can be expressed in terms of τ and γ_i as

$$P_{target}(s) = a_0 \left[\left\{ \sum_{i=2}^{n} \left(\prod_{j=1}^{i-1} \frac{1}{\gamma_{i-j}^j} \right) (\tau s)^i \right\} + \tau s + 1 \right]. \quad (17)$$

Placing the chosen design parameters into $P_{target}(s)$ above and equating (5) with (17),

$$A(s)D(s) + N(s)B(s) = P_{target}(s) \quad (18)$$

is obtained. Assuming a_0=1 in (17) and solving this equation, the parameters of CDM controller are found as

$$l_1 = (\gamma_1^2\gamma_2\theta^3 + 2\tau\gamma_1^2\gamma_2\theta^2 + 4\tau^2\gamma_1\gamma_2\theta + 8\tau^3)/[4\gamma_1^2\gamma_2\theta(T_0\theta + 2T_1)]\,,$$
$$k_2 = (\gamma_1^2\gamma_2 T_1 l_1\theta - 2\tau^3)/(\gamma_1^2\gamma_2 K\theta)\,,$$
$$k_1 = (\tau + 0.5\theta - T_0 l_1)/K\,,$$
$$k_0 = 1/K\,. \quad (19)$$

Note that the proposed design method needs only two stability indices, γ_1 and γ_2. Finally, the PID controller parameters are obtained from (7).

The numerator polynomial *F(s)* which is described as a proportional controller is determined to be

$$F(s) = P(s)/N(s)|_{s=0} = P(0)/N(0) = 1/K\,. \quad (20)$$

In this case, any steady-state error occurring in the time response is reduced to zero. Finally, the feedforward controller in Fig. 1 is turned into

$$C_f(s) = \frac{F(s)}{B(s)} = \frac{k_0}{k_2 s^2 + k_1 s + k_0} = \frac{1}{T_i T_d s^2 + T_i s + 1}\,. \quad (21)$$

Remark 3.2: In this method, the designer does not need to make extra calculations for the feedforward controller. Because the parameters of $C_f(s)$ depend on the PID parameters directly as shown in (21).

D. Graphical Optimization

The main purpose of the transient response control is to design the controller ensuring the unit step response with desired settling time and maximum overshoot requirements, which are specified prior to design, for the closed loop system. As mentioned in Section 2, using the CDM and standard Manabe form, this purpose can be achieved for the LTI systems easily. However, for the time delay systems, transient response results may not meet the specified performance because of the time delay in the plant. Furthermore, some stability index values which are different from the values of standard Manabe form can give the better performance results. Unfortunately, a certain rule for the selection of the stability indices for the time delay systems has not reported in the literature until now. Therefore, a graphical optimization technique is incorporated to the proposed PID tuning method.

The graphical optimization technique uses two colored figures which are obtained from the colored contour of their 3-D figures. The abscissa of the figures is the first stability index (γ_1) and the ordinate is the equivalent time constant (τ). In the first figure, the maximum overshoot (M_p) values of the closed loop unit step responses calculated by using (7) and (21) versus γ_1 for the interval of (γ_{1min}, γ_{1max}) and τ for the interval of (τ_{min}, τ_{max}) are plotted. Here, γ_{1min}, γ_{1max}, τ_{min}, τ_{max} are the minimum and maximum values of the γ_1 and τ. The internal (γ_{1min}, γ_{1max}) for the first stability index are chosen so that the standard Manabe values are in the middle of this interval. The recommended initial interval is (2, 3) and this interval can be modified according to design requirements. The selection of the interval (τ_{min}, τ_{max}) depends on the settling time needs of the designer. In the second figure, the settling time (t_s) values of the closed loop unit step responses using (7) and (21) versus γ_1 and τ are plotted for the same interval in the first figure. These two figures are called as *transient response-map* (*tr-map*). Since the proposed method has three design parameters (γ_1, γ_2 and τ) for the FOPTD system, to consider the second stability index γ_2 on the same figures is difficult. However, it is noted that different choices of γ_2 lead to different transient response performances. By changing γ_2 in the range of (2, 3) with 0.1 steps, the set of tr-maps is obtained.

The most important advantage of the graphical optimization technique is that the PID controller parameters which are calculated according to the FOPTD model are optimized in consideration of the real plant. Furthermore, an important advantage of this graphical optimization on the mathematical optimization procedures is that the designer can make a decision for the desired performance in a wide performance range visually. It is possible to change the selections of the design parameters according to various transient response alternatives.

In order to show the effectiveness of the graphical optimization, we consider a first-order plus time delay system $G(s) = e^{-1.2s}/(s+1)$. When γ_2=2 is chosen as in the standard Manabe form, the tr-map of the control system designed by the proposed method is obtained as shown in Fig. 3a. As can be seen from this figure, the standard Manabe form values γ_i={2.5, 2} gives the unit-step response without overshoot and with the shortest settling time at the value of τ=3.3. If τ is decreased for obtaining the less settling time, the overshoot of the unit step response exceeds the limit of 2%. From Fig. 3a, however, the shorter settling time without overshoot can be obtained at γ_1=2.65 and τ=2.5. Note that the chosen γ_1 is different from the value in the standard Manabe form in this case. Furthermore, the better performances can be obtained by changing γ_2. For the various γ_2 values in the range of (2, 3), new tr-maps can be plotted. For example, a tr-map for γ_2=2.6 is shown in Fig. 3b. From this figure, it can be seen that the values γ_1=2.5 and τ=2.2 give the shorter settling time.

For three cases, the unit step responses of the closed loop system are shown in Fig. 4. This figure shows that the last case (γ_i={2.5, 2.6}, τ=2.2) gives the shortest settling time. For all cases, the unit step responses are without overshoot.

The presented PID tuning algorithm for stable, unstable or integrating time delay system is summarized as follows:

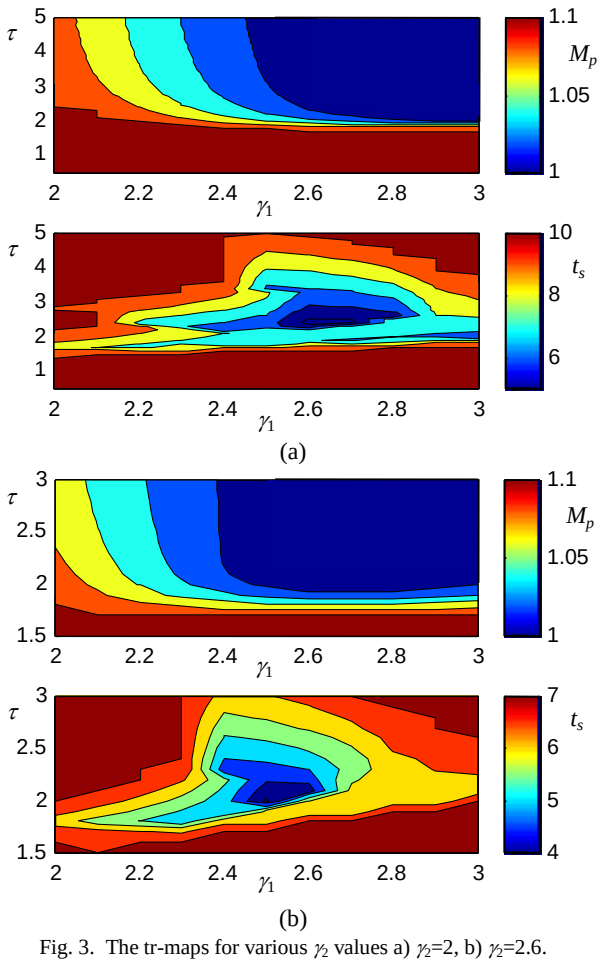

Fig. 3. The tr-maps for various γ_2 values a) γ_2=2, b) γ_2=2.6.

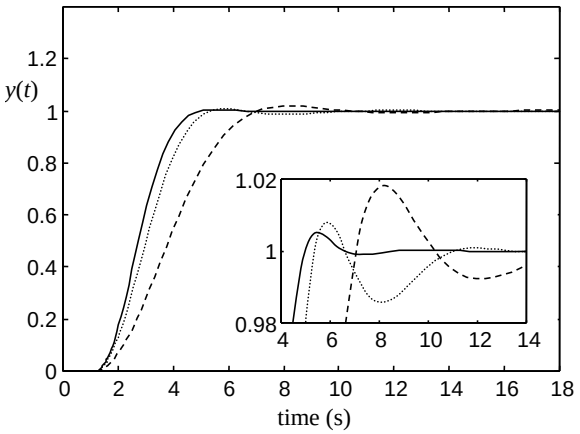

Fig. 4. Unit step responses: (Case 1: ── γ_i={2.5 2.6}, τ=2.2; Case 2: ····· γ_i={2.65 2}, τ=2.5; Case 3: - - - - γ_i={2.5 2}, τ=3.3)

1. Determine a FOPTD model of the time delay system using the methods given in [21-23].

2. Obtain the set of tr-maps by using various values of γ_2:

a) For a first value of γ_2 (γ_2=2), plot the tr-map using (7) and (21) (The abscissa of the tr-map is γ_1 in the range of (γ_{1min}-γ_{1max}) and the ordinate is τ in the range of (τ_{min}-τ_{max})).

b) Repeat the same process for the γ_2 values in the range of (2, 3) with 0.1 steps.

3. Specify the optimal values of γ_1, γ_2 and τ.

4. Calculate the PID parameters using γ_1, γ_2 and τ.

III. Simulation Examples

In this section, three simulation examples containing systems of different dynamics are given to demonstrate the wide applicability of the introduced PID control method. The first example which considers an unstable FOPDT plant shows the improved performance of the proposed PID tuning method compared to the performances of some methods in the literature. The second example takes into account an integrating FOPDT plant, where it is observed that the proposed method yields significantly improved results relative to recent two PID control methods. In the third example, a higher order system are controlled.

A. *Example 1*

Consider a first order unstable system with a time delay $G(s) = 4e^{-2s}/(4s-1)$. The PID controller parameters calculated by ISTE optimization method of Visioli [24] are K_p=0.652, T_i=8.261, T_d=0.9671 and Taylor series expansion method of Sree *et al* [25] are K_p=0.548, T_i=11.117, T_d=1.024. Simulation results show that the best settling time for these PID control systems is about 25 s. Therefore, a smaller settling time than this value is aimed to obtain the better performance for the proposed method. First of all, a set of tr-maps computed for the various values of γ_2 in the range of (2, 3) are plotted. From these tr-maps, the choice of γ_2=2.2 gives the shortest settling time without overshoot as shown in Fig. 5. Also seen from this figure that τ=5.7 and γ_1=2.4 values for γ_2=2.2 is the best selection. Therefore, the PID controller parameters are calculated as K_p=0.5384, T_i=12.5086, T_d=0.6891 and the feedforward controller is obtained as $C_f(s) = 1/(8.6197s^2 + 12.509s + 1)$.

The unit step responses of the proposed PID control system and two PID control systems designed by Visioli and Sree *et al* are shown in Fig. 6a while the control signals produced by these control systems are shown in Fig. 6b. It is apparent that the proposed PID controller produces a unit step response without an overshoot and with the smallest settling time, and this is achieved by a control signal having a smaller magnitude.

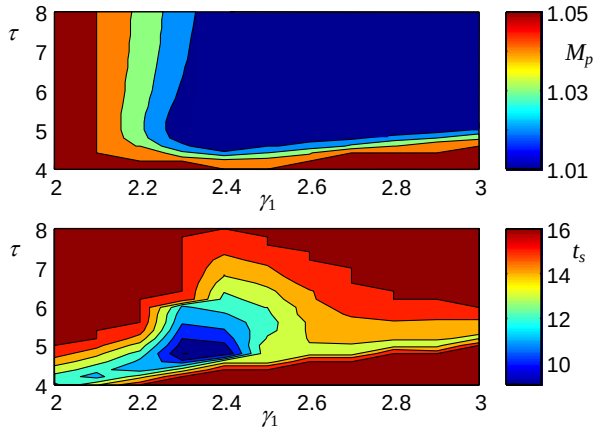

Fig. 5. The optimal tr-map for Example 1.

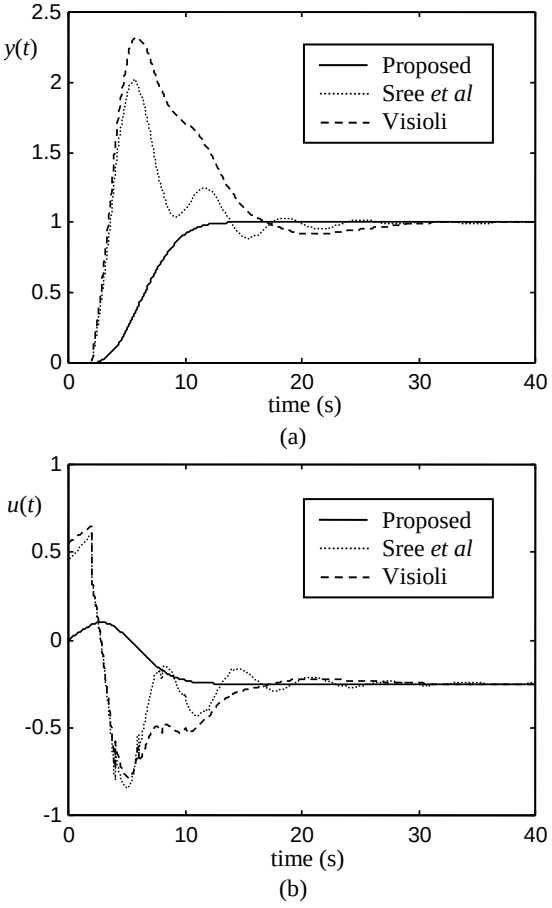

Fig. 6. a) Unit step responses, b) Control signals (Example 1).

B. *Example 2*

An integrating plant transfer function $G(s) = e^{-s}/5s$ is considered in this example. The PID controller parameters for ISTE optimization method of Visioli [24] are obtained as K_p=6.7, T_i=1.83, T_d=0.49 and for the frequency response method of Wang and Cluett [26] are calculated as K_p=4.794, T_i=3.043, T_d=0.391. The Wang and Cluett's method gives the best settling time which is 7.5s.

For the proposed method, the optimal tr-map which is obtained for γ_2=2.3 is shown in Fig. 7. In accordance with this map, the PID controller parameters obtained by using the graphical optimization method with the design parameters τ=2.3 and γ_i={2.4, 2.3} are K_p=5.1461, T_i=2.8 and T_d=0.3156. The feedforward controller is $C_f(s) = 1/(0.8837s^2 + 2.8s + 1)$.

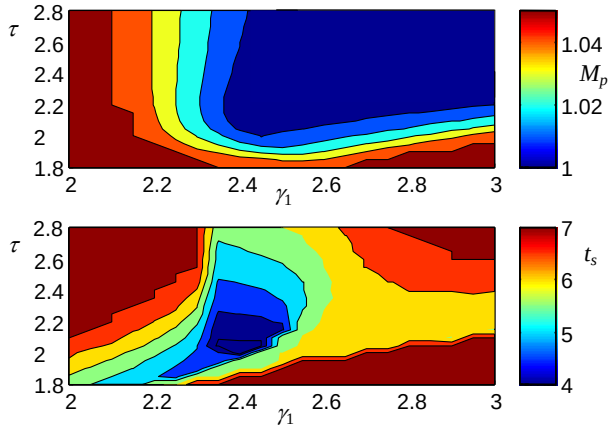

Fig. 7. The optimal tr-map for Example 2.

The unit step response of the proposed PID control system is compared with those of control systems using the previous PID controllers are shown in Fig. 8a for a step load-disturbance change with magnitude of d=-0.5 applied at time 20 s. From this figure, the proposed design method results in an improved performance with shorter settling time and without overshoot. Fig. 8b illustrates the control signals, which show that the introduced design method requires less effort for the improved control action, for all PID methods.

C. *Example 3*

A high order plant transfer function of $G(s) = 1/(s+1)^8$, which was given in Wang and Shao [29], is taken into account in this example. The FOPDT model for this plant was given as $G(s) = e^{-5.1s}/(4.35s+1)$ in [27]. The PID parameters were determined as K_p=0.677, T_i=4.3314 and T_d=1.6489 using the method of Wang and Shao and estimated as K_p=0.716, T_i=5.4589 and T_d=1.3380 through the method of Cluett and Wang [28]. For the improved performance, the design parameters of the proposed method are chosen as τ=8.4 and γ_i={2.05, 4.2} for the optimal tr-map shown in Fig. 11. The PID parameters with these values are calculated as K_p=1.0012,

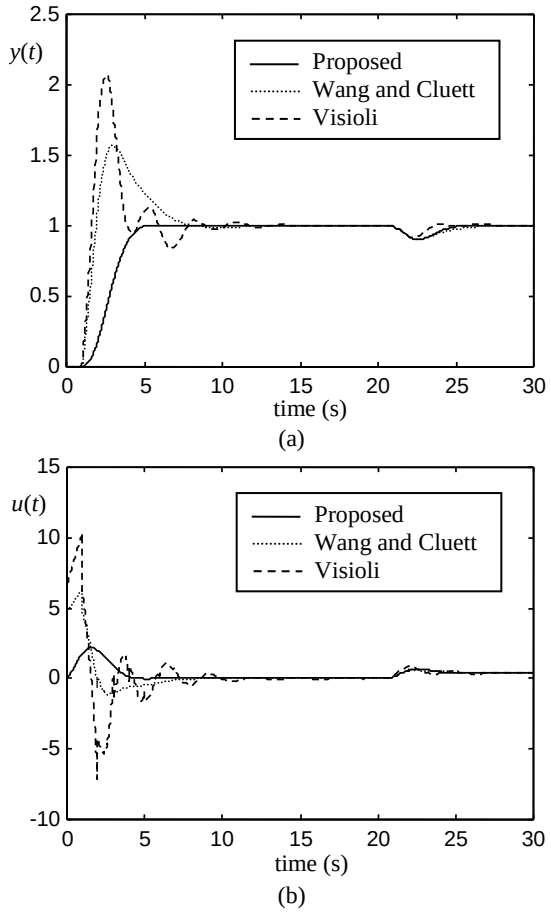

Fig. 8. a) Unit step responses, b) Control signals (Example 2).

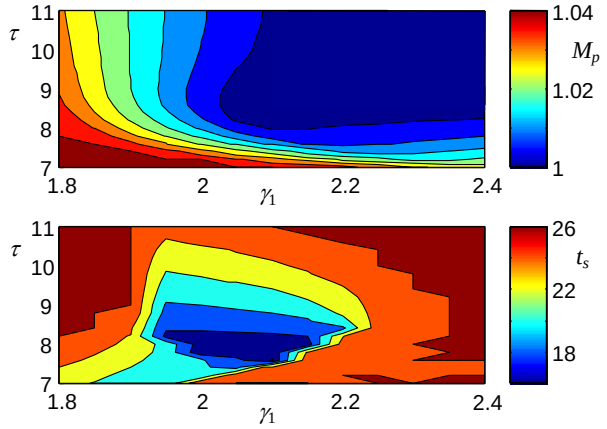

Fig. 11. The optimal tr-map for Example 3.

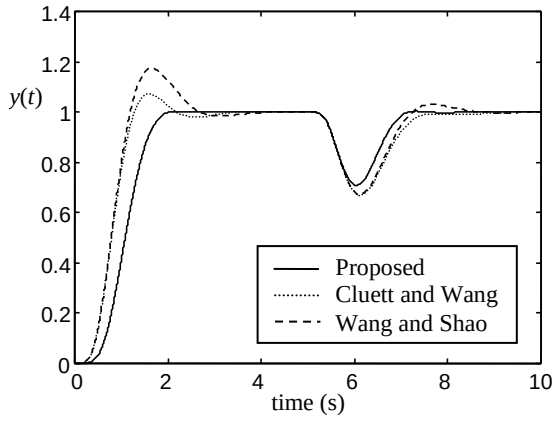

Fig. 12. Unit step responses (Example 3).

T_i=5.4782 and T_d=1.9411 and the feedforward controller is obtained as $C_f(s) = 1/(10.6336s^2 + 5.4782s + 1)$. The outputs to a unit step input and step load disturbance of magnitude -0.5 introduced at time 50s. are shown in Fig. 12 for all the design studies. It can be shown from this figure that the proposed method provides excellent control for the high-order plant in terms of settling time and overshoot.

IV. CONCLUSIONS

In this paper, the earlier results on transient response control which was successfully applied to the control of linear time-invariant systems using higher order polynomial controllers have been extended to the case of the control of linear time delay systems using PID controllers. The solution to the problem of PID transient response control presented here is based on first obtaining the explicit PID tuning formulae using the FOPTD model of the plant. To achieve this, the design parameters which are called as the stability indices and the equivalent time constant are considered. Then, the optimal PID controller is obtained by the graphical optimization technique which makes use of transient responses maps (tr-maps). The dominant merit of the proposed method is that the numerical quantities of the desired settling time and maximum overshoot values for the unit step response of the closed-loop system are specified before starting the design. As evidenced by the simulation results, it can be concluded that the proposed method gives reliable and accurate results for the stable, integrating and unstable time delay systems.

REFERENCES

[1] K. Ogata, *Modern Control Engineering*, Prentice-Hall, Englewood Cliffs, NJ, 1970.

[2] J. Zheng, P. Guo, and J.D. Wang, "STFC-self-tuning fuzzy controller," in *Proc. IEEE Conf. on Systems, Man and Cybernetics*, Chicago, 1992.

[3] Y.C. Kim, L.H. Keel, and S.P. Bhattacharyya, "Transient response control via characteristic ratio assignment," *IEEE Trans. on Automatic Control*, vol. 48, pp. 2238-2244, 2003.

[4] A.S. Hauksdóttir, "Analytic expression of transfer function responses and choice of numerator coefficients (Zeros)," *IEEE Trans. on Automatic Control*, vol. 41, pp. 1482–1488, 1996.

[5] S. Jung, and R.C. Dorf, "Novel analytic technique for PID and PIDA controller design," in *Proc. 13th IFAC World Congress*, San Francisco, USA, 1996.

[6] G.C. Goodwin, A.R. Woodyatt, R.H. Middleton, and J. Shim, "Fundamental limitations due to *jw*-axis zeros in SISO systems," *Automatica*, vol. 35, pp. 857-863, 1999.

[7] B.A. Leon de la Barra, "On undershoot in SISO systems," *IEEE Trans. on Automatic Control*, vol. 39, pp. 578-581, 1994.

[8] D. Graham, and R.C. Lathrop, "The synthesis of "optimum" transient response: criteria and standard forms," *AIEE Transactions*, vol. 72, pp. 273-288, 1953.

[9] G.F. Franklin, and J.D. Powell, and A. Emami-Naeini, "Feedback control of dynamic systems," Addison-Wesley, 1994.

[10] C. Kessler, "Ein beitrag zur theorie mehrschleifiger regelungen," *Regelungstechnik*, vol. 8, pp. 261-266, 1960.

[11] N.K. Sinha, *Control Systems*, 2nd ed. John Wiley & Sons Inc, 1994.

[12] M. Zhuang, and D.P. Atherton, "Automatic tuning of optimum PID controllers," *IEE Proc. D*, vol. 140, pp. 216-224, 1993.

[13] P. Naslin, *Essentials of Optimal Control*, Boston Technical Publishers, Massachusetts, 1969.

[14] Y.C. Kim, L.H. Keel, and S.P. Bhattacharyya, "Transient response control via characteristic ratio assignment and pulsatance assignment," in *Proc. 21th American Control Conference*, Anchorage, 2002.

[15] S. Manabe, "Coefficient diagram method," in *Proc. 14th IFAC Symposium on Automatic Control in Aerospace*, Seoul, 1998.

[16] S.E. Hamamci, "A robust polynomial-based control for stable processes with time delay," *Electrical Engineering*, vol. 87, pp. 163–172, 2005.

[17] T. Liu, W. Zhang, and D. Gu, "Analytical design of two-degree-of-freedom control scheme for open-loop unstable processes with time delay," *Journal of Process Control*, vol. 15, pp. 559–572, 2005.

[18] A.S. Rao, and M. Chidambaram, "Enhanced two-degrees-of-freedom control strategy for second-order unstable processes with time delay," *Ind. Eng. Chem. Res.*, vol. 45, pp. 3604-3614, 2006.

[19] S. Manabe, and Y.C. Kim, "Recent development of Coefficient Diagram Method," in *Proc. 3rd Asian Control Conference*, Shanghai, 2000.

[20] M. Araki, and H. Taguchi, "Two-degree-of-freedom PID controllers," *Int. J. of Control, Automation, and Systems*, vol. 1, pp. 401-411, 2003.

[21] I. Kaya, and D.P. Atherton, "Exact parameter estimation from relay autotuning under static load disturbances," in *Proc. 20th American Control Conference*, Arlington, 2001.

[22] A. Visioli, "Time-optimal plug&control for integrating and FOPDT processes," *Journal of Process Control*, vol. 13, pp. 195–202, 2003.

[23] S. Majhi, and D.P. Atherton, "Online tuning of controllers for an unstable FOPDT process," *IEE Proc.- Control Theory Appl.*, vol. 147, pp. 421-427, 2000.

[24] A. Visioli, "Optimal tuning of PID controllers for integral and unstable processes," *IEE Proc.-Control Theory Appl.*, vol. 148, pp. 180–184, 2001.

[25] R.P. Sree, M.N. Srinivas, and M. Chidambaram, "A simple method of tuning PID controllers for stable and unstable FOPDT systems," *Comput. Chem. Eng.*, vol. 28, pp. 2201–2218, 2004.

[26] L. Wang, and W.R. Cluett, "Tuning PID controllers for integrating processes," *IEE Proc.- Control Theory Appl.*, vol. 144, pp. 385-392, 1997.

[27] I. Kaya, "Tuning PI controllers for stable processes with specifications on gain and phase margins," *ISA Transactions*, vol. 43, pp. 297-304, 2004.

[28] W.R. Cluett, and L. Wang, "New tuning rules for PID control," *Pulp and Paper Canada*, vol. 3, pp. 52-55, 1997.

[29] Y.G. Wang, and H.H. Shao, "PID autotuner based on gain- and phase-margin specifications," *Ind. Eng. Chem. Res.*, vol. 38, pp. 3007–3012, 1998.

BIOGRAPHY

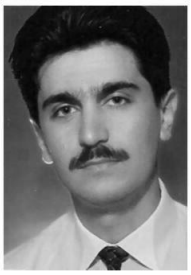

SERDAR E. HAMAMCI received the B.S. degree in electronics engineering from Erciyes University in 1992 and the M.S. and Ph.D. degrees in electrical-electronics enginnering from Firat University in 1997 and 2002 respectively.

From 1993 to 2009, he was a Research Assistant with the Electrical-Electronics Engineering Department at Inonu University. Since 2009, he has been an Associate Professor with the same department. His research interest includes control system design, stabilization and fractional order systems.

Nussbaum Gain for Adaptive Fuzzy Global Non Singular Sliding Mode Power System Stabilizer

E. Nechadi, M. N. Harmas, N. Essounbouli and A. Hamzaoui

***Abstract*—Power systems stability is enhanced through a novel stabilizer developed around a non singular adaptive fuzzy terminal integral sliding mode approach using the Nussbaum function applied to a nonlinear model of a single machine power system connected to an infinite bus via a double transmission lines subjected to severe faults. Nussbaum gain is used to avoid the problem of controllability of the system. Stability is insured through Lyapunov synthesis. Severe operating conditions are used in a simulation study to test the validity of the proposed method, indicating better performance and satisfactory transient dynamic behavior.**

Index Terms—**Power system stabilizer, adaptive fuzzy global sliding mode; Nussbaum function, Lyapunov stability.**

I. Introduction

THESE power systems are complex nonlinear systems that often exhibit low frequency oscillations due to insufficient damping caused by adverse operating conditions which can lead to a devastating loss of synchronism [1].

Power system stabilizers are used to suppress these oscillations and improve the overall stability [1-4]. The computation of the fixed parameters of these stabilizers is usually based on the linearized model of the power system around a nominal operating point [5-7]. The operating condition often change as a result of load variation and/or major disturbances, making the dynamic behaviour of the power system different, thus requiring new adjustment of stabilizer parameters for if the latter are kept fixed, controlled power system performance is greatly degraded [7].

Conventional stabilizers, consisting of cascade connected lead–lag compensators derived from a linear model representing the power system at a certain operating point, have long been used to damp oscillations regardless of the varying loading conditions or disturbances [8-12]. However, a lot of research about the design of power system stabilizers has been conducted, using a wide range of strategies, such as sliding controller [13,14], adaptive controller [15-16], adaptive fuzzy controllers [17,18] and a comparison of some approaches to designing power system stabilizers has been presented in [19,20].

E. NECHADI and M. N. HARMAS are with the Electrical Engineering Department, Ferhat Abbas University of Sétif1, Algeria (e-mail: nechadiamira@yahoo.fr, mharamas@yahoo.fr).

N. ESSOUNBOULI and A. HAMZAOUI are with Centre of Research for Science and Information Technology and Communication Laboratory, Champagne Ardennes University, France e-mail: najib.essounbouli@univ-reims.fr, abdelaziz.hamzaoui@univ-reims.fr).

One of these possible methods is the application of adaptive fuzzy sliding controller. Remarkable research effort has been done in the last decade putting forward intelligent fuzzy logic based power system stabilizer as well as optimality in adapting to changing operating conditions as in [21-23].

However, this linear model based control strategies often fail to provide satisfactory results over a wide range of operating conditions besides during severe disturbances, PSS action may actually cause the generator under its control to lose synchronism in an attempt to control its excitation field. In [24] the authors applied the Nussbaum gain with the conventional sliding mode control but the results are unsatisfied.

This paper introduces briefly in the next section the terminal sliding mode control approach used, followed by the second section in which adaptive fuzzy technique is tackled. In third section the design of the non singular adaptive fuzzy terminal sliding mode stabilizer using a Nussbaum gain is undertaken and stability issue addressed. The power system model is presented in the ensuing section followed by simulation and a presentation of results for different operating conditions.

II. Global Sliding Mode Control

Consider a SISO nonlinear system described by:

$$\begin{cases} \dot{x}_1 = x_2 \\ \dot{x}_2 = f(x,t) + g(x,t)u \end{cases} \tag{1}$$

where $x = [x_1 \quad x_2]^T \in R^2$ is the state vector, $u \in R$ is the input, $f(x,t)$ and $g(x,t)$ are the unknown functions nonlinear.

Then, $f(x,t)$ and $g(x,t)$ can be written as:

$$f = f_0 + \Delta f \tag{2}$$

$$g = g_0 + \Delta g \tag{3}$$

where f_0, g_0 are the nominal functions, Δf and Δg are uncertainties satisfy the conditions:

$$|\Delta f| \le F \tag{4}$$

$$\frac{g}{g_0} \le G \tag{5}$$

where F and G are positive.

The terminal sliding switching surface as follows:

$$S = \int_0^t x_1^{\lambda}(\tau)d\tau + \alpha x_1 + \beta x_2 \quad (6)$$

where α, β and λ are the constants positive.

Control law enabling satisfaction of the attraction phase condition (7) and the equivalent control to maintain state trajectories on the sliding surface is typically given by (8) assuming g is non-singular.

$$S\dot{S} \prec 0 \quad (7)$$

Theorem 1: For the nonlinear system (1), if we choose the following control law:

$$u_{GSMC} = -g^{-1}\left(\frac{1}{\beta}x_1^{\lambda} + \frac{\alpha}{\beta}x_2 + f + \frac{k^*}{\beta}sign(S)\right) \quad (8)$$

where k^* indicates the control gain with the sliding function, then the system is stable.

Proof:
Choosing the Lyapunov function candidate to be

$$V = \frac{1}{2}S^T S \quad (9)$$

Therefore

$\dot{V} = S^T\dot{S}$

$\dot{V} = S^T\left[x_1^{\lambda} + \alpha x_2 + \beta\dot{x}_2\right]$

$\dot{V} \le -k^*|S|$

thus: $\dot{V} \le 0$.

III. Adaptive Fuzzy Global Sliding Mode Control

In this section, the procedure to construct an adaptive fuzzy gain to the terminal sliding mode controller. $\hat{k}$ is the approximation of the k^*, using the singleton fuzzifier, product fuzzy inference and center gravity defuzzifier, the inferred output is:

$$\hat{k}(x,\theta_k) = \xi^T(x)\theta_k \quad (10)$$

where $\theta_k = [\theta_{1k},\theta_{2k},...,\theta_{mk}]$ is the vector of parameters, $\xi = [\xi_1,\xi_2,...,\xi_m]^T$ is the vector of fuzzy basis functions.
The minimum approximation error is:

$$\varepsilon_k = k^* - \xi^T(x)\theta_k^* \quad (11)$$

where θ_k^* is the optimal approximation parameter and $\tilde{\theta}_k = \theta_k - \theta_k^*$.

Theorem 2: For the nonlinear system (1), if we choose the following control law:

$$u_{AFGSMC} = -g_0^{-1}\left(\frac{1}{\beta}x_1^{\lambda} + \frac{\alpha}{\beta}x_2 + f_0 + \frac{\hat{k}}{\beta}sign(S)\right) \quad (12)$$

and if,

$$k^* \ge \frac{1}{G}\eta + \left|\frac{\beta F}{G} + \left(\frac{1-G}{G}\right)\left(x_1^{\lambda} + \alpha x_2 + \beta f_0\right)\right| + |\varepsilon_k| \quad (13)$$

and choose the adaptation law:

$$\dot{\theta}_k = \gamma G|S|\xi^T(x) \quad (14)$$

then the system is stable.

Proof:
Choosing the Lyapunov function candidate to be

$$V = \frac{1}{2}S^T S + \frac{1}{2\gamma}\tilde{\theta}_k^T\tilde{\theta}_k \quad (15)$$

Therefore

$$\dot{V} = S^T\dot{S} + \frac{1}{\gamma}\tilde{\theta}_k^T\dot{\theta}_k$$

$$\dot{V} = S^T\left[\left(x_1^{\lambda} + \alpha x_2 + \beta f\right) - \beta\left(\frac{g}{g_0}\right)\left(\frac{1}{\beta}x_1^{\lambda} + \frac{\alpha}{\beta}x_2 + f_0 + \frac{\hat{k}}{\beta}\mathrm{sgn}(S)\right)\right] + \frac{1}{\gamma}\tilde{\theta}_k^T\dot{\theta}_k$$

$$\le -\eta|S| + S\left((1-G)\left(x_1^{\lambda} + \alpha x_2 + \beta f\right) + \beta F\right) + G\hat{k}|S| + \frac{1}{\gamma}\tilde{\theta}_k^T\dot{\theta}_k$$

$$\le -\eta|S|.$$

IV. Non Singular Adaptive Fuzzy Global Sliding Mode Control

Definition

A function is called a Nussbaum-type function if it has the following properties:

$$\limsup_{y\to\infty}\frac{1}{y}\int_0^y N(\varsigma)d\varsigma = +\infty \quad (16)$$

$$\liminf_{y\to\infty}\frac{1}{y}\int_0^y N(\varsigma)d\varsigma = -\infty \quad (17)$$

Through out this paper the even Nussbaum function:

$$N(\varsigma) = \exp(\varsigma^2)\cos((\pi/2)\varsigma) \quad (18)$$

is employed and ς is a variable determined later.
In this section, the fuzzy logic model is expressed as the following form:

$$\hat{f}(x) = \theta_f\xi^T(x) \quad (19)$$

approximates the unknown system function $f(x)$ with the approximation error δ_f, such that:

$$\delta_f = f(x) - \xi^T(x)\theta_f \quad (20)$$

where $\theta_f = [\theta_{1f}, \theta_{2f}, ..., \theta_{mf}]$ is the vector of parameters, $\xi = [\xi_1, \xi_2, ..., \xi_m]^T$ is the vector of fuzzy basis functions.

V. Adaptive Fuzzy Global Sliding Mode Control Using Nussbaum Function

In previous research on indirect adaptive fuzzy method, the controller with $1/\hat{g}(x)$ can be singular because it cannot be guaranteed that $\hat{g}(x)$ is note equal to zero at any moment where $\hat{g}(x)$ denotes the approximation of $g(x)$. A Nussbaum function is used to avoid appearance of the singularity problem and should satisfy the following condition:

$$gN(\varsigma) \le \chi \tag{21}$$

Theorem 3: For the nonlinear system (1), if we choose the following control law:

$$u_{NTSMC} = -N(\varsigma)\left(\frac{1}{\beta}x_1^{\lambda} + \frac{\alpha}{\beta}x_2 + \hat{f} + \frac{\hat{k}}{\beta}sign(S)\right) \tag{22}$$

and if

$$k^* \ge \frac{1}{\chi}\eta + \left|\frac{\beta F}{\chi} + \left(\frac{1-\chi}{\chi}\right)\left(x_1^{\lambda} + \alpha x_2\right)\right| + |\varepsilon_k| \tag{23}$$

with

$$\dot{\varsigma} = x_1^{\lambda} + \alpha x_2 \tag{24}$$

and choose the adaptation law:

$$\dot{\theta}_k = \gamma_2 \chi |S| \xi^T(x) \tag{25}$$

$$\dot{\theta}_f = -\gamma_1 \beta (1-\chi) S \xi^T(x) \tag{26}$$

then the system is stable.

Proof:

Choosing the Lyapunov function candidate to be

$$V = \frac{1}{2}S^T S + \frac{1}{2\gamma_1}\theta_f^T\theta_f + \frac{1}{2\gamma_2}\tilde{\theta}_k^T\tilde{\theta}_k \tag{27}$$

Therefore;

$$\begin{aligned}\dot{V} &= S^T\dot{S} + \frac{1}{\gamma_1}\theta_f^T\dot{\theta}_f + \frac{1}{\gamma_2}\tilde{\theta}_k^T\dot{\tilde{\theta}}_k \\ &= S^T\left[(1-gN(\varsigma))\left(x_1^{\lambda} + \alpha x_2 + \beta\hat{f}\right) + \beta\delta_f - gN(\varsigma)\hat{k}sign(S)\right] \\ &\quad + \frac{1}{\gamma_1}\theta_f^T\dot{\theta}_f + \frac{1}{\gamma_2}\tilde{\theta}_k^T\dot{\tilde{\theta}}_k \\ &\le -\eta|S| + S(1-\chi)\beta\xi^T(x)\theta_f + \frac{1}{\gamma_1}\dot{\theta}_f^T\theta_f - \chi\xi^T(x)|S|\tilde{\theta}_k \\ &\quad + \frac{1}{\gamma_2}\tilde{\theta}_k^T\dot{\theta}_k \\ &\le -\eta|S|.\end{aligned}$$

VI. Power System Model

The power system model considered in this paper is a nonlinear model representing a synchronous machine connected to an infinite bus via a double circuit transmission line. The power system schematic diagram including turbine, transformer, automatic voltage regulator and PSS is shown in Fig.1 [25-26].

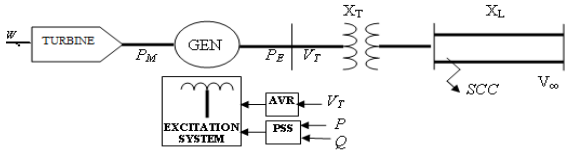

Fig.1 One-line SMIB diagram with AVR and PSS.

A fourth order classic representation is:

$$\begin{aligned}\dot{\delta} &= \omega_0(\omega - \omega_{ref}) \\ \dot{\omega} &= \frac{1}{M}(P_m - P_e) \\ \dot{e}_q' &= \frac{1}{T_{d0}'}(e_{fd} - e_q) \\ \dot{e}_{fd} &= \frac{1}{T_A}\left(K_A(E_{ref} - V_t + u) - e_{fd}\right)\end{aligned} \tag{28}$$

A nonlinear representation the machine during a transient period after a major disturbance has occurred in the system is follows:

$$\begin{cases}\dot{z}_1 = \dfrac{1}{M}z_2 \\ \dot{z}_2 = f(z,t) + g(z,t)u\end{cases} \tag{29}$$

where the state variable are expressed as: $z = [\Delta\omega \quad \Delta P]$, with $\Delta\omega$ is speed deviation, $\Delta P = P_m - P_e$ is the accelerating power and M is inertia moment coefficient.

The fact that the governor time constant is large compared to the time constants of the synchronous machine and its exciter, so that during the first few seconds after the occurrence of a severe disturbance the governor function can be ignored. Therefore the mechanical input power is constant during the transient integral, say less than 5 seconds after the disturbance has occurred [19].

Then, (29) can be written in form of system (1), if you make a change of variable as follows:

$$\begin{cases}x_1 = z_1 \\ x_2 = \dfrac{1}{M}z_2\end{cases} \tag{30}$$

The parameters of the single machine infinite bus system are as follows:

$x_e = 0.2\,p.u, x_q = 0.36\,p.u, x_d = 1.86\,p.u, x'_d = 0.25\,p.u, D = 0,$
$T'_{d0} = 6s, H = 4s, T_A = 0.05, K_A = 50, V = 1p.u, P_0 = 0.9\,p.u,$
$Q_0 = 0.3\,p.u.$

VII. SIMULATION

The soundness of the proposed PSS was tested and performance as well as robustness tests were conducted and compared to a classic CPSS [13] confirming, through computer simulations, good transient behaviour with the proposed control despite severe operating conditions illustrated by the following case studies. Five fuzzy sets for each input are sufficient for the PSS to be designed.

The fuzzy sets for inputs $\Delta\omega$ and ΔP are defined according to the membership functions shown in Fig.2.1 and Fig.2.2. The initial value of the θ_f, θ_k is chosen to be zero and the 0.09 respectively.

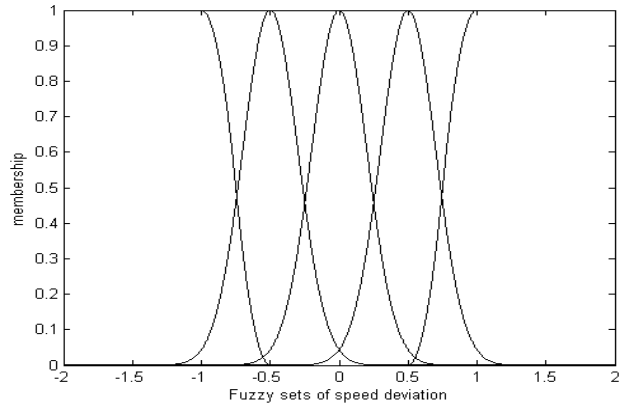

Fig.2.1 Fuzzy sets for input $\Delta\omega$.

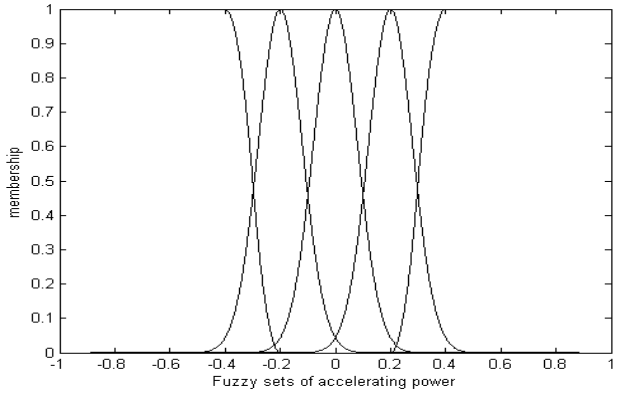

Fig.2.2 Fuzzy sets for input ΔP.

Case 1: First the simulation results for normal load condition are shown in Fig.3 with PSS calculated on proposed control. Performances of the proposed PSS are clearly superior while a greater control effort is solicited.

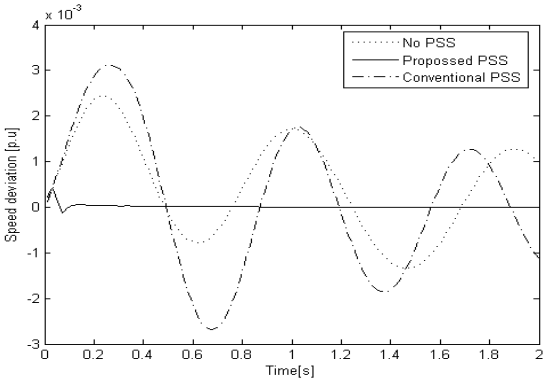

Fig.3.1 Speed deviation.

Case 2: Operating conditions change abruptly from light to heavy load condition, i.e. Q is changed from 0.3 p.u. to 0.8 *p.u* and x_e= 0.45 *p.u*. The simulation results in Fig.4 show a better transient performance for the proposed control.

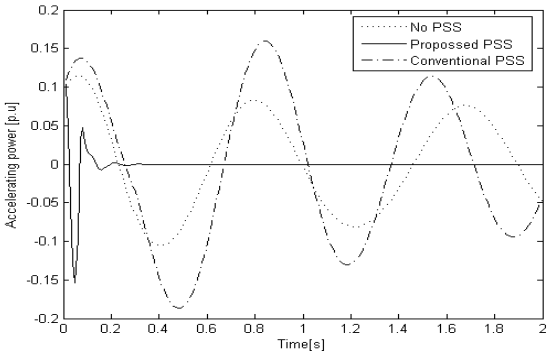

Fig.3.2 Accelerating power.

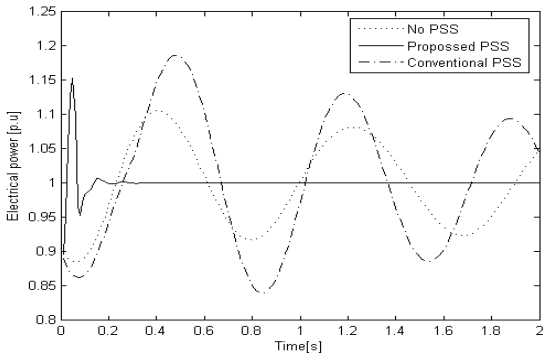

Fig.3.3 Electrical power.

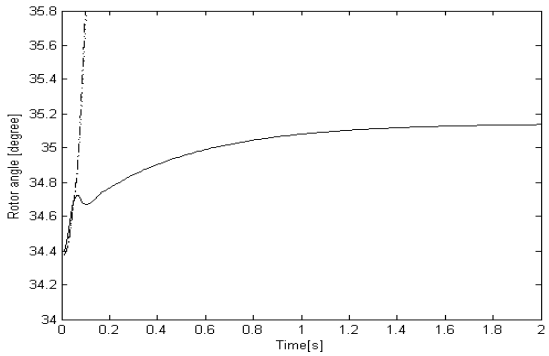

Fig.3.4 Rotor angle.

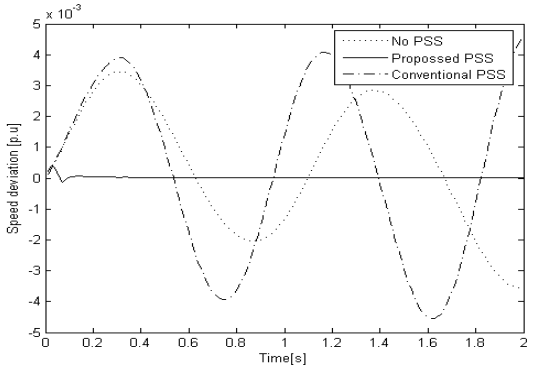

Fig.4.1 Speed deviation in heavy reactive power case.

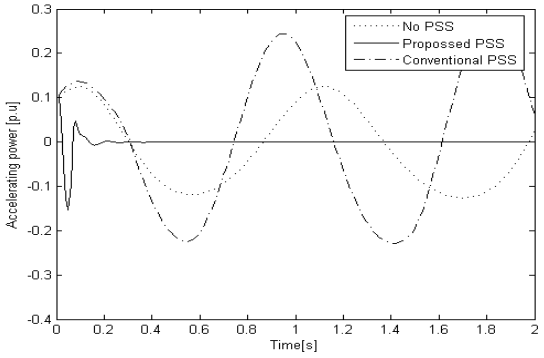

Fig.4.2 Accelerating power in heavy reactive power case.

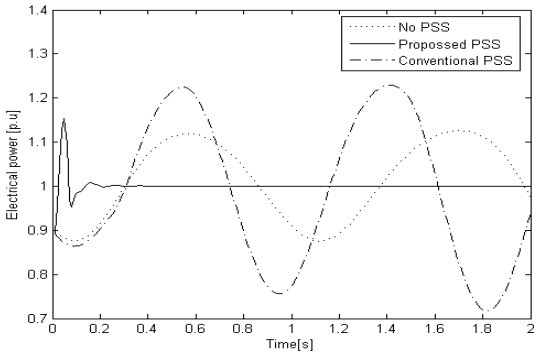

Fig.4.3 Electrical power in heavy reactive power case.

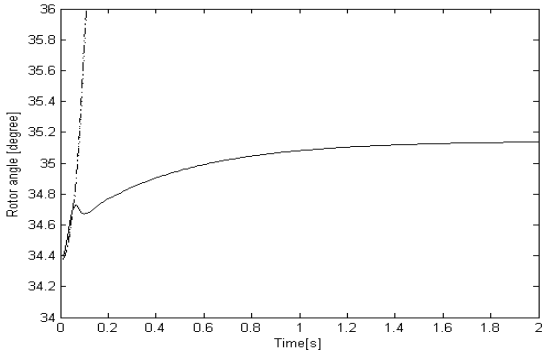

Fig.4.4 Rotor angle in heavy reactive power case.

Case 3: We now consider the case of the sudden occurrence of importing reactive power causing a change in Q from the light value to *-0.3 p.u* and strong connection ($x_e = 0.1$ *p.u*). Again the simulation results shown in Fig.5 seem to indicate a good transient behaviour with superior performance due to the proposed PSS.

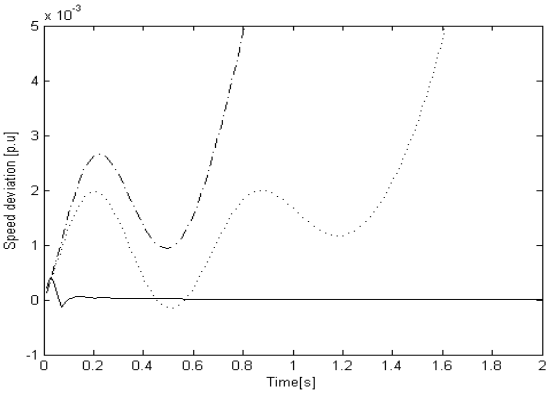

Fig.5.1 Speed deviation for case 3.

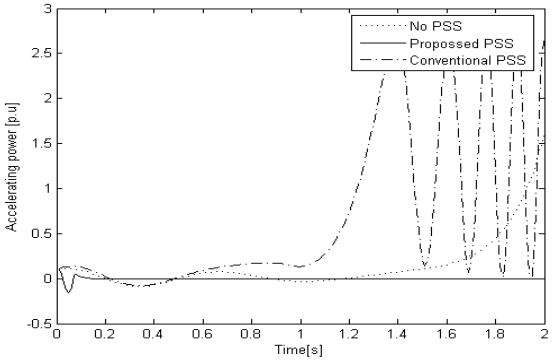

Fig.5.2 Accelerating power for case 3.

VIII. CONCLUSION

We introduced in this paper, based on the adaptive fuzzy terminal sliding mode controller and the Nussbaum gain, a new non singular power system stabilizer that enhances damping and improves transient dynamics of a single synchronous machine using a nonlinear model of the power system. Different load conditions as well as severe perturbations were used to evaluate the proposed power system stabilizer effectiveness in rapidly reducing oscillations that could lead to loss of synchronism if not treated. Simulation results exhibit superior performance over classical PSS and in absence of PSS.

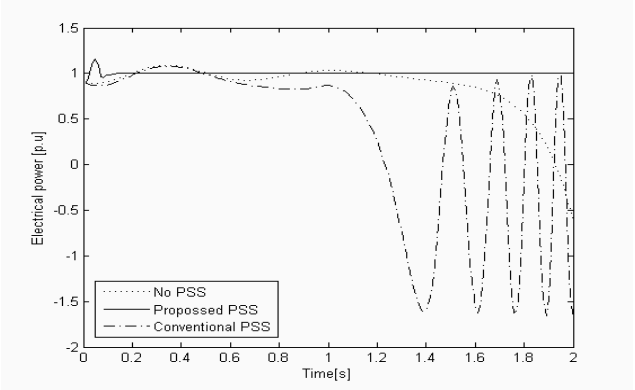

Fig.5.3 Electrical power for case 3.

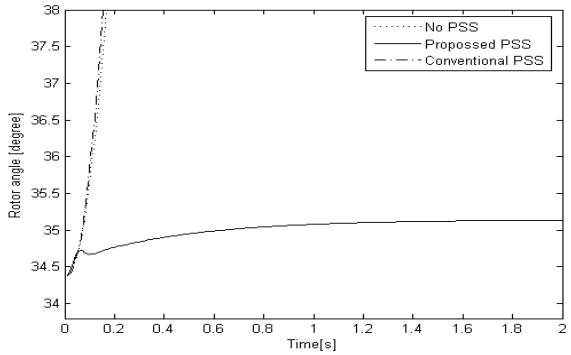

Fig.5.4 Rotor angle for case 3.

REFERENCES

[1] P. Kundur, Power System Control and Stability, Ed. McGraw-Hill Inc, 1994.

[2] F.P. DeMello, C.A. Concordia, Concept of synchronous machine stability as affected by excitation control, IEEE Trans. Vol.PAS-88, No.4, 1969, pp.316–329.

[3] P.M. Anderson, A.A. Fouad, Power system control and stability, Iowa State University Press, Ames.

[4] E.V. Larsen, D.A. Swann, Applying power system stabilizers, Part I, II, III, IEEE Trans. on Power App. and Syst., PAS-100, 1981, pp.3017-3041.

[5] M.L. Kothari, J. Nanda, K. Bhattacharya, Design of variable structure power system stabilizers with desired eigenvalues in the sliding mode, IEE Proc. Gen., Trans. and Distr., Vol140, No.4, 1993, pp.263-268.

[6] K. Bhattacharya, M.L Kothari and J. Nanda, Design of Discrete-Mode Variable Structure Power System Stabilisers, Electrical power & Energy System, Vol.17, No.6, 1995, pp.399-106.

[7] Y.M. Park, W. Kim, Discrete time adaptive sliding mode power system stabilizer with only input/output measurements, Electrical power & Energy systems, 18, 1996, pp.509-517.

[8] Z. Jiang, Design of Power System Stabilizers Using Synergetic Control Theory, Power Engineering Society General Meeting, IEEE, 2007, pp.1-8.

[9] A.L. Elshafei, K. El-Metwally, A.A. Shaltout, A variable structure adaptive fuzzy logic stabilizer for single and multi-machine power systems, Control Engineering Practice, 13, 2005, pp.413-423.

[10] P. Hoang, K. Tomsovic, Design and analysis of an adaptive fuzzy power system stabilizer, IEEE Transactions on Energy Conversion, Vol.11, No.2, 1996, pp.455-461.

[11] T.T. LieGuojie, C. B. Soh, G.H. Yang, Design of state-feedback decentralized nonlinear Hinf controllers in power systems , Electrical Power & Energy Systems, Vol.24, 2002, pp.601-610.

[12] A. D. Falehi, A. Dankoob, S. Amirkhan, H. Mehrjardi, Coordinated Design of STATCOM-Based Damping Controller and Dual-Input PSS to Improve Transient Stability of Power System, International Review of Automatic Control, 2011, pp.1308-1317.

[13] A.Y. Sivaramakrishnan, M. V. Hariharan, M. C. Srisailam, Design of a variable-structure load controller using pole assignment technique, Int. J. Contr.,40, 1984, 487-498.

[14] G. Shahgholian, A. Rajabi, B. Karimi, Analysis and Design of PSS for Multi-Machine Power System Based on Sliding Mode Control Theory, International Review of Automatic Control, 2010, pp.2241-2250.

[15] A. Ghosh, G. Ledwich, O.P. Malik, G.S. Hope, Power system stabilizer based on adaptive control techniques, IEEE Trans. PAS 103, 1984, pp.1983–1989.

[16] S.J. Chang, Y.S. Chow, O.P. Malik, G.S. Hope, An adaptive synchronous machine stabilizer, IEEE Trans. PWRS 1, 1986, pp.101–109.

[17] A. Pierre, A perspective on adaptive control of power systems, IEEE Trans. PWRS, Vol.2, 1987, pp.387–396.

[18] N.H. Zadeh, A. Kalam, A direct adaptive fuzzy power system stabilizer, IEEE Transaction on Energy Conversion, 14, 1999.

[19] N.H. Zadeh, A. Kalam, An indirect adaptive fuzzy-logic power system stabiliser, Electrical power & Energy systems, 24, 2002, pp.837-842.

[20] I. Ngamroo, Augmentation of Electrolyzer Control Effect by PSS for Microgrid Stabilization using PID-based Mixed H2/H∞ Control, International Review of Automatic Control, 2011, 3073-3080.

[21] S.S. Lee and J.K. Park, Design of power system stabilizer using observer / sliding mode, observer/sliding mode model following and H∞ / sliding mode controllers for small signal stability study, Electrical Power & Energy Systems, Vol.20, No.8, 1998, pp.543-553.

[22] T. Hussein, M.S. Saad, A.L. Elshafei, A. Bahgat, Damping inter-area modes of oscillation using an adaptive fuzzy power system stabilizer, Electric Power Systems Research, Vol.80, 2010, pp.1428-1436.

[23] G.H. Hwang, D.W. Kim, J.H. Lee, Y.J. An, Design of Fuzzy Power System Stabilizer Using Adaptive Evolutionary Algorithm, Engineering Applications of Artificial Intelligence, Vol.21, 2008, pp.86-96.

[24] E. Nechadi, M. N. Harmas, N. Essounbouli, A. Hamzaoui, Adaptive Fuzzy Sliding Mode Power System Stabilizer Using Nussbaum gain, International Journal of Automation and Computing, Vol.10, No.4, August 2013, pp.281-287.

[25] H. M. Soliman, A.L. Elshafei, F. Bendary, W. Mansour, LMI Static output-feedback Design of Fuzzy Power System Stabilizers, Expert Systems with Applications, Vol.36, 2009, pp.6817-6825.

[26] H.M. Soliman, A.L. Eshafei, A.A. Shaltout, M.F. Mors, Robust Power System Stabiliser, IEE Proc-Elec. Power Appl., 147, 2000, pp.285-291.

BIOGRAPHY

EMIRA NECHADI, received her bachelor degree in Control Systems in 2002; her Master's in Control Systems in 2004, and her doctorate in Control Systems in 2013, from the University of Sétif, Algeria. Her research interests include sliding mode control, adaptive fuzzy control, fuzzy systems, synergetic control and power systems.

MOHAMED NAGUIB HARMAS, presently professor at Sétif University, doctorate in control systems from UFA Sétif and MSEEE from CSU Sacramento, main research interests include robust nonlinear control, power system and power electronics control, and fuzzy synergetic design.

NAJIB ESSOUNBOULI, received his bachelor degree in electrical engineering from the University of Sciences and Technology of Marrakech (FSTG) in Morocco, his D.E.A. in 2000, and his Ph.D. in 2004 and it's Habilitation from Reims University of Champagne Ardennes, all in electrical engineering. from september 2005 to 2010, he is an assistant professor with IUT of Troyes, Reims Champagne Ardennes University. Since september 2010, he has been a professor with the same institute. His current research interests include fuzzy logic control, robust adaptive control, renewable energy and control drive.

ABDELAZIZ HAMZAOURI, received his bachelor degree in electrical engineering from the Polytechnic School of Algiers (ENPA), Algeria, in 1982, and his D.E.A. (1989) and Ph.D. (1992) from Reims University of Champagne Ardennes, both in electrical engineering. He is a currently a professor and the director of the Technology Institute of Troyes, Reims Champagne Ardennes University. His research interests include intelligent control, fuzzy control, and robust adaptive control.

Optimization of Insulator Shape Using GA and HGAPSO Methods

M. R. Salimian, and H. Javadi

***Abstract*—The flashover voltage of insulator is relative to the distribution of the electric field. The distribution of the electric field on the insulator is contributed to the shape of insulator. For this, we must optimize the shape of insulator. In this paper, we use FEM, GA and HGAPSO for optimizing the shape of insulator. The tangential electric field and the area of insulator are optimized by GA and HGAPSO. Then, the results obtained from GA and HGAPSO are compared with each other.**

Index Terms—**FEM, GA, HGAPSO, insulator, electric field.**

I. Introduction

THE flashover voltage is an important parameter of insulator. The low flashover voltage may be caused to electric discharge. The flashover voltage of insulator can be increased by optimizing the shape of insulator. Numerical methods for optimizing the shape of insulator are presented in [1-3]. These methods are complex and may find local optimum.

CSM [4-7] and DAGA [8-9] are used in [10] for optimizing the shape of Taiwan power insulator. CSM which is used for computing the tangential electric field is not accurate. DAGA which is used for optimizing is relative to initial population. For this, the final shape of insulator is similar to the initial shape.

In this paper, the average and variance of tangential electric field and the area of insulator are optimized by GA and HGAPSO. Finite element method (FEM) [11] is used for computing the tangential electric field of insulator. At the end, the optimal design obtained from GA and HGAPSO are compared with each other and with original Taiwan power company insulator.

II. Objective Function

In this paper, the shape of Taiwan power company insulator which is shown in Fig 1 has been optimized. 41 control points are considered for optimizing the shape of insulator. Search space of optimization is between ±1cm of the initial state of control points. Cubic spline function is used for smoothing the shape of insulator. Tangential electric field and the area of insulator are optimized. The objective function is presented in [1].

$$objectivefunction = a_1 E_{ave} + a_2 \sigma_E + a_3 A_s \quad (1)$$

$$E_{ave} = \frac{\sum_{i=1}^{41} E_i}{41} \quad (2)$$

$$\sigma_E = \sqrt{\frac{\sum_{i=1}^{41} (E_i - E_{ave})^2}{41}} \quad (3)$$

constraints,

$$y_j^{Down} - y_j^{Up} < 0 \quad (4)$$

$$y_j^{Down} \geq y_{Min} \quad (5)$$

$$y_i^{Up} - y_{i+1}^{Up} > 0 \quad (6)$$

$$N_{extreme} \leq N_{max} \quad (7)$$

A_s is the area of insulator shown in Fig 1.

y_j^{Up} shows the altitude of the jth control points on the upper surface of insulator.

y_j^{Down} shows the altitude of the jth control point on the lower surface of insulator.

$N_{extreme}$ shows the number of extremes on the lower surface of insulator.

E_i is the tangential electric field of the control point i.

M. R. SALIMAN is with the Department of Electrical Engineering, Faculty of Shahid Abbaspour, Shahid Beheshti University, Tehran, Iran (e-mail: bmsalimian@gmail.com).

H. JAVADI is with the Department of Electrical Engineering, Faculty of Shahid Abbaspour, Shahid Beheshti University, Tehran, Iran (e-mail: javadih@yahoo.com).

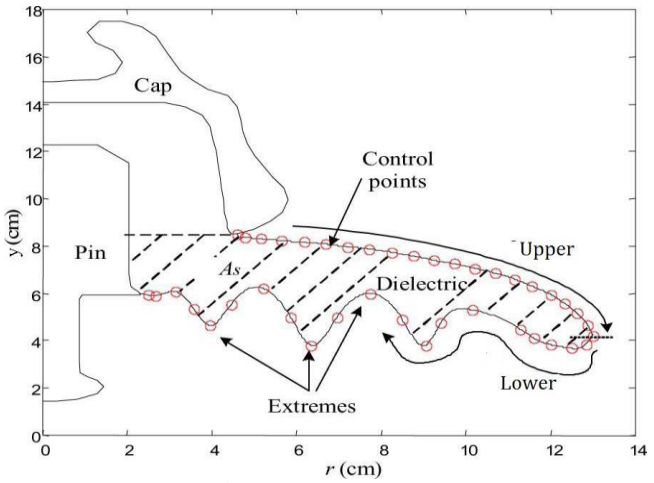

Fig.1 the original shape of Taiwan power insulator [10]

III. HYBRID GA AND PSO (HGAPSO)

This method is compound of GA and PSO. PSO is replaced by mutation in GA and change the position of population members by (8).

$$X_j^n = X_j^{n-1} + vel_j^n \quad (8)$$

$$vel_j^n = w_n \times vel_j^{n-1} + c \times R \otimes (Gbest - X_j^{n-1}) \quad (9)$$

$w_n$is the inertia of the nth generation which is changed from 0.9 to 0.4.

$R$is a random vector.
$Gbest$is the best member of population.
$X_j^n$is the position of the jth member in the nth generation.
$c$is a constant which is considered as 2.

IV. SIMULATION RESULT

MATLAB PDE toolbox [12] is used for computing the tangential electric field of insulator by FEM method. HGAPSO and GA which are coding by MATLAB are used for minimizing objective function. The population size, crossover fraction and the maximum number of generation are considered as 61, 0.8, and 30, respectively. The permittivity of dielectric and the voltage of electrode are considered as 2.5 and 1 p.u, respectively.

The results obtained from HGAPSO and GA for $y_{Min} = 2.45$ cm and $a_3 = 0.166$ are presented in Fig 2 and 3, respectively. The optimal design of of insulator obtained from GA and HGAPSO which are shown in Fig 4-5 are compared with original insulator in Fig 6-7, respectively. The minimum of objective function obtained from HGAPSO is equal to 14.3268 which is smaller than the results obtained from GA that is equal to 14.6213.
The average and variance of tangential electric field and the area of insulator are compared for different cases in Table 1.

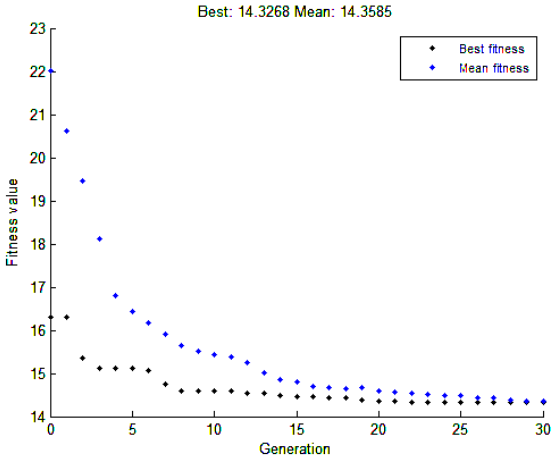

Fig.2 the minimum values of objective function obtained from HGAPSO ($a_3 = 0.166$)

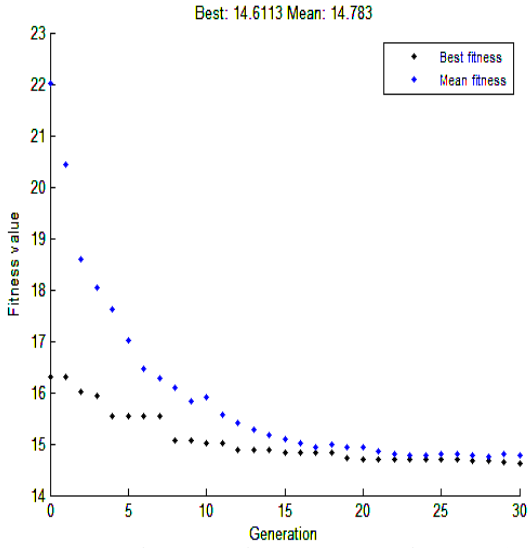

Fig.3 the minimum values of objective function obtained from GA ($a_3 = 0.166$)

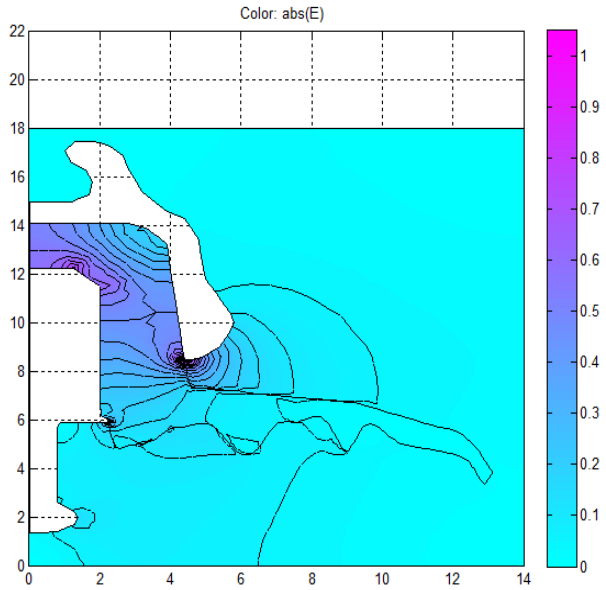

Fig.4 optimal shape of insulator obtained from HGAPSO ($a_3 = 0.166$)

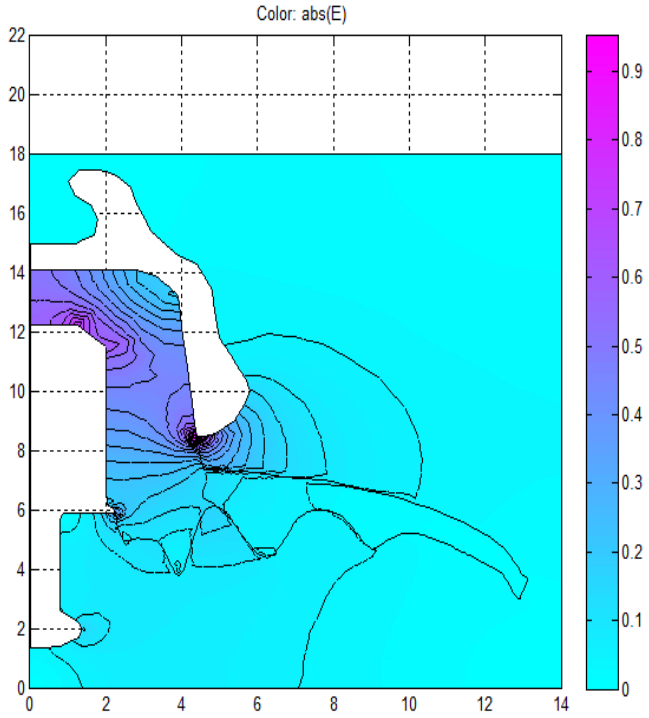

Fig.5 optimal shape of insulator obtained from GA ($a_3 = 0.166$)

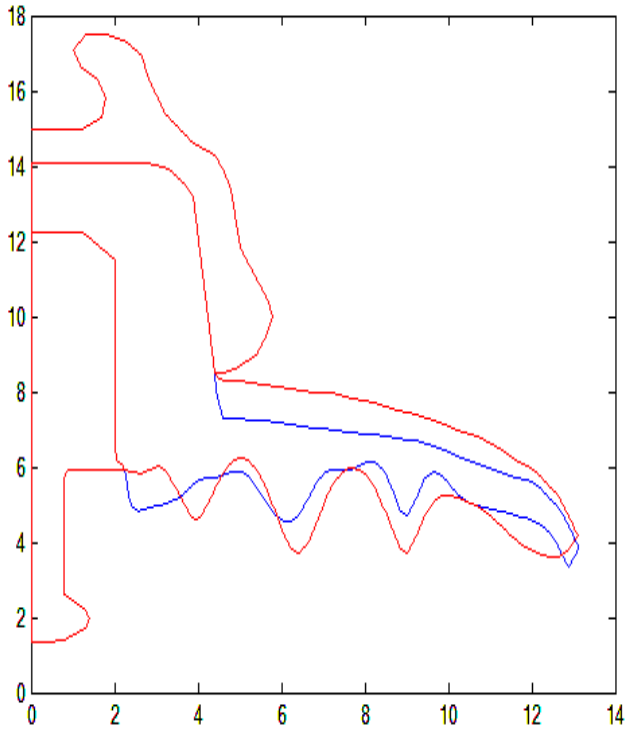

Fig.6 comparison of the optimal shape obtained from HGAPSO with the original shape ($a_3 = 0.166$)

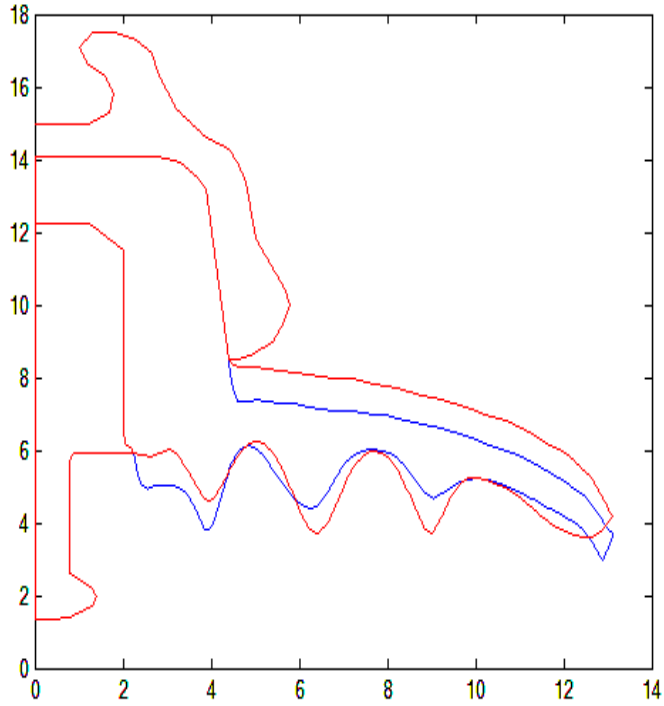

Fig.7 comparison of the optimal shape obtained from GA with the original shape ($a_3 = 0.166$)

TABLE I.
COMPARISON OF THE RESULTS OBTAINED FROM GA and HGAPSO WITH THE VALUES OF ORGINAL INSULATOR ($a_3 = 0.166$)

	GA	HGAPSO	Original Insulator
E_{ave}	0.0618	0.0628	0.0949
σ_E	0.0494	0.0489	0.1226
A_s	21.0240	19.0207	28.3146

The results obtained from HGAPSO and GA for $y_{Min} = 2.45$ cm and $a_3 = 0$ are presented in Fig 8 and 9, respectively. The optimal design of of insulator obtained from HGAPSO and GA which are shown in Fig 10-11 are compared with original insulator in Fig 12-13, respectively. The minimum of objective function obtained from HGAPSO is equal to 10.7081 which are smaller than the results obtained from GA that is equal to 10.997.

The average and variance of tangential electric field and the area of insulator are compared for different cases in Table 2.

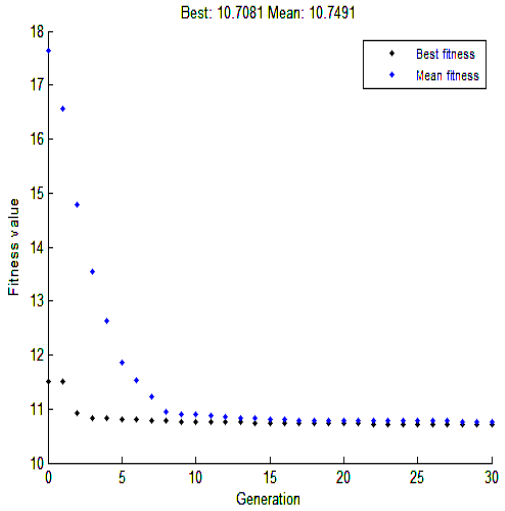

Fig.8 the minimum values of objective function obtained from HGAPSO ($a_3 = 0$)

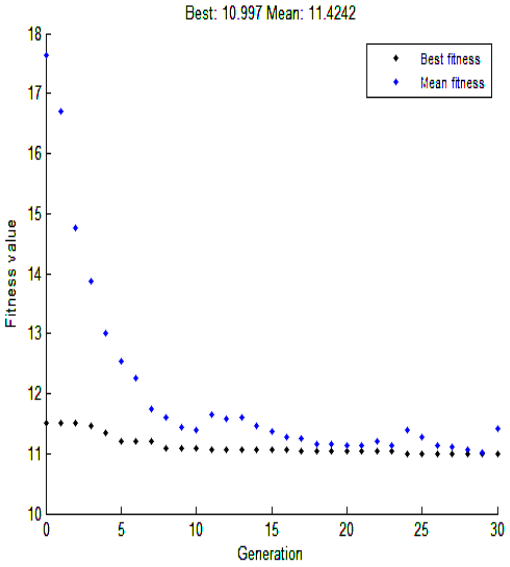

Fig.9 the minimum values of objective function obtained from GA ($a_3 = 0$)

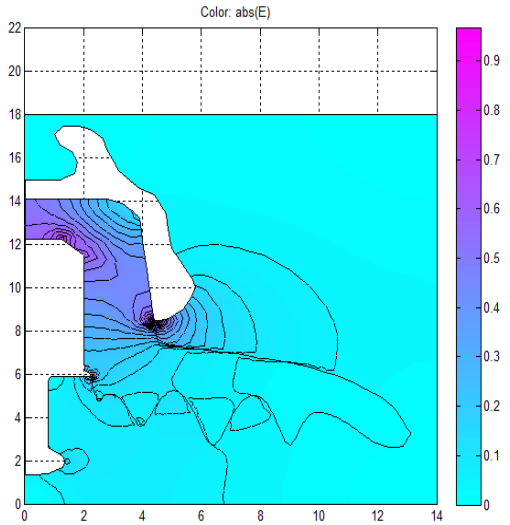

Fig.10 optimal shape of insulator obtained from HGAPSO ($a_3 = 0$)

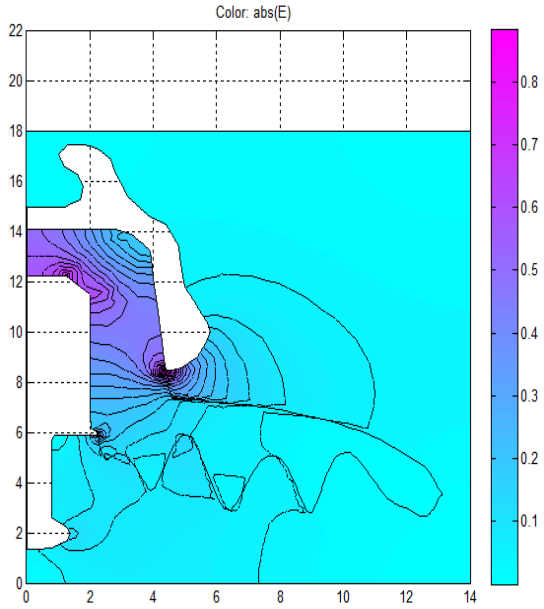

Fig.11 optimal shape of insulator obtained from GA ($a_3 = 0$)

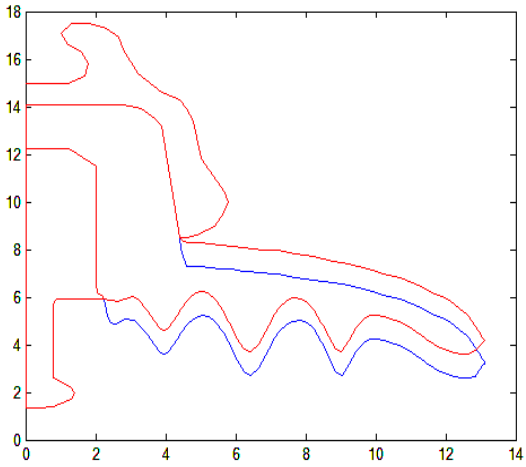

Fig.12 comparison of the optimal shape obtained from HGAPSO with the original shape ($a_3 = 0$)

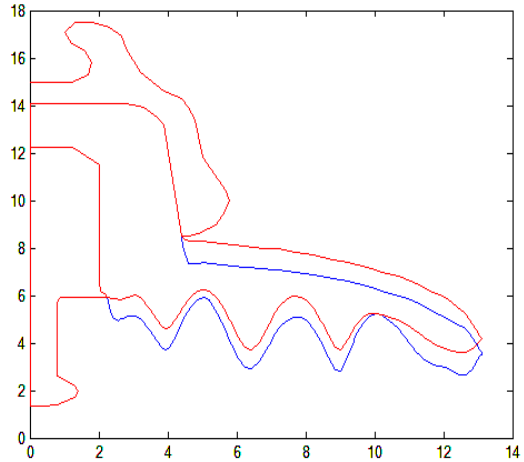

Fig.13comparison of the optimal shape obtained from GA with the original shape ($a_3 = 0$)

TABLE II.
COMPARISON OF THE RESULTS OBTAINED FROM GA and HGAPSO WITH THE VALUES OF ORGINAL INSULATOR ($a_3 = 0$)

	GA	HGAPSO	Original Insulator
E_{ave}	0.0599	0.0588	0.0949
σ_E	0.0501	0.0483	0.1226
A_s	28.8557	30.6432	28.3146

V. CONCLUSION

The minimum of objective function obtained from HGAPSO is smaller than GA. This shows the total coefficients of average and variance of electric field and the area of insulator obtained from HGAPSO is smaller than the result of GA. Therefore, HGAPSO is better than GA for optimizing the shape of insulator. Also, the average and variance of electric field of control points obtained from HGAPSO are smaller than the values of original shape. This shows, we can use HGAPSO for enhancing the distribution of electric field on the insulator.

REFERENCES

[1] M. Abdel-Salam and E. K. Stanek, "Optimizing field stress of highvoltageinsulators," *IEEE Trans. Electr.Insul.*, vol. 22, no. 1, pp. 47–56,Feb. 1987.

[2] M. Abdel-Salam and E. K. Stanek, "Field optimization of high-voltageinsulators," IEEE Trans. Ind. Appl., vol. IA-22, no. 4, pp. 594–601, Jul.1986.

[3] Z. Stih, "High voltage insulating system design by application of electrodeand insulator contour optimization," IEEE Trans. Elect.Insul.,vol. 21, no. 4, pp. 579–584, Aug. 1986.

[4] H. Singer, H. Steinbigler, and P. Weiss, "A charge simulation method for the calculation of high voltage fields," IEEE Trans. Power App.Syst., vol. 126, no. 1, pp. 1660–1668, Feb. 1974.

[5] P. K. Mukherjee and C. K. Roy, "Computation of fields in and around insulators by fictitious point charges," IEEE Trans. Electr. Insul., vol.EI-13, no. 1, pp. 24–31, Feb. 1978.

[6] N. H. Malik, "A review of the charge simulation method and its applications," IEEE Trans. Elect. Insul., vol. 24, no. 1, pp. 3–19, Feb. 1989.

[7] H. El-Kishky and R. S. Gorur, "Electric potential and field computation along ac HV insulators," IEEE Trans. Dielectr.Elect.Insul., vol. 1, no. 6, pp. 982–990, Dec. 1994.

[8] V. Cingoski, K. Kaneda, H. Yamashita, and N. Kowata, "Inverse shape optimization using dynamically adjustable genetic algorithms," IEEETrans. Energy Convers., vol. 14, no. 3, pp. 661–666, Sep. 1999.

[9] R. Hinterding, H. Gieleski, and T. C. Peachey, "The nature of mutation in genetic algorithm," in Proc. 6th Int. Conf. Genetic Algorithms, Jul.1995, pp. 65–72.

[10] W. Chen, H. Yang, and H. Huang, "Contour Optimization of Suspension Insulators Using Dynamically Adjustable Genetic Algorithms," IEEE Trans. Power Delivery, vol. 25, no. 3, pp. 1220–1228, Jul. 2010.

[11] O. W. Andersen, "Finite element solution of complex potential electric fields," IEEE Trans. Power App. Syst., vol. PAS-96, no. 4, pp.1156–1161, Jul./Aug. 1977.

[12] MATLAB PDE Toolbox User's Guide, Version 7.6, 2008.

BIOGRAPHIES

MOHAMMAD REZA SALIMAN was born in Tehran, Iran, in 1986. He received the B.Sc. degree from the Semnan University, Semnan, Iran, MSc degree from Imam Khomeini International University, Qazvin, Iran, and Ph.D. degree from Shahid Beheshti University, Tehran, Iran, all in electrical engineering. His research interests are power system protection and dynamics.

HAMID JAVADI is with the Department of Electrical Engineering, Faculty of Shahid Abbaspour, Shahid Beheshti University, Tehran, Iran. His research interest is power system protection.

Stabilization of Switched Systems Using Only A Single Fractional Order PI Controller

S. E. Hamamci and I. Işık

***Abstract*—In this study, stabilization of switched systems is investigated using only a single controller. Due to providing a rich variety in the control performance, fractional order PI controller is selected as stabilizing controller. For the stabilization process, well known D-partition method is utilized. The proposed method is based on obtaining stability regions in (k_p, k_i)-plane for each sub-system of switched system and then determining a common stability region from intersection of these stability regions. The common region includes the controllers making the overall closed loop system stable for all sub-systems. By changing the order of the integrator in the controller fractionally, a set of common stability regions are obtained. A switched system with two sub-systems was simulated to demonstrate the efficiency of the method.**

***Index Terms*— Switched systems, Fractional order PI controller, Stabilization, Common stability region.**

I. Introduction

SWITCHED systems are a category of hybrid systems composed of different sub-systems and a switching rule specifying the active sub-system in the timetable. [1-3]. The most important property of these systems is to have a decisive impact of switching operation on behavior of the whole system. Although all of the sub-systems in a switched system are stable, the switching operation may lead to unstable or chaotic behaviors in the overall system. Similarly, a switched system with some unstable sub-systems may exhibit a stable behavior with the switching operation [4]. There are many application areas of the switched systems in control of industrial systems and modeling of engineering and physical systems like the switching power converters, automotive industry, aircraft and air traffic control, communication systems, and many other fields [5-7 and references therein]. The most important reason of this, a lot of system can be expressed as "having the switching dynamic between the local models" [4].

Recently, many studies have been reported about the switched systems in literature. In general, these studies can be grouped under two main headings. One of them is analysis of switching system dynamics that is mostly focused on stability [1, 5, 8] and controllability/observability [9, 10] issues. On the other hand, second one is control system design which supply desired performance. There are some studies on the control of switched systems in literature [11-14]. In these studies, the numbers of the used controllers are as the number of sub-systems generally. However, HosseinNia *et al* [15] employed only a single controller for the switched systems. The utilization of single controller is an important idea because of providing the easier design effort.

In this study, the switched systems and their control with single fractional order PI controller is investigated. The objective of the control is to obtain all stabilizing set of fractional order PI controllers for the overall switched system rather than better performance. First, the stability regions using the fractional order PI controller for each sub-systems are obtained separately by Neimark's D-partition method [16]. This region includes the fractional order PI controller parameters that stabilize their sub-systems. Then, plotting these stability regions on a same graph, the common stability region of fractional order PI controller which makes the overall switched system stable are obtained by intersecting these stability regions. Every pair of (k_p, k_i) in this common region gives the stable closed loop control response for each instant of switching. Finally, a set of common stability regions for the various values of fractional order in the controller is determined. An important advantage of the method is that the designer eliminates the controllers which make the overall switched control system unstable.

II. Switched Control System

In literature, the most commonly used control system structure for the switched systems shown in Fig. 1 was suggested by Liberzon and Morse [17]. This structure contains the same number of sub-systems and sub-controllers. In each switching period, only one sub-system and one sub-controller are active. Switching unit decides which the pair of sub-system and sub-controller will be selected. But the major disadvantage of this structure for the designer is to design the sub-controllers as many as the number of sub-systems. Therefore, HosseinNia *et al* [15] suggested an alternative control system structure shown in Fig. 2 instead of the structure of Liberzon and Morse. As can be seen from the figure, the design of only one controller for the switched system control will be sufficient. However, the major

S. E. HAMAMCI is with the Department of Electrical-Electronics Engineering Department, Inonu University, Malatya, Turkey (e-mail: serdar.hamamci@inonu.edu.tr).

İ. IŞIK is with the Department of Electrical-Electronics Engineering Department, Inonu University, Malatya, Turkey (e-mail: ibrahim.isik@inonu.edu.tr).

disadvantage of this structure for the designer is to design a controller which must control all the sub-system is very difficult. But HosseinNia *et al* showed in their publications [15] and [18] that the successful control results can be obtained if the suitable design methods are developed.

In a switched linear system, the transfer function corresponding to each sub-system is defined as

$$G_i(s) = \frac{N_i(s)}{D_i(s)} = \frac{\sum_{k=0}^{p} b_{ik}s^k}{\sum_{k=0}^{q} a_{ik}s^k} \qquad i=1\sim n \tag{1}$$

where i determines which sub-system is active, k refers to indices of polynomial coefficients and n denotes the number of sub-systems. Here $N_i(s)$ and $D_i(s)$ are the numerator and denominator polynomials of $G_i(s)$. p and q are the degrees of the polynomials $N_i(s)$ and $D_i(s)$, respectively. In (1), the condition $p<q$ must be fulfilled for the strictly properness property. The characteristic polynomial of the control system changes for each position of switching. Therefore, the characteristic polynomial for any switching status is described as

$$P_i(s) = 1 + G_i(s)C(s) \qquad i=1\sim n\,. \tag{2}$$

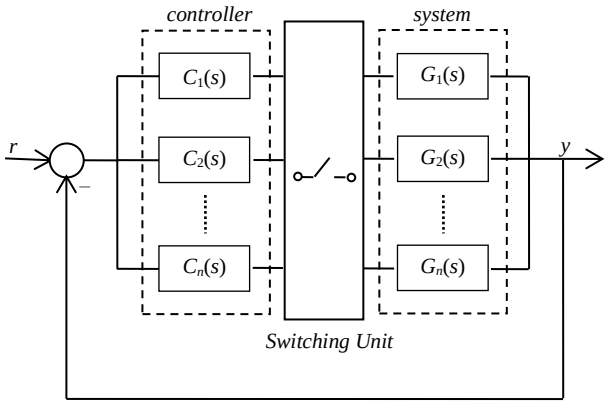

Fig. 1. Switched control system structure containing multi controller.

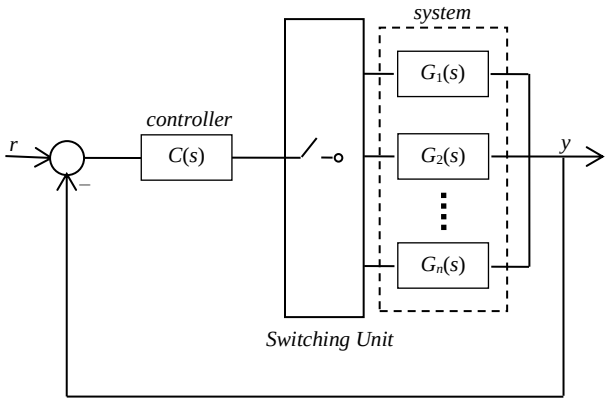

Fig. 2. Switched control system structure containing only one single controller.

Each characteristic polynomial must be Hurwitz stable for the stability of overall closed-loop system.

The controller to be used in this study is in the type of fractional order PI controller [19] and defined by

$$C(s) = k_p + \frac{k_i}{s^\lambda} = \frac{k_p s^\lambda + k_i}{s^\lambda}\,. \tag{3}$$

where λ is fractional order of the integrator part of the controller and its value may vary in the range of (0, 2). This is an advantage because the time and frequency responses can be shaped using functions and, as a consequence, the performance of the closed loop can be improved over the use of integer-order controllers [20]. For λ=1, the fractional order PI controller turns into the classical integer order PI controller.

III. COMPUTATION OF ALL COMMON STABILITY REGIONS

It is well known that the stability of a control system is determined by locating it's all poles to the left half plane (LHP) of the complex plane. The stability region for the control system is expressed by a conformal mapping of the LHP to the controller parameter plane. This region contains a controller parameters set that makes the closed loop system stable. Therefore, the characteristic polynomial of the control system plays an important role for obtaining the stability region.

As mentioned above, the switched control system has many characteristic polynomials as defined in (2). Substituting the transfer function of the switched system in (1) and the controller transfer function in (3) into (2), we obtain

$$\begin{aligned} P_i(s) &= 1 + \frac{\sum_{k=0}^{p} b_{ik}s^k}{\sum_{k=0}^{q} a_{ik}s^k} \cdot \frac{k_p s^\lambda + k_i}{s^\lambda} \\ &= \sum_{k=0}^{q} a_{ik}s^{k+\lambda} + k_p \sum_{k=0}^{p} b_{ik}s^{k+\lambda} + k_i \sum_{k=0}^{p} b_{ik}s^k\,. \end{aligned} \tag{4}$$

For obtaining the stability regions, there are some methods in the literature, for example parameter space approach [21], Hermite Biehler theorem [22], D-partition method [16], etc. In this study, the D-partition method is preferred because of its easy and systematic methodology. The method is based on the calculation of stability boundaries as summarized in Appendix after Section 5. Hence, for each sub-systems, the real root boundary (RRB) line putting s=0 into (4) is obtained as

$$k_i = 0\,. \tag{5}$$

The infinite root boundary does not exist because of $m<n$. Finally, the complex root boundary (CRB) is obtained by equating the real and imaginary parts of $P_i(jw)$ to zero. In this case, Equation (4) is returned to two equations:

$$w^\lambda A(w)k_p + B(w)k_i = w^\lambda P(w) \tag{6}$$

$$w^\lambda C(w)k_p + D(w)k_i = w^\lambda Q(w) \tag{7}$$

where,

$A(w) = \sum_{k=0}^{p} b_{ik} x_k w^k$,
$B(w) = \sum_{k=0}^{p} b_{ik} z_k w^k$,
$C(w) = \sum_{k=0}^{p} b_{ik} y_k w^k$,
$D(w) = \sum_{k=0}^{p} b_{ik} t_k w^k$,
$P(w) = -\sum_{k=0}^{q} a_{ik} x_k w^k$,
$Q(w) = -\sum_{k=0}^{q} a_{ik} y_k w^k$,

$x_k = \Re\{j^{(k+\lambda)}\}$, $y_k = \Im\{j^{(k+\lambda)}\}$, $z_k = \Re\{j^k\}$ and $t_k = \Im\{j^k\}$. Here, $\Re$ and $\Im$ denote the real and imaginary parts of a complex number or variable. After solving these two equations, we obtain k_p and k_i parameters with the following equations:

$$k_p = [Q(w)B(w) - P(w)D(w)]/[B(w)C(w) - A(w)D(w)] , \quad (8)$$

$$k_i = w^{\lambda}\{[Q(w)B(w) - P(w)D(w)]/[B(w)C(w) - A(w)D(w)]\} . \quad (9)$$

Changing w between (0, ∞), many (k_p, k_i) points can be marked as a point in (k_p, k_i)-plane. Connecting these points, the complex root boundary can be obtained as a line or curve.

Plotting complex and real root boundaries together on a same (k_p,k_i)-plane, the parameter plane is divided into a large number of parts. The most important feature of these parts is that all (k_p,k_i) pairs in a region are produce the characteristic polynomials at the same stability property. Therefore, these parts can be tested by substituting any test point, which is selected randomly from each part, into characteristic polynomial. The part is determined as the stability region whose all roots of the characteristic polynomial are in LHP.

For i=1~n, a set of stability regions corresponding to each subsystems is found. Intersection of these stability regions are called as *common stability region*. Any (k_p, k_i) pairs chosen in the common region make the control system stable for all situations of switch. Similarly, changing the order of integrator in controller in the range of (0, 2), a set of common stability regions is determined. As a result, the designer has a large facility for the performance decision.

IV. SIMULATION EXAMPLE

In this section, a simulation example to show the efficiency of the proposed method will be given. Since the widely used switched systems in industry are with two sub-systems, a switched system having two sub-system with second order considered in [15] is studied in this example. The transfer functions of the system is given by

$$G_1(s) = \frac{2}{s^2+0.6s+0.1} \quad (10)$$

$$G_2(s) = \frac{0.5}{s^2+0.3s+0.023} \quad (11)$$

The purpose of this example is to obtain the common stability regions for different values of λ.

The characteristic polynomials for the sub-systems can be obtained as

$$P_1(s) = s^{\lambda+2} + 0.6s^{\lambda+1} + (0.1 + 2k_p)s^{\lambda} + 2k_i \quad (12)$$

$$P_2(s) = s^{\lambda+2} + 0.3s^{\lambda+1} + (0.023 + 0.5k_p)s^{\lambda} + 0.5k_i \quad (13)$$

The RRB for both $G_1(s)$ and $G_2(s)$ are the line $k_i = 0$ as given in (5). From (8) and (9), the CRB for each sub-systems are calculated as below:

– Sub-system 1:

$$k_p = \frac{1}{2y_0}[-y_2w^2 - 0.6y_1w - 0.1y_0] \quad (14)$$

$$k_i = \frac{w^{\lambda}}{2y_0}[(x_0y_2 - x_2y_0)w^2 - 0.6(x_0y_1 - x_1y_0)w] \quad (15)$$

– Sub-system 2:

$$k_p = \frac{2}{y_0}[-y_2w^2 - 0.3y_1w - 0.023y_0] \quad (16)$$

$$k_i = \frac{2w^{\lambda}}{y_0}[(x_0y_2 - x_2y_0)w^2 - 0.3(x_0y_1 - x_1y_0)w] \quad (17)$$

where $x_2 + jy_2 = j^{(\lambda+2)}$, $x_1 + jy_1 = j^{(\lambda+1)}$ and $x_0 + jy_0 = j^{\lambda}$.

In case of λ=1, the view of RRB and CRB in the parameter plane are given in Figs. 3 and 4 for each sub-systems. It is obviously seen that the parameter planes in these figures is partitioned to three parts:

1. above of CRB,
2. between CRB and RRB,
3. under of RRB.

When the stability of these parts are examined for each (k_p,k_i) points taken from the parts randomly, one concludes that the triangular region is stable between CRB and RRB for both of sub-systems. Note that there is not any boundary at the right side of this triangular region. It is seen from the figures, the stability region of first sub-system is greater than that of second sub-system. This implies that the number of PI controllers making the first sub-system stable is greater than ones for making the second sub-system stable. If Figs. 3 and 4 are plotted on a same frame as shown in Fig. 5, the intersection of two stability regions (1st region in Fig. 5) is called as *common stability region*. The PI controllers selected from this region makes the overall closed-loop system stable in every switching stage. Thus the designer can choose any PI controller from the common region without considering the switching status and the subsystems. In the second region drawn with horizontal lines and outside of common region in

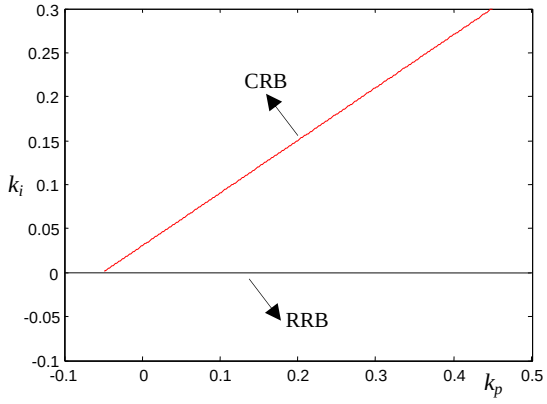

Fig. 3. PI stability region belonging to $G_1(s)$ sub-system.

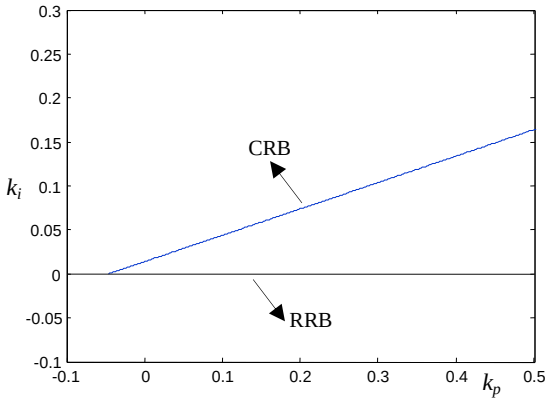

Fig. 4. PI stability region belonging to $G_2(s)$ sub-system.

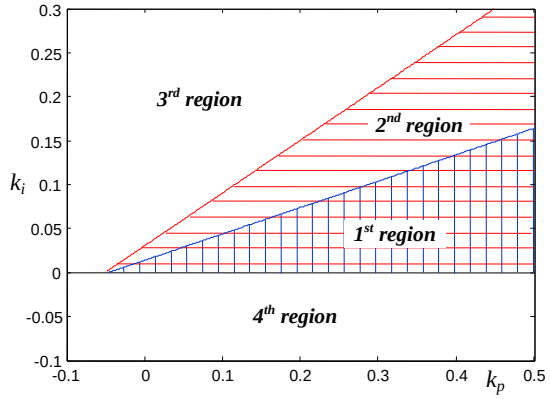

Fig. 5. Common stability region of the overall control system.

Fig. 5, the overall control system is stable for first sub-system but unstable for the second sub-system. In the third and fourth regions where they are not drawn with any lines, the control system is unstable for both of sub-systems. Furthermore, it is seen from Fig. 5 that there is not any region in the parameter space where the overall control system is stable for the second sub-system and is unstable for the first sub-system.

To verify the results in Fig.5, the unit step responses for the PI controllers (λ=1) selected from four different places of Fig. 5 are analyzed. In this analysis, the unit step signal is applied to the input of control system and switching from first sub-system to second sub-system is made at t=75s. Firstly, the unit step response of the overall control system for the PI controller parameters which are selected as k_p=0.05, k_i=0.01 from the common stability region (1st region) randomly is shown in Fig. 6a It is clearly seen from the figure, stable responses for the overall control system are produced by both first sub-system/PI controller pairs at first 75s and second sub-system/PI controller pairs at next 75s. In Fig. 6b, the unit step response of the overall control system for k_p=0.3, k_i=0.1 values selected on boundary line between first and second regions is given. In this case, the control system is stable for the first 75s but an oscillating response is occurred after switching. On the other hand, in Figs. 6c and 6d, the output

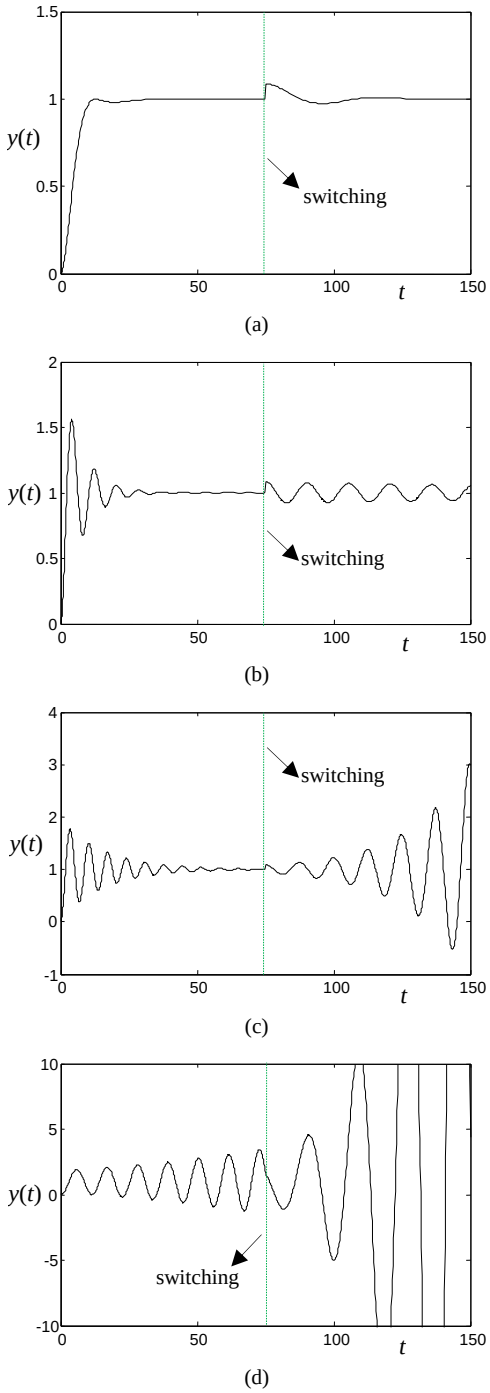

Fig. 6. Unit step responses of switched control system for four different PI controllers: a) k_p=0.05, k_i=0.01; b) k_p=0.3, k_i=0.1; c) k_p=0.4, k_i=0.2 and d) k_p=0.1, k_i=0.1.

responses of closed loop system are given for k_p=0.4, k_i=0.2 and k_p=0.1, k_i=0.1 values selected from second and third regions. Unit step response of the overall control system is stable before switching and unstable after the switching for PI controller values selected from second region while the unit step response of the control system is unstable before and after switching for the PI controller values chosen from third region.

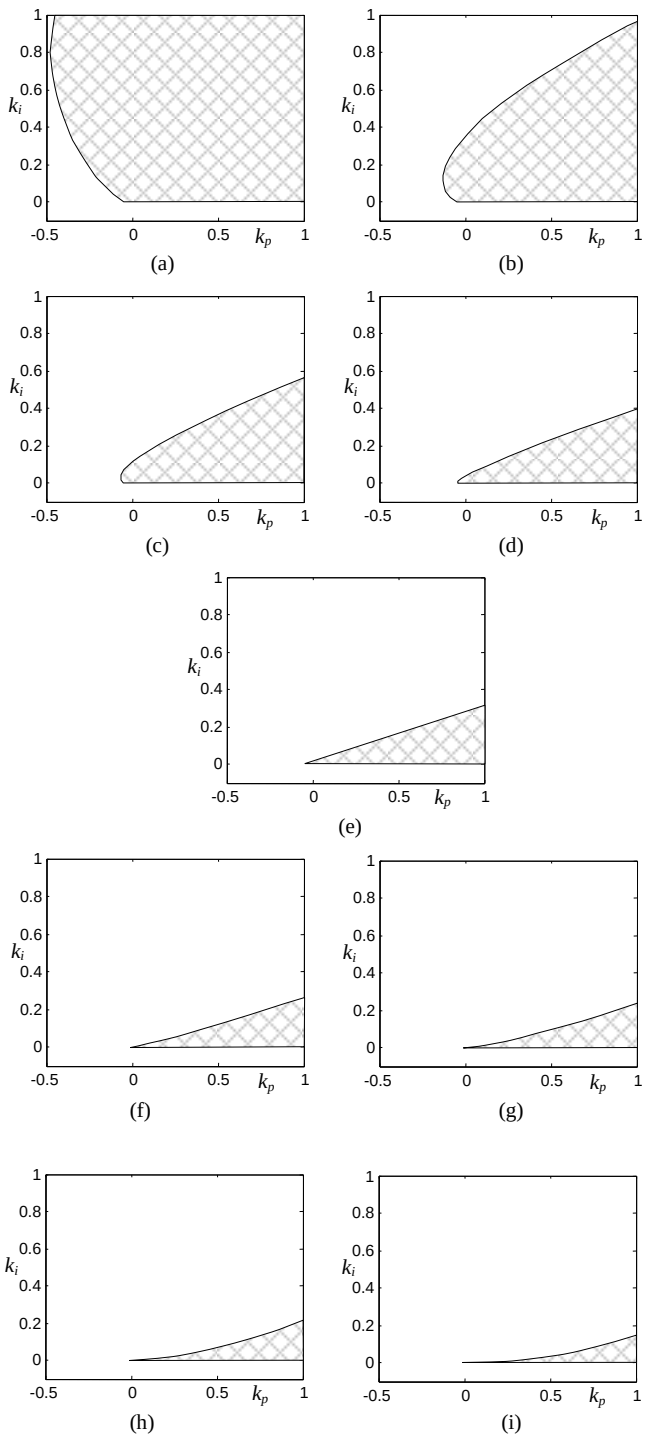

Fig. 7. The common stability regions for the values of λ in the range of (0, 2): a) λ=0.2, b) λ=0.4, c) λ=0.6, d) λ=0.8, e) λ=1, f) λ=1.2, g) λ=1.4, h) λ=1.6, i) λ=1.8.

Finally, changing λ from 0 to 2, the set of common stability regions are obtained as shown in Fig. 7. It is seen from Fig. 7 that smaller λ gives bigger common stability region.

Remark: The fractional order PI controllers with smaller value of λ than 1 provide bigger stability regions according to integer order PI controller. This is an important result that can give new ideas to the designers in industry.

The obtained results clearly show that the presented method gives a successful way to find a stability map for the fractional order PI switched control system.

V. CONCLUSIONS

In this paper, a study on obtaining the stability map for the switched systems using a single fractional order PI controller is given. The common stability region presented in this study contains all controllers which make the overall control system stable without considering the switching status. For obtaining the common stability region, it is made use of D-partition method. The method in this paper may be considered as an extended version of the method given in [23]. In the previous version, the switched systems with only two subsystems and the conventional PI controller are considered. In this paper, however, the switched systems with more subsystems and the fractional order PI controller which is generalized version of conventional PI controller are examined. Thus, a set of common stability regions using fractional PI controller is obtained instead of only a common stability region using the classical PI controller. This provides to the designer more flexibility for his/her decision in the controller selection process. Simulation results confirm the results. However, note that the performance of the overall switched control system is a different topic. Whether bigger stability region gives better performance or not is an open issue that must be studied.

APPENDIX: SUMMARY FOR D-PARTITION METHOD

Consider a characteristic polynomial with unknown x_i (i=1~n) parameters which is defined by

$$P(s; x_1, x_2, \ldots x_n) = P_0(s) + P_1(s)x_1 + \cdots + P_n(s)x_n \,. \qquad \text{(A.1)}$$

Here, $P_i(s)$ refers to known parts of polynomial for i=1~n. To find x_i unknown values, the D-partition method has been proposed by Neimark [16] as an effective technique which finds a set of x_i values stabilizing the polynomial in (A.1). In other words, all the set of x_i values are found so that all roots of the polynomial are remained in LHP. This method gives very good results in stability analysis and design of control systems. These sets of x_i values constitute a stability region in (x_1, x_2,…, x_n)-parameter space.

For obtaining the stability region in the parameter space, three important stability boundaries are used [21, 24]. These regions are defined as follows.

– *Real Root Boundary (RRB):* This boundary is determined by the equation $P(s; x_1, x_2, \ldots \ldots x_n)|_{s=0} = 0$. This equation always gives a line in the parameter space if this boundary exists.

– *Infinite Root Boundary (IRB):* This boundary is obtained by the equation $P(s; x_1, x_2, \ldots \ldots x_n)|_{s=\infty} = 0$. The equation means equating the largest coefficient of the polynomial to zero. This equation also always gives a line in the parameter space if this boundary exists.

– *Complex Root Boundary (CRB):* This boundary is found by the equation $P(s; x_1, x_2, \ldots \ldots x_n)|_{s=jw} = 0$. For obtaining this boundary, putting jw instead of s in the characteristic polynomial and equating the real and imaginary parts of the

polynomial to zero separately. This equation usually gives a curve (sometimes a line in the simple systems) in the parameter space if this boundary exists.

These boundaries are partitioned the parameter space to many parts. Stability test is applied for each parts. In the results of the stability test, the stability region can be obtained.

REFERENCES

[1] D. Liberzon, *Switching in Systems and Control*, Birkäuser, 2003.

[2] J. Daafouz, P. Riedinger, and C. Lung, "Stability analysis and control synthesis for switched systems: A switched Lyapunov function approach," *IEEE Trans. on Automatic Control*, vol. 47, no. 11, pp. 1883–1887, 2002.

[3] S.L. Chen, Y.Yao, and X. Di, "Robust Stabilization for a Class of Uncertain Discrete-time Switched Linear Systems," In: *Discrete Time Systems*, edited by M.A. Jordán, InTech-Open Access Company.

[4] D.J. Leith, R.N. Shorten, W.E. Leithead, O. Mason, and P. Curran, "Issues in the design of switched linear control systems: A benchmark study," *Int. J. Adapt. Control Signal Process*, vol. 17, no. 2, pp. 103–118, 2003.

[5] S. Kim, S.A. Campbell, and X. Liu, "Stability of a Class of Linear Switching Systems With Time Delay," *IEEE Trans. on Circuits and Systems-I: Regular Papers*, vol. 53, no. 2, pp. 384-393, 2006.

[6] Z. Sun, and S.S. Ge, "Analysis and synthesis of switched linear control systems," *Automatica*, vol. 41, no. 2, pp. 181-195, 2005.

[7] K. Wulff, *Quadratic and Non-Quadratic Stability Criteria for Switched Linear Systems*, Ph.D Thesis, National University of Ireland, 2004.

[8] M.S. Branicky, "Stability of switched and hybrid systems," in: *Proc. the 33rd IEEE Conf. on Decision and Control*, pp. 3498-3503, 1994.

[9] Z. Sun, S. S. Ge, and T. H. Lee, "Controllability and reachability criteria for switched linear systems," *Automatica*, vol. 38, no. 5, pp. 775–786, 2002.

[10] J.P. Hespanha, D. Liberzon, D. Angeli, and E.D. Sontag, "Nonlinear norm-observability notions and stability of switched systems," *IEEE Trans. Automat. Control*, vol. 52, no. 2, pp. 154–168, 2005.

[11] S. Solmaz, R. Shorten, K. Wulff ve F.Ó. Cairbre, "A design methodology for switched discrete time linear systems with applications to automotive roll dynamics control," *Automatica*, vol. 44, no. 9, pp. 2358-2363, 2008.

[12] X. Xu and P. J. Antsaklis, "Optimal control of switched systems based on parameterization of the switching instants," *IEEE Trans. Automat. Control*, vol. 49, no. 1, pp. 2–16, 2004.

[13] K. Wulff, F. Wirth, and R. Shorten, "A control design method for a class of switched linear systems," *Automatica*, vol. 45, no. 11, pp. 2592-2596, 2009.

[14] C. Chen, S. Fei, K. Zhang, and Y. Lu, "Control of switched linear systems with actuator saturation and its applications," *Mathematical and Computer Modelling*, vol. 56, no. 1-2, pp. 14-26, 2009.

[15] S.H. HosseinNia, I. Tejado, B.M. Vinagre, "Robust Fractional order PI Controller for Switching Systems," in: *Proc. the 5th Symp. on. Fractional Differentiation and its Applications (FDA'2012)*, Hohai University, 2012.

[16] Y.I. Neimark, "D-decomposition of the space of quasi-polynomials (on the stability of linearized distributive systems)," *American Mathematical Society Translations*, vol. 102, pp. 95-131, 1973.

[17] D. Liberzon, ve A.S. Morse, "Basic problems in stability and design of switched systems," *IEEE Control Systems Magazine*, vol. 19, pp. 59–70, 1999.

[18] S.H. HosseinNia, I. Tejado, B.M. Vinagre, "A method for the design of robust controllers ensuring the quadratic stability for switching systems," *J. of Vibration and Control*, vol. 20, no. 7, pp. 1085-1098, 2014.

[19] I. Podlubny, "Fractional Order Systems and $PI^{\lambda}D^{\mu}$ Controllers," *IEEE Trans. on Automatic Control*, vol. 44, no. 1, pp. 208-214, 1999.

[20] J. Hwang, J.-F. Leu, and S.-Y. Tsay, "A note on time-domain simulation of feedback fractional-order systems," *IEEE Trans. on Automatic Control*, vol. 47, no. 4, pp. 625-631, 2002.

[21] J. Ackermann, D. Kaesbauer, "Design of robust PID controllers," in: *Proc. the European Control Conference*, pp. 522-527, 2001.

[22] M.-T. Ho, A. Datta, and S.P. Bhattacharyya, "A new approach to feedback stabilization," in: *Proc. The 35th Conf. on Decision and Control*, Kobe, Japan, 1996.

[23] İ. Işık, and S.E. Hamamci, "Anahtarlamalı Sistemleri Kararlı Yapan PI Kontrolör Setinin Hesabı," in: *Proc. the TOK 2013 Turkish Automatic Control National Meeting*, Malatya, Turkey, 2013, (in Turkish).

[24] Y.C. Cheng, and C. Hwang, "Stabilization of unstable first-order time-delay systems using fractional-order PD controllers," *J. of the Chinese Inst. of Engineers*, vol. 29, pp. 241-249, 2006.

BIOGRAPHIES

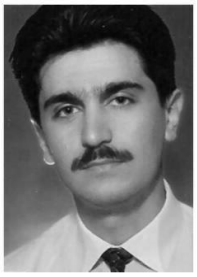

SERDAR E. HAMAMCI received the B.S. degree in electronics engineering from Erciyes University in 1992 and the M.S. and Ph.D. degrees in electrical-electronics enginnering from Firat University in 1997 and 2002 respectively.

From 1993 to 2009, he was a Research Assistant with the Electrical-Electronics Engineering Department at Inonu University. Since 2009, he has been an Associate Professor with the same department. His research interest includes control system design, stabilization and fractional order systems.

A Review Study on Mathematical Methods for Fault Detection Problems in Induction Motors

E. Ayaz

***Abstract*—Induction motors are frequently used in industrial processes. Failure of these machines may cause economic, quality and safety losses. In this paper, the mathematical methods used in detection of mechanical and electrical faults of these motors are reviewed together with theory and application examples on the current and vibration data which is acquired during performance tests of the motors followed by accelerated aging.**

Index Terms—**Induction motor, fault detection, aging, signal processing**

1. INTRODUCTION

INDUCTION motors are widely used electrical drives in industrial processes due to their wide power range, simple and rugged structure. When the motor ages or a fault occurs in the motors, these may cause losses in their efficiency, economic and safe operation of industrial processes. The faults can be categorized into as being mechanical or electrical faults. According to the statistical surveys performed on motors revealed that 41% of failures are resulted from bearing faults, 37% of them are from stator faults, 10% is from rotor faults, and 12% are from other faults such as unbalanced phase supply, soft foot, asymmetries in the magnetic circuits etc. [1-7]

This paper addresses fault detection methods in induction motors together with theory and applications on experimental data acquired during performance test of the motors subjected to accelerated aging [6-7]. Detection of eccentricity fault [7-9], bearing fault [10-18], and stator insulation fault [19-20] is considered. Applications of statistical methods, power spectral density analysis, coherence analysis, continuous and discrete wavelet transform, autoregressive modeling method, adaptive neuro-fuzzy inference system, artificial neural network is presented by means of the experimental data.

2. MATHEMATICAL METHODS

This section includes mathematical methods used in signal analysis for fault detection and diagnosis studies. These are frequency domain methods, time-frequency/scale domain methods, stochastic methods, and soft computing methods.

2.1. FREQUENCY DOMAIN METHODS

Since different fault types generate different frequency spectrum distributions, the diagnosis results are based on frequency features of signals. Frequency content of a signal at frequency $m\Delta f$ can be found by Fourier transform given as below [21-22]

$$X(m\Delta f) = \sum_{k=0}^{N-1} x(k\Delta t)\, \exp\left(-\frac{j2\pi km}{N}\right) \qquad (1)$$

where N is the number of samples, Δf is the frequency resolution, m is integer number and Δt is the data-sampling interval. The auto-power spectral density (APSD) of $x(t)$ is estimated as

$$S_{xx}(f) = \frac{1}{N}|X(m\Delta f)|^2 \ , \quad f = m\Delta f \qquad (2)$$

The cross power spectral density (CPSD) between $x(t)$ and $y(t)$ is similarly estimated. The statistical accuracy of the estimate in Equation (2) increases as the number of data points or the number of blocks of data increases.

The cause and effect relationship between two signals or the commonality between them is generally estimated using the coherence function. The coherence function is given by

$$\gamma_{xy}(f) = \frac{|S_{xy}(f)|}{\sqrt{S_{xx}(f)\, S_{yy}(f)}} \ , \quad 0 < \gamma_{xy} < 1 \qquad (3)$$

where S_{xx} and S_{yy} are the APSD's of $x(t)$ and $y(t)$, respectively, and S_{xy} is the CPSD between $x(t)$ and $y(t)$. A value of coherence close to unity indicates highly linear and close relationship between the two signals.

2.2. TIME-FREQUENCY/SCALE DOMAIN METHODS

To find time localization of the frequency content of the signal short-time Fourier transform (STFT) can be used which is defined as [23-24]

$$STFT(\tau, f) = \int_{-\infty}^{\infty} x(t)\, g(t-\tau) \exp[-2\pi f t]\ dt. \qquad (4)$$

E. AYAZ is with the Faculty of Electrical and Electronic Engineering, Istanbul Technical University, Istanbul, Turkey (e-mail: ayaze@itu.edu.tr).

In STFT, the signal $x(t)$ is first windowed using different type of window functions $g(t)$ such as triangular window, rectangular window, Gaussian window etc. centered at time location τ. Then Fourier Transform of resulting windowed signal is taken. This gives the STFT of signal for particular time. As window slides along time axis, so basically STFT maps input signal $x(t)$ into two dimensional function in a time-frequency plane with fixed resolution.

Wavelet transform can be used to separate the signal into frequency bands and to get variable resolution which is good time resolution for rapidly changing signals and good frequency resolution for slowly changing signals. The continuous wavelet transform is defined as

$$W_f(a,b) = \int_{-\infty}^{\infty} x(t)\ \psi_{a,b}(t)\ dt \tag{5}$$

where

$$\psi_{a,b}(t) = \frac{1}{\sqrt{|a|}}\ \psi\left(\frac{t-b}{a}\right)\ ; \quad a,b \in R\ ; a \neq 0 \tag{6}$$

ψ is called the mother wavelet. The dilation parameter a controls the scale or frequency of wavelet, and the translation parameter b controls the position of the wavelet in time. The parameters a and b are defined as $a = a_0^j, b = nb_0a_0^j$ where $n, j \in Z,\ a_0 > 1,$ and $b_0 > 0,$ the Discrete Wavelet Transformation (DWT) is given as

$$DWT[j,k] = \frac{1}{\sqrt{a_0^j}} \sum_n x[n]\ \psi\left[\frac{k - nb_0a_0^j}{a_0^j}\right] \tag{7}$$

S. Mallat introduced an efficient algorithm to perform the DWT known as the Multi-Resolution Analysis (MRA). The MRA is similar to a two-channel sub-band coder used in high-pass and low-pass filters, from which the original signal can be reconstructed.

The frequency decomposition of the signal is shown schematically (Fig.1). The low-frequency sub-band is referred to as approximation a_i and the high-frequency sub-band by detail d_i. Thus, at the second stage the signal may be reconstructed as

$$S = a_2 + d_1 + d_2 \tag{8}$$

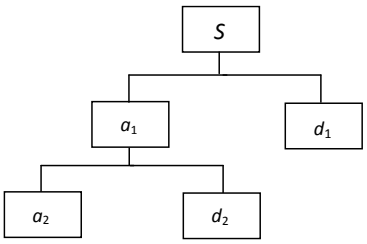

Fig.1. Signal decomposition at the second stage.

2.3. STOCHASTIC METHODS

This section gives statistical methods and time series modeling methods.

2.3. 1. STATISTICAL METHODS

Several statistical parameters, calculated in the time domain, are generally used to define average properties of machinery data. The two basic parameters are the mean value μ and the standard deviation σ. For a given data set $\{x_i\}$ these are defined as follows [25]:

$$\mu = \frac{1}{N}\sum_{i=1}^{N} x_i \tag{9}$$

$$\sigma = \sqrt{\frac{1}{N}\sum_{i=1}^{N}(x_i - \mu)^2} \tag{10}$$

where N is the number of the data points. For the Gaussian (normal) probability distribution, two parameters that reflect the departure from the normal distribution are skewness (c) and kurtosis (k). These are calculated as follows.

$$c = \frac{\left[\frac{1}{N}\sum_{i=1}^{N}(x_i - \mu)^3\right]}{\sigma^3} \tag{11}$$

$$k = \frac{\left[\frac{1}{N}\sum_{i=1}^{N}(x_i - \mu)^4\right]}{\sigma^4} \tag{12}$$

For a perfect normal distribution, c is equal to zero. A negative value is due to skewness towards lower values while a positive value indicates non-symmetry towards higher values. For small data sets, one often gets values that differ from zero. The kurtosis or flatness k, is very close to unity for a normal distribution. These statistical parameters may be used to perform a quick check of the changes in the statistical behaviour of a signal.

2.3. 2. TIME SERIES MODELING METHODS

In time series analysis the autoregressive (AR) modeling method is used commonly due its simplicity and ability to show sharp peaks in the frequency domain. The AR method establish the mathematical model for regression and forecast, hence the AR coefficients of the model represent the signal features, and can be used for fault detection purposes [16,26].

AR modeling is a parametric method and represents the signal as a linear combination of its previous values plus an error term. AR model of order p for the signal $x(n)$ is given as

$$x(n) + \sum_{k=1}^{p} a_k\ x(n-k) = v(n) \tag{13}$$

where a_k for $k = 0,1,\ldots, p$ are AR coefficients and $v(n)$ is the white noise with variance σ_v^2. The filter coefficients are determined using the autocorrelation sequence of the AR process which satisfies the Yule-Walker equations given by

$$r_x(k) + \sum_{l=1}^{p} a_l\, r_x(k-l) = \sigma_v^2 \delta(k) \;\; ; \;\; k \geq 0 \qquad (14)$$

where $\delta(k)$ is the unit sample sequence. Thus given the autocorrelations $r_x(k)$ for $k = 0,1,\ldots, p$ these equations can be solved for the AR coefficients a_k and σ_v. In most applications $r_x(k)$ is unknown and estimated from a sample realization of the process. Given $x(n)$ for $0 \leq n \leq N$, where N is the number of samples, $r_x(k)$ is estimated using the sample autocorrelation

$$\hat{r_x}(k) = \frac{1}{N}\sum_{n=0}^{N-1} x(n)x(n-k) \qquad (15)$$

Order selection is important in terms of to get less error between signal and its AR model. And also there must be enough number of coefficients, but not too much, to diagnose faults conveniently. Akaike's Information Criteria (AIC) can be used for order selection and given as follows

$$AIC(p) = N\, ln(\, \sigma_v^2) + 2p \qquad (16)$$

2.4. SOFT COMPUTING METHODS

The relation matrix between fault types and fault features extracted from vibration, current, temperature signals can be too complicated to determine fault types by this matrix with human inference. Intelligent methods like artificial neural networks (ANN) and adaptive neuro-fuzzy inference system (ANFIS) can be used for classification and pattern recognition.

2.4.1. ARTIFICIAL NEURAL NETWORKS

ANN is an interconnection of computational elements known as neurons [27]. Each neuron has multi inputs from other neurons with assigned weights. The output of a neuron is computed by summing of all the weighted inputs and then passing it through a function. ANN consists of one or more layers of neurons in interconnected topology (Fig.2).

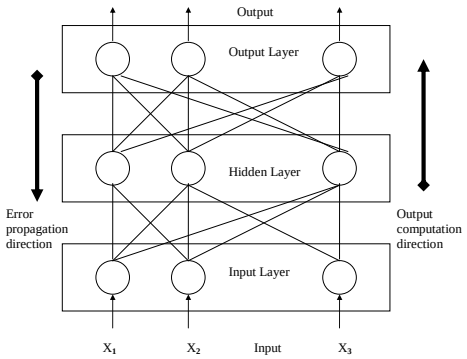

Fig.2. Topology of a feed forward neural network with three layers.

The backpropagation learning algorithm is widely used to determine input-output relationship of a system. It is an iterative gradient search algorithm which adjust each weight in a multilayer network so as to reduce the error in the outputs. It works by propagating errors backward from the output layer. For a three layer ANN with I inputs, one hidden layer with J neurons and K outputs neurons, the error function is

$$E = \frac{1}{2}\sum_{p=1}^{P}\sum_{k=1}^{K}(y_{kp} - d_{kp})^2 \qquad (17)$$

where y_{kp} and d_{kp} are the actual and desired outputs of the pattern respectively. Individual weight adjustment between the hidden layer and the output layer for pattern p are computed by

$$\Delta\omega_{kj} = -\eta\frac{\partial E_p}{\partial \omega_{kj}} \qquad (18)$$

where j=1,2,…J and η is a constant learning rate. The weights between hidden and output layers are adjusted using the recursive formula given as

$$\omega_{kj}(n+1) = \omega_{kj}(n) + \eta\Delta\omega_{kj} \qquad (19)$$

where n is the iteration number. Similar weight adjustment formulas can be obtained between the input and output layers by changing the indices from k to i.

2.4.2. ADAPTIVE NEURO-FUZZY INFERENCE SYSTEM

Adaptive neuro-fuzzy inference system (ANFIS) is an implementation of a fuzzy logic inference system with the architecture of a five-layer feed-forward network [18,19,27,28]. With this way ANFIS uses the advantages of learning capability of neural networks and inference mechanism similar to human brain provided by fuzzy logic. The architecture of ANFIS with two inputs, one output and two rules is given (Fig.3). Here x, y are inputs, f is output, the circles represent fixed node functions and squares represent adaptive node functions. This is a Sugeno-type fuzzy system, where the fuzzy *IF-THEN* rules have the following form:

Rule 1: If x is A_1 and y is B_1 then $f_1 = p_1\, x + q_1\, y + r_1$
Rule 2: If x is A_2 and y is B_2 then $f_2 = p_2\, x + q_2\, y + r_2$

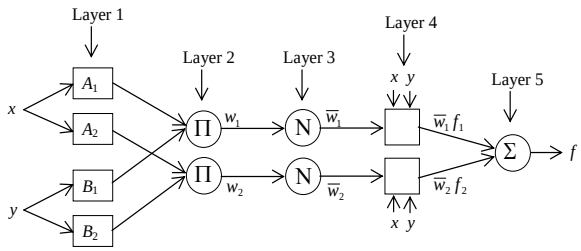

Fig.3. ANFIS architecture with two rules.

The operation of each layer is as follows:

Layer 1 called fuzzification layer and it fuzzify the values of the input variables according to a membership function. This layer forms the antecedents of the fuzzy rules (*IF* part). Generalized bell membership function (Fig.4) is popular for specifying fuzzy sets because of their smoothness and concise notation. The parameters $\{a_i, b_i, c_i\}$ of the membership function are called as premise parameters where i denotes the node number.

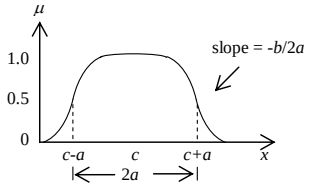

Fig.4. Generalized bell function.

Layer 2 is rules layer and performs fuzzy AND operation at the nodes. Thus the output is the product of all incoming signals and represents the firing strength of each rule. Layer 3 is normalization layer. Layer 4 is fuzzy inference or consequent layer which estimates the rule's output (*THEN* part). The parameters $\{p_i, q_i, r_i\}$ of each rule's output are referred as consequent parameters. Layer 5 is called defuzzification layer and calculates the sum of the outputs of all the rules. Learning of ANFIS is done using hybrid learning procedure given in Table 1. This algorithm combines backpropagation gradient descent and least squares method for identification of premise and consequent parameters in such a way that ANFIS output matches the training data.

Table 1. Hybrid learning procedure.

	Forward pass	Backward pass
Premise parameters	Fixed	Gradient descent
Consequent parameters	Least squares	Fixed
Signals	Node outputs	Error signals

3. CASE STUDIES

In this section example applications of mathematical methods on experimental data for detection of mechanical and electrical faults in induction motors are given. Detection of eccentricity fault, bearing fault, and insulation fault is considered. For this purpose 5 HP, three phases, four poles induction motor is subjected to bearing damage and winding insulation damage as well as thermal and chemical aging [6-7]. After each aging cycle the data is collected at 12 kHz sampling frequency under 100 % load condition. Seven aging cycle is performed until the motor is broken down.

3.1. MECHANICAL FAULTS AND THEIR DETECTION

Airgap eccentricity (Non-uniform air gap):

Air gap eccentricity may be the consequence of bearing, wear or bearing failure, bad motor assembly with rotor unbalance or a rotor which is not perfectly centered [4,8-9]. This eccentricity causes anomalies in the air gap flux density and creates frequency side bands at around the supply frequency of the stator current signal for each phase. The side-band frequencies caused by the dynamic eccentricity are given as

$$f_{ecc} = f_e\left[1 \mp k\left(\frac{1-s}{p/2}\right)\right] = |f_e \mp k f_r| \ , \ k = 1, 2, 3, \ldots \quad (20)$$

where f_e is the electrical supply frequency, s is the per unit slip, p is the number of poles, and f_r is the rotor speed in Hz. Slip $s = (f_s - f_r)/f_s$, where f_s is the synchronous frequency.

The side-band effects of the motor current signals both of the healthy and faulty cases by means of their power spectral density variations at around supply frequency 60 Hz is shown in (Fig.5a) and (Fig.5b).

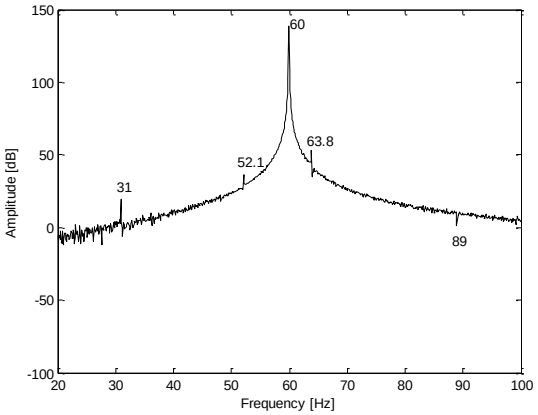

(a) APSD for healthy case.

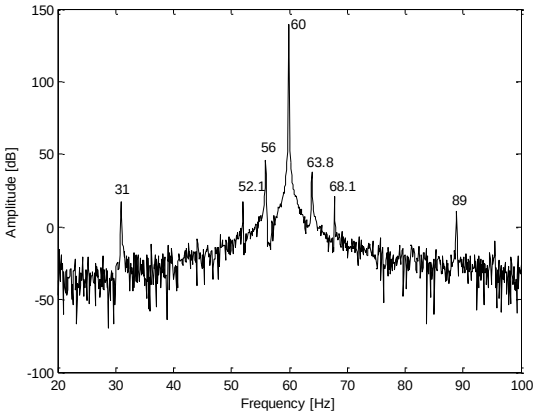

(b) APSD for aged case.

Fig.5. APSD variations of current signals

The big amplitudes defined as side-band frequencies (Fig.5b), which are appeared at around the fundamental frequency 60 Hz with difference of 4 Hz, indicate the rotor eccentricity. Here the side-band frequencies (f_{sb}) can be defined by the following equation

$$f_{sb} = f_e(1 \mp 2ks) \quad (21)$$

where k is an integer. In this application f_r=1800/60=30 Hz and f_r=1742/60=29.03 Hz. Taking k=1,2 and s=0.032, from the Eq. (21), all side-band frequency values can be found at 52, 56, 64 and 68 Hz (Fig.5b). Also, comparing the Fig.5a and Fig.5b the

other important frequency components can be determined at 31 Hz and 89 Hz. These are the rotor eccentricity frequencies and they can be defined between the rotational frequency (f_r) and fundamental frequency (f_e) by Equation (20).

Bearing faults:

One cause of premature bearing failure is the passage of electrical current through the bearing and it is known as electrical discharge machining or fluting [1-3]. A severe damage is a source of audible bearing noise. The surface degradation of bearing races and rolling elements results in extreme vibration levels and eventual bearing failure.

Statistical properties of vibration signal can be investigated for detecting the fault [10-11]. The deviation between statistical parameters for the healthy and the faulty cases are compared as given in Table 2. The healthy and faulty vibration signals in time domain and their amplitude probability density functions (histograms) is shown in (Fig.6). These results indicate that the signals have a normal distribution and the overall standard deviation has increased by a factor of about 6, showing the damage.

Table 2. Statistical parameters of vibration signal

	Healthy	Faulty
Mean	0.0016	0.0030
Standard Deviation	0.1135	0.6040
Skewness	0.0591	-0.0060
Kurtosis	2.9266	3.0093

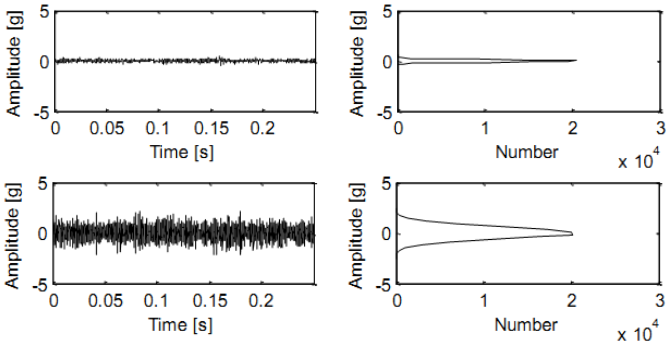

Fig.6. Accelerometer signal waveforms: (a) Baseline. (b) Final aged cycle. (c) Probability density functions of a) and b).

Bearing faults can be diagnosed by frequency domain analysis of vibration signals [12-14]. When a fault occurs in any bearing components, this creates vibrations at characteristic frequencies defined by the bearing geometry. These characteristic fault frequencies can be calculated by using either the bearing geometry or approximate formulas for the bearings which have the number of balls between six and twelve as below:

Cage Frequency: $f_c = 0.4\ f_r$

Ball Pass Frequency of the Outer Race (BPFO): $f_o = 0.4\ N_b\ f_r$

Ball Pass Frequency of the Inner Race (BPFI): $f_i = 0.6\ N_b\ f_r$

Ball Spin Frequency (f_b) is calculated using the bearing data provided by the bearing manufacturer. Here f_r is the rotor frequency and N_b is the number of balls. In this study, the motor speed is 1742 min^{-1} and then the rotor frequency is calculated as f_r = 1742/60 = 29.03 Hz. The number of balls in the bearing is N_b = 9. The characteristic frequencies are calculated as f_c = 11.6 Hz, f_o = 104.5 Hz, and f_i = 156.7 Hz. Ball Spin Frequency is calculated as f_b = 136.9 Hz for the given rotational speed.

The characteristic bearing frequencies and its harmonics occur when the bearing has a fault. The variations that are produced by the air gap eccentricity due to bearing defect generate stator currents that are related to these characteristic bearing frequencies (f_v)

$$f_{bng} = |f_e \mp m f_v|\ ,\ \ m = 1, 2, 3, \ldots \qquad (22)$$

where f_v is one of the characteristic bearing frequencies namely f_c , f_o , f_i , f_b .

The characteristic bearing frequencies are remarkable when the bearings have single point defects. If the defects are scattered on the bearing components, an increase is seen in the high frequency region of the vibration spectrum. From the power spectral density (Fig.7) of vibration signals for the healthy and faulty case, it is clear that there is an increase in the signal energy for the frequency ranges 1.5-4 kHz are due to frosting on the surface of bearing elements, caused by material removal by pitting. Data acquisition system has a low-pass filter with the cutoff frequency at 4 kHz.

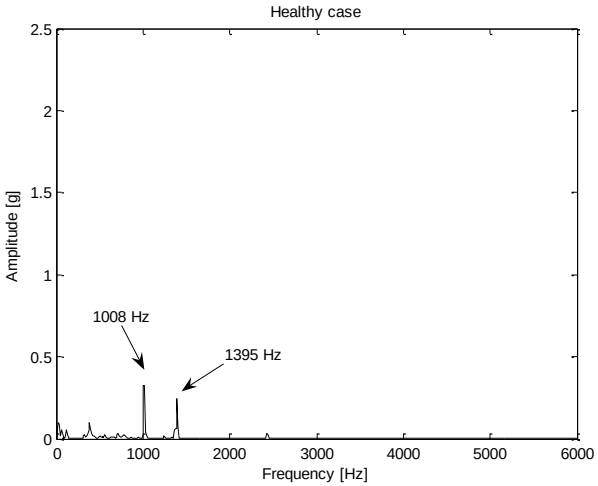

(a)

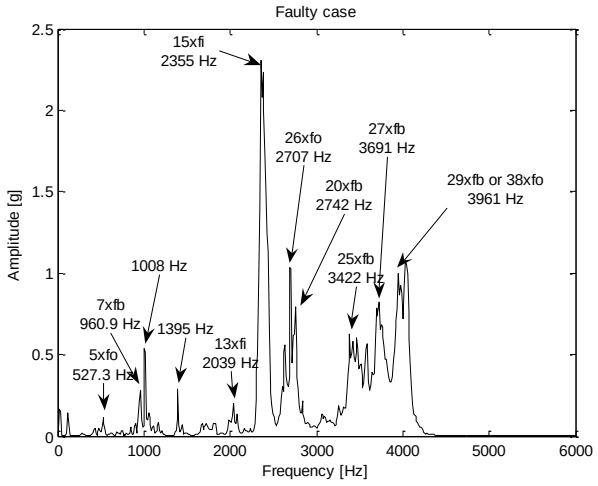

(b)

Fig.7. Power spectral densities of vibration signals (a) healthy, (b) aged cases.

The coherence function (Fig.8) indicates that the most dominant frequency values, where motor current and vibration signals are correlated, are located at 234 Hz and 469 Hz [8-9]. The side-band frequency due to the dynamic eccentricity is

$$f_{ecc} = 60 + 6(29.03) = 234 \text{ Hz}.$$

The gap eccentricity generated current due to the bearing defect is

$$f_{bng} = 60 + 3(136.9) = 470.7 \text{ Hz}.$$

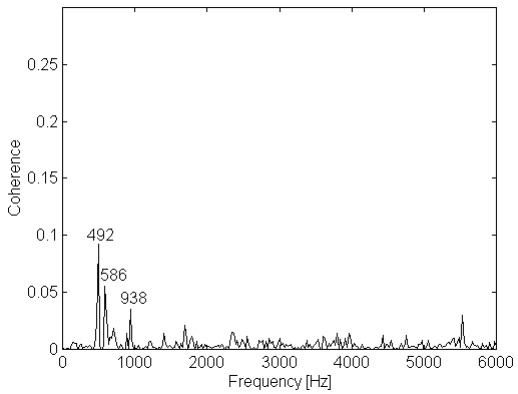

(a)

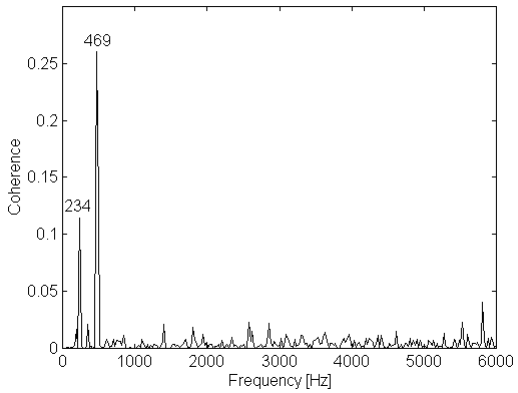

(b)

Fig.8. The coherences for healthy (a) and faulty (b) cases.

The coherence function between the motor current and accelerometer signals at the 234 Hz and 470.7 Hz has increased by a factor of 2.5 in the 200-500 Hz frequency range. The coherence between the motor current and vibration signals indicates that rotor eccentricity and bearing faults are reflected in the motor current spectrums. Also the location of bearing fault is balls in the bearing as a result of coherence analysis.

In order to determine precisely which frequency band reflects the bearing fluting damage, the sub-band or the MRA of the faulty signals was performed by dividing them into eight sub-bands in the frequency range 0-6 kHz [7,12,14]. These are given in Table 3 in terms of details (d_i) and approximations (a_i).

Table 3. Frequency sub-bands of the vibration signal

Approxi-mations	Sub-bands (Hz)	Details	Sub-bands (Hz)
$a1$	0 – 3000	$d1$	3000 – 6000
$a2$	0 – 1500	$d2$	1500 – 3000
$a3$	0 – 750	$d3$	750 – 1500
$a4$	0 – 375	$d4$	375 – 750
$a5$	0 – 187.5	$d5$	187.5 – 375
$a6$	0 – 93.75	$d6$	93.75 – 187.5
$a7$	0 – 46.875	$d7$	46.875 – 93.75
$a8$	0 – 23.4375	$d8$	23.4375 – 46.875

MRA implementation is shown in (Fig.9) and (Fig.10). According to these results, 3-6 kHz frequency band, which is named as first detail (d_1) in MRA, is the most dominant band in terms of the similarity. The ratio, which can be calculated between the RMS (root-mean-square) values of vibration measurement and the RMS values of (d_1), increases as the motor bearing degrades toward failure. If looked at other sub-bands of the vibration measurement, a good trend cannot be seen. For this reason, high frequency vibrations, which take place between 3 kHz and 6 kHz, are very affective in bearing fluting. Hence, a feature extraction from considered data could be very effectively realized by using the multi-resolution wavelet analysis technique.

(a)

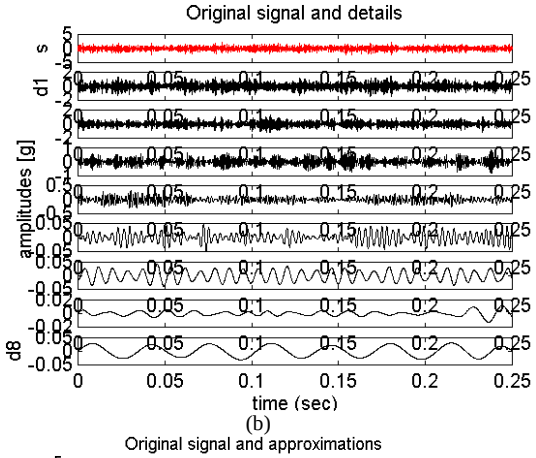

(b)

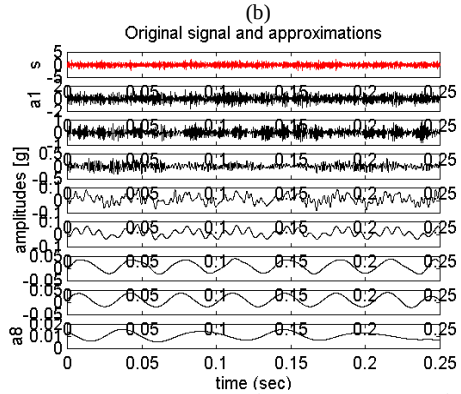

Fig.9. Details and approximations of vibration signal (s) after final aging cycle. (a) Detail sub bands ($d1$-$d8$) vibration signal (s) for aged case. (b) Approximation sub bands ($a1$-$a8$) vibration signal (s) for aged case.

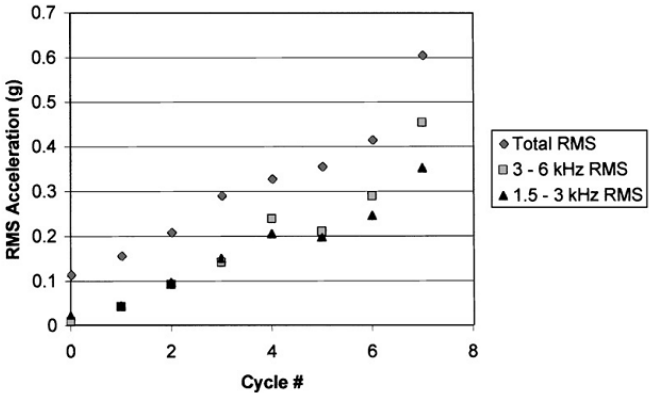

Fig.10. RMS values of vibration signal and two sub-bands (d1 and d2) after final aging cycle.

And also, short-time Fourier transformation (STFT) (Fig.11) of the first detail (d_1) shows that the observed frequency band is between 2 and 4 kHz because of the usage low-pass filter which has a cut-off frequency at 4 kHz during the data acquisition process.

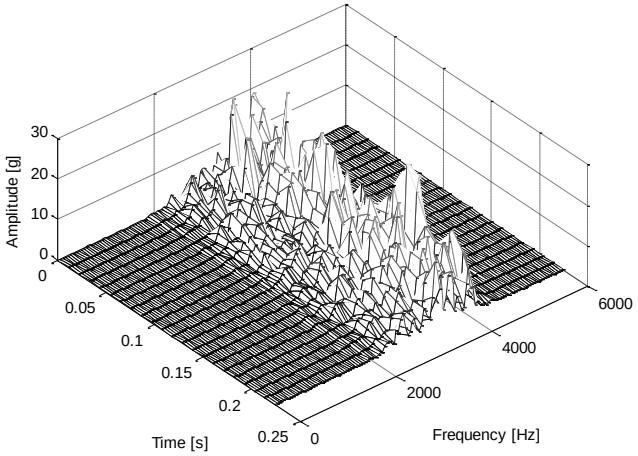

Fig.11. STFT presentation of the sub-band (d_1) related to bearing damage.

The fundamental feature, which is indicated (Fig.11) in the frequency range 2-4 kHz, denotes the bearing damage as a result of the bearing fluting test procedures. At this point, we want to ask the question how to detect this before it becomes severe. To answer this, the continuous wavelet transform (Fig.12) is recommended to reveal the potential existence of the bearing damage in early case using only healthy case data.

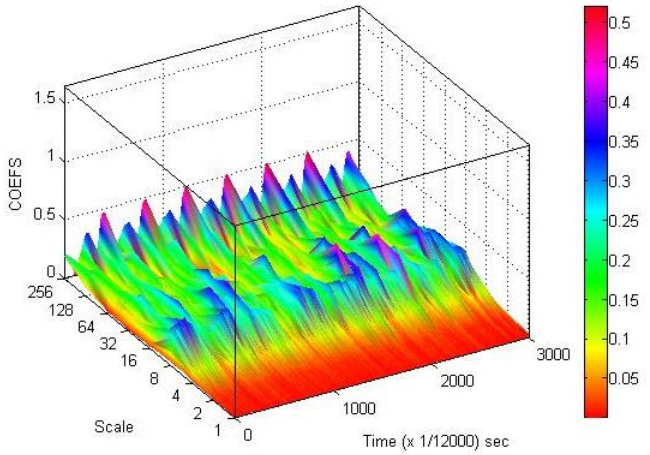

Fig.12. Absolute values of continuos wavelet transform coefficients for scales 1, 2, 4, 8, 16, 32, 64, 128, 256 of vibration signals for healthy case.

If the first scale variation is taken outside to plot it individually (Fig.13), it gives the high frequency components which are represented by very small amplitudes, to indicate the origin of the bearing damage as a potential defect.

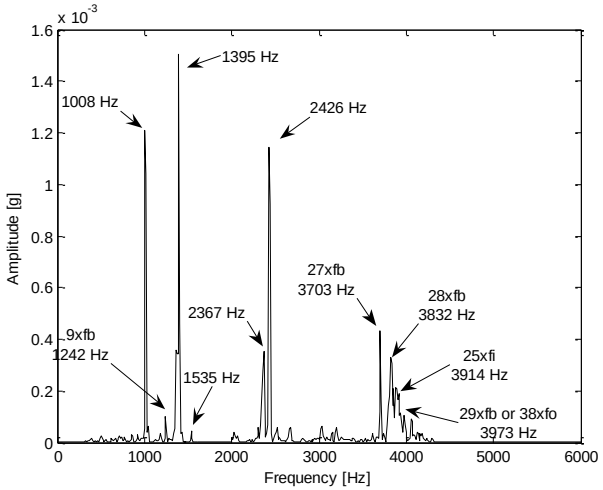

Fig.13. First scale spectrum of vibration signals in healthy case as a potential defect.

AR method is used to model vibration signals parametrically and to determine how the model parameters changes with the aging [15]. The sixtieth order model is chosen to construct AR models of vibration signals. The first AR coefficient and variance of white noise input to drive the AR model is increased with the aging (Fig.14 and Fig.15).

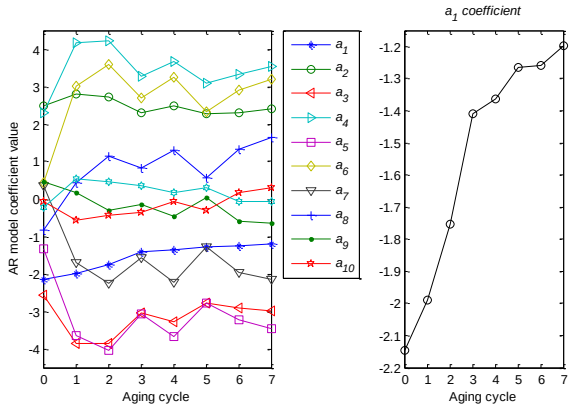

Fig.14. Variation of first 10 AR coefficients (left) and the a_1 coefficient (right) with aging cycles.

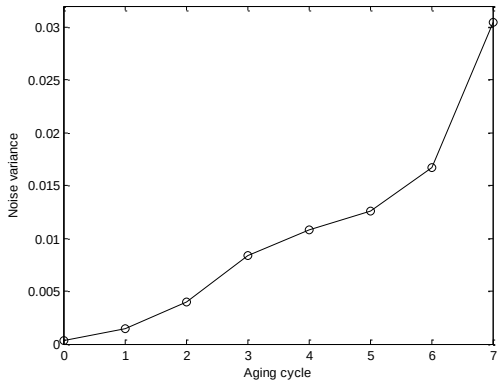

Fig.15. Variance of white noise input to drive the AR models.

Except from vibration and current signals, bearing temperature gives valuable information about the health of the bearings [17] since temperature is an important factor for lubricant. High temperatures reduce the viscosity of lubricant inside of the bearing, and cause early bearing failure. From the relationship between bearing surface temperature and aging (Fig.16), it is seen that the bearing temperature increase with the degradation of the motor. The temperature rise is at most 5°C for M8 by comparing the temperature values of the healthy motors which is cycle #0 and faulty motors which is cycle #7. The increase in temperature give information about anomaly, but it is not enough for precise decision on the severity of the fault.

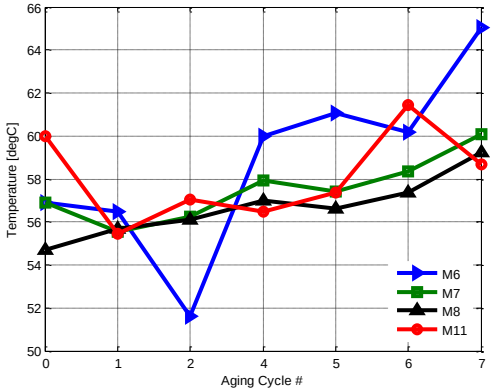

Fig.16. Process-end bearing surface temperature.

ANFIS is used to combine information from several sensors to perform automatic fault detection of bearing failure (Fig.17). The inputs of ANFIS are current, vibration and temperature as given in Table 4, and the output is motor's condition labeled as healthy (H) or faulty (F).

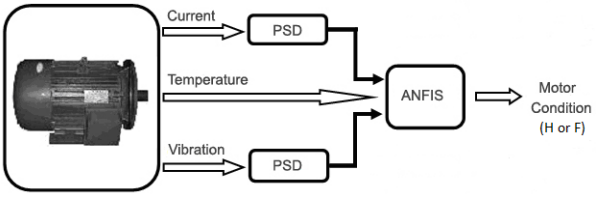

Fig.17. ANFIS based fault detection structure.

Table 4. Inputs used in ANFIS.

	Input #	Frequency band intervals
Vibration	1	0 – 732 Hz
	2	2199 – 2930 Hz
	3	2931 – 4028 Hz
Current	4	0 – 53 Hz
	5	123 – 234 Hz
	6	240 – 352 Hz
Temperature	7	-

The classification performance of ANFIS as healthy or faulty condition is calculated by taking a threshold value of 0.5. Hence 97.8% of test data is classified correctly (Fig.18).

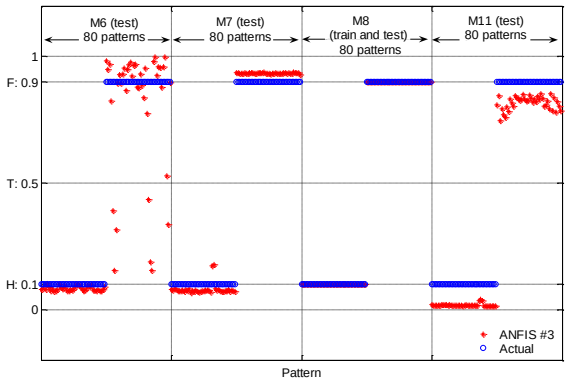

Fig.18. Training and test results for ANFIS.
H: Healthy, F: Faulty, T: Threshold

3.2. ELECTRICAL FAULTS AND THEIR DETECTION

Stator winding insulation faults are also a common source of failure of electric motors. Especially the use of motor drives creates some undesirable effects with the eventual failure of motors [20]. In this section, detection of stator winding insulation fault of main-fed induction motor is addressed.

Stator current imbalances based upon the stator insulation damage act on the stator magneto motor force (mmf) and cause motor vibrations. In this sense the cross spectral approach which is the calculation of coherence function between the motor current and vibration signals for the initial and aged cases (Fig.19) is used to detect the insulation damage.

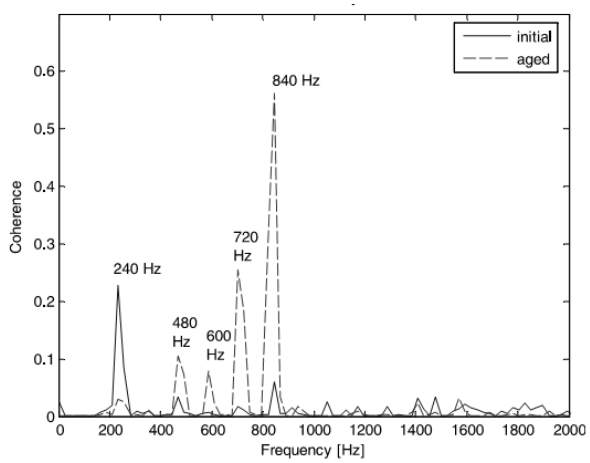

Fig.19. Coherence variation between motor current and vibration signal.

By comparing the initial and aged cases (Fig.19), the even harmonics of line frequency between 4th and 16th in the range 0-1000 Hz, namely the frequencies 240, 360, 480, 600, 720, 840, and 960 Hz appear due to insulation aging.

A neuro-detector is designed for the automatic fault detection using the coherence approach to determine the even harmonic effects, which characterize the stator insulation damage. The artificial neural network topology has an auto-associative structure, which uses the same input-output pairs in the frequency domain. Each input-output pairs obtained by coherence approach cover the frequency band of 0-1000Hz, which contains the most effective even harmonics, and they are defined as training patterns of the training data set of the neural structure. The feed forward neural structure has 50 nodes in terms of the input and output nodes, while number of the hidden nodes is 10. At the first step, the neural network is trained for the normal condition that is healthy stator insulation case using a learning algorithm. After that, the aged case is asked to it as an unknown case. In this case, the neural network produces different responses at the output nodes with a big error changes (Fig.20). Even harmonic values related to the insulation degradation can be detected looking through the error change.

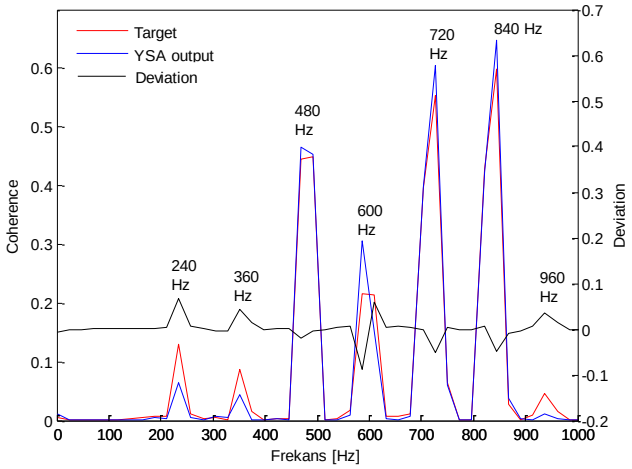

Fig.20. Testing result of the neural network for the aged case.

4. CONCLUSIONS AND DISCUSSIONS

In this paper fault detection and diagnosis in induction motors using mathematical methods are discussed with theory and example applications. Eccentricity detection, bearing fault detection and stator winding insulation faults are considered.

Eccentricity is detected by spectrum of stator current and coherence between current and vibration signals.

The statistical analysis of vibration signals give information about the anomaly. Power spectral analysis of vibration signal give the features of bearing fault as an increase of energy in the high frequency region of spectrum The most dominant frequency band is determined by multi-resolution wavelet analysis of vibration signals. Potential bearing fault is detected using continuous wavelet transform. Coherence calculation revealed the location of fault in bearing. AR modeling give the first coefficient of model can be used as a feature of bearing fault. ANFIS application helps to make decision about the condition of motor using spectral features of current and vibration signals, and bearing temperature.

Features for stator winding insulation fault is determined as even harmonics between 4th and 16th in coherence function. A neuro-detector can be used to detect the changes of these harmonics.

REFERENCES

[1] S.Nandi, H.Toliyat, XLi, (2005). Condition monitoring and fault diagnosis of electrical motors – a review. IEEE Transactions on Energy Conversion. 20 (4), pp.719-729.

[2] A.K.S.Jardine, D.Lin, D.Banjevic, (2006). A review on machinery diagnostics and prognostics implementing condition-based maintenance. Mechanical Systems and Signal Processing. (20), pp.1483–1510.

[3] A.H.Bonnett, (2000). Root Cause AC Motor Failure Analysis with a Focus on Shaft Failures. IEEE Transactions on Industry Applications. 36 (5), pp.1435-1448.

[4] R.R.Schoen, T.G.Habetler, F.Kamran, R.G.Bartheld, (1995). Motor Bearing Damage Detection Using Stator Current Monitoring. IEEE Transactions on Industry Applications. 31 (6), pp.1274-1279.

[5] IEEE Standard Test Procedure for Evaluation of Systems of Insulation Materials for Random-wound AC Electric Machinery, IEEE Std 117-1974.

[6] A.S.Erbay, B.R.Upadhyaya, (1999) Multi sensor fusion for induction motor aging analysis and fault diagnosis. Research Report, UTK,UTNE/BRU/99-01. Knoxville, TN, USA.

[7] S.Şeker, E.Ayaz, B.R.Upadhyaya, A.S.Erbay, Analysis of Motor Current and Vibration Signals for Detecting Bearing Damage in Electric Motors. Maintenace And Reliability Conference. Knoxville, TN, USA, 8-10 May 2000, (1) pp.29.01-29.14.

[8] S.Seker, (2000). Determination of Air-Gap Eccentricity in Electric Motors Using Coherence Analysis. IEEE Power Engineering Review. July, pp.48-50.

[9] S.Şeker, E.Ayaz, E.Türkcan, (2003). Elman's Recurrent Neural Network Applications to Condition Monitoring in Nuclear Power Plant and Rotating Machinery. Engineering Applications of Artificial Intelligence. 16 (7-8), pp.647–656.

[10] S.Şeker, E.Ayaz, (2003). A Reliability Model for Induction Motor Ball Bearing Degradation. Electric Power Components & Systems. 31 (7), pp.639-652.

[11] S.Şeker, E.Ayaz, (2002). A Study on Condition Monitoring for Induction Motors Under the Accelerated Aging Processes. IEEE Power Engineering Review. 22 (7), pp.35-37.

[12] S.Şeker, E.Ayaz, (2003). Feature extraction related to bearing damage in electric motors by wavelet analysis. Journal of the Franklin Institute. 340 (2), pp.125-134.

[13] E.Ayaz, S.Şeker, E.Türkcan, B.Barutçu, Combination Of Spectral And Multi-Resolution Wavelet Analysis For Fault Detection In Electric Motors. ELECO'2003, Third International Conference on Electrical and Electronics Engineering. Bursa, Turkey, 3-7 December 2003, pp.94-98.
[14] E.Ayaz, A.Öztürk, S.Şeker, B.R.Upadhyaya, (2009). Fault detection based on continuous wavelet transform and sensor fusion in electric motors. COMPEL: The International Journal for Computation and Mathematics in Electrical and Electronic Engineering. 28 (2), pp.454-470.
[15] E.Ayaz, (2014). Autoregressive modeling approach of vibration data for bearing fault diagnosis in electric motors. Journal of Vibroengineering. 16 (5), pp.2130-2138.
[16] C.C.Wang, Y.Kang, P.C.Shen, Y.P.Chang, Y.L.Chung, (2010). Applications of fault diagnosis in rotating machinery by using time series analysis with neural network. Expert Systems with Applications. (37), pp.1696–1702.
[17] M.S.Yilmaz, E.Ayaz, Adaptive Neuro-Fuzzy Inference System for Bearing Fault Detection in Induction Motors Using Temperature, Current, Vibation Data. EUROCON 2009-International IEEE Conference. Saint-Petersburg, Russia, May 18-23, 2009.
[18] N.T.Nguyen, H.H.Lee, Bearing fault diagnosis using adaptive network based fuzzy inference system. International Symposium on Electrical & Electronics Engineering. Vietnam, 24- 25 October 2007.
[19] M.S.Ballal, Z.J.Khan, H.M.Suryawanshi, R.L.Sonolikar, (2007). Adaptive neural fuzzy inference system for the detection of inter-turn insulation and bearing wear faults in induction motor. IEEE Transactions on Industrial Electronics. 54 (1).
[20] E.Ayaz, M.Uçar, S.Şeker, B.R.Upadhyaya, (2009). Neuro-detector based on coherence analysis for stator insulation in electric motors. Electric Power Components and Systems. 37 (5), pp.533-546.
[21] V.S.Vaseghi, (1996) Advanced signal processing and digital noise reduction, New York: John Wiley.
[22] T.K.Moon, W.C.Stirling, (1999) Mathematical Methods and Algorithms for Signal Processing, Prentice Hall.
[23] S.Qian, D.Chen, (1996) The joint Time -Frequency Analysis-Methods and Applications. Englewood Cliffs, NJ: Prentice-Hall.
[24] I. Daubechies, (1990). The wavelet transform, time-frequency localization and signal analysis. IEEE Transactions on Information Theory 36 (5) pp.961-1005.
[25] A.Papoulis, (1987) Probability, Random Variables and Stochastic Processes. McGraw Hill International Edition, 5th printing, Singapore.
[26] M.H.Hayes, (1996) Statistical Digital Signal Processing and Modeling. John Wiley&Sons, Inc.
[27] L.H.Tsoukalas, R.E.Uhrig, (1997) Fuzzy and neural approaches in engineering. New York: Wiley.
[28] J.S.R.Jang, (1993). Adaptive-network-based fuzzy inference system. IEEE Transactions on Systems, Man, and Cybernetics 23 (3).

ACKNOWLEDGMENT

The author gratefully thanks to Prof. Serhat Seker from the Istanbul Technical University and Prof. Belle R. Upadhyaya from the University of Tennessee, Knoxville for their support.

BIOGRAPHIES

EMINE AYAZ received the BS, MS and PhD. degrees from the Istanbul Technical University (ITU), Electrical Engineering Department, in 1993, 1997 and 2002 respectively. In 1999, she joined to the University of Tennessee, Nuclear Engineering Department and Maintenance & Reliability Centre to do research on accelerated aging studies of the electric motors. She is currently associate professor in Electrical Engineering Department of ITU. Her research interests are signal processing, soft computing, and condition monitoring in electric power systems.

Balkan Journal of Electrical & Computer Engineering
BAJECE
An International Peer Reviewed Refereed indexed and Open Access Journal

ISSN: 2147- 284X
Vol: 2
No: 3
Year: September 2014

CONTENTS

BALKAN JOURNAL OF
ELECTRICAL & COMPUTER ENGINEERING
(An International Peer Reviewed, Refereed, indexed and Open Access Journal)

Contact
https://www.bajece.com

e-mail: editor@bajece.com
bajece.editor@gmail.com